Composites Part B 224 (2021) 109173

Contents lists available at ScienceDirect

Composites Part B

journal homepage: www.elsevier.com/locate/compositesb

Research advances in composition, structure and mechanisms of microwave absorbing materials

Huifang Pang, Yuping Duan *, Lingxi Huang, Lulu Song, Jia Liu, Tuo Zhang, Xuan Yang, Jiangyong Liu, Xinran Ma, Jingru Di, Xiaoji Liu

Key Laboratory of Solidification Control and Digital Preparation Technology (Liaoning Province), School of Materials Science and Engineering, Dalian University of Technology, Dalian, 116085, PR China

ARTICLE INFO

Keywords:
Microwave absorbing materials
Metamaterials
Structural materials
Infrared stealthy material
Nanocomposite
High-temperature microwave absorbant

ABSTRACT

The earliest microwave absorbing materials (MAMs) are fabricated in the early 20th century for military purpose to inhibit radar detection. Currently, the application of MAMs has been existing in every part of human's life to prevent radiation and interference. The microwave absorbant and microwave absorbing coatings classified by composition including alloys, metal oxides, conductive polymers, carbon materials, ceramic materials both in traditional and innovative forms are introduced in this work. Considering the harsh and complex application environment, MAMs with high temperature resistance and infrared-compatible stealth performance are involved. Metamaterials, showing excellent electromagnetic properties which are far beyond that of the materials can achieve, including perfect absorber, digitally coded control metamaterials, bionic structural materials, and adjustable smart metamaterials, are also introduced specifically in this work. In addition, to investigate electromagnetic response of absorbant, the first-principles calculations works are overviewed. The electromagnetic properties, loss mechanisms, structure, fabrication method, regulation approaches, designing principles, current applications, and future prospects of MAMs are involved in this work. This work gives a comprehensively overview over the MAMs for their theoretical and experimental advances in recent years including the military radar (frequency range of 2–18 GHz) stealth materials, relevant infrared compatible (infrared-visible, infrared-radar, infrared-laser) stealth materials, and other stealth materials with multifrequency adaptability.

1. Introduction

The MAMs are first proposed in the early age of the 20th century for military purpose, are initially applied for commercial usage in second world war period, and rapidly evolve in mid-late page of that century. Materials will interact with electromagnetic (EM) waves impinging on them in the forms of reflection, absorption, transmission, also secondary reflection and transmission based on optic rules. The MAMs can attenuate and absorb the EM waves by convert electromagnetic energy to heat or other forms energy to reduce the wave reflection and transmission. Currently, the MAMs has been applied in every part of human's life including anti-radiation devices, buildings, clothes, and stealth coatings on warplanes, warship, vehicle, etc., to protect human beings' health, prevent electromagnetic interference, and avoid radar detection. To satisfy the increasing requirement on MAMs, various advanced materials have been explored. Certainly, the development of MAMs cannot happen without the extensive support from other fields of science and technology including nanotechnology, material chemistry, polymer science, solid state physics, optics, and electromagnetism, etc.

MAMs are generally composed of absorbent with effective microwave attenuation, and matrix materials with good wave transmission properties [1–7]. Besides the type of materials, the loss mechanisms consisting of dielectric loss, magnetic loss and conductive loss, are the most general way to classify the absorbant of MAMs [8–11]. As the microwaves can be regarded as a coupling of an oscillatory, intergenerative electric field and magnetic field propagating in the same direction, MAMs attenuate and absorb them through interacting with either or both of these two fields. According to the Maxwell's equations, the EM field perturbation resulting from the interaction with the materials medium on either of these two fields may induce a response on another field. Dielectric and conductive loss are the characteristic directly applied on the electronic field to attenuate the whole electromagnetic field. When the EM wave impinge on a non-magnetic dielectric material, with rare electronic carriers participating in the conduction

* Corresponding author.;
E-mail address: duanyp@dlut.edu.cn (Y. Duan).

https://doi.org/10.1016/j.compositesb.2021.109173
Received 7 May 2021; Received in revised form 19 July 2021; Accepted 21 July 2021
Available online 27 July 2021

process, the bound charges and other particles are drawn in similar motion in a very limited displacement to reach a polarization state, but reverse and recover very fast corresponding to the oscillating electric field. In that repeated arrangement process of particles, the misalignment between the motion and external EM field appears, that makes the permittivity become a complex parameter ($\varepsilon = \varepsilon' - \varepsilon'' j$). The imaginary permittivity (ε''), quantifies the dielectric loss of EM wave in this process [1,12–14]. The real part (ε') quantifies the lossless potential generated by the materials medium on EM wave, when the dielectric polarized particles returns to its original state [15,16]. In general, the dielectric polarization comes from the bound charges, atoms, ions, specific functional groups, and is sensitive to interfaces, defects, crystal structure, impurities, particle shape, grain size, porosity, microcracks, and crystal orientation. While the conductive loss always occurs in the conductive materials, whose large number of free electronic carriers can form induced current under the alternating EM field and produce heat to attenuate the EM energy. According to the Debye's theory, $\varepsilon'' = \varepsilon_p'' + \varepsilon_c''$, where $\varepsilon_p'' = (\varepsilon_s - \varepsilon_\infty)\omega\tau/(1 + \omega^2\tau^2)$, $\varepsilon_c'' = \sigma(T)/\varepsilon_0\omega$, and $\sigma(T)$ are associated to dielectric loss, conductive loss and temperature-dependent electrical conductivity, respectively. The conductive loss increases with the increasing electrical conductivity of materials, and also can be quantified by the imaginary part of permittivity. Magnetic loss is the dominated loss mechanisms occurring in magnetic materials and is the specific interaction for magnetic field. Similar to the electrical loss (dielectric and conductive loss), magnetic loss can be also expressed by a complex characteristic which is known as complex permeability($\mu = \mu' - \mu'' j$) [17]. The μ'' quantifies the magnetic loss caused by the eddy current, natural resonance, magnetic hysteresis loss, domain-wall resonance, magnetic aftereffect, etc. Due to the frequency-dependent character of these mechanisms, magnetic hysteresis loss, domain-wall resonance, and magnetic aftereffect can be neglected, while the eddy current and natural resonance dominate the loss mechanism in the gigahertz frequency band [17]. As eddy current loss increases as the increasing electrical conductivity, the magnetic alloys always have a huge eddy current loss. Besides the intrinsic characteristics of materials, magnetic properties of MAMs also depend on the particles size, crystal defects, internal stress, and particles shape, etc. More details on the magnetic characteristics and magnetic loss mechanisms will be introduced.

The most applied dielectric-loss dominated MAMs is the non-magnetic metal oxides such as ZnO, TiO_2, MnO_2 and $BaTiO_3$, dielectric ceramic such as SiC, and other inorganic nonmetal materials such as SiO_2. The conductive-loss dominated MAMs refer to that with excellent electrical conductivity such as carbon materials [18,19] and conductive polymer. The magnetic-loss dominated MAMs often contain the materials with high permeability such as magnetic alloys and magnetic metal oxide. It is easy to form a large conduction current in the conductive materials. While, only pursuing a large conductivity or permittivity will turn into the opposite, because the huge 'difference' leading to the impedance mismatching between materials and free space will make most of the EM waves reflected before impinging inside the materials. On this account, to balance the requirement of lightweight, high absorption and wide absorbing bandwidth, materials are always used in the form of mixture and composites. In addition, the approaches to improve the performance of MAMs such as atom doping, composition design, microstructure regulation, etc., are also comprehensively discussed in this review.

In addition, the MAMs are often required to work in harsh high-temperature environments. For example, the temperature of the surface of a high-speed-flying aircraft can reach over 300 °C even though in a high altitude, the temperature of some critical parts such as engine's jettube and adjustment sheets can even reach up to over 700 °C. As we know, the electrical conductivity and magnetic properties of materials are strongly influenced by temperature. Besides, according to Debye theory we mentioned above, τas the temperature-dependent relaxation time will influence the dielectric polarization process and dielectric loss [20–23]. Therefore, the thermal properties including high-temperature stability, high-temperature oxidation resistance, and high temperature microwave absorbing properties will be crucial for the MAMs in a practical application. We also review the recently progress for high-temperature MAMs in this work, their influence factors and developing prospects are also discussed.

The current numerical techniques make it possible to investigate electromagnetic response of absorbant through calculation by using validated theoretical methods to support their experimental research. Permittivity and permeability can be researched by analyzing the information of magnetic moment, charge transfers, and electric dipole, etc., which are essentially depends on the electron structure and behavior. The relationship between electromagnetic response and electron behaviors involves the integration of atomic level dynamics, nonequilibrium thermodynamics, and defect physics, etc., which can be further researched by first-principles calculations based on density functional theory (DFT) [24–28]. We will present some theoretical researches in this paper.

Besides the absorbant mentioned above, the subwavelength-scale structure of MAMs also plays important role in the absorbing performance. Many structural absorbing systems achieve excellent absorbing properties that are far beyond those of the same synthetic materials. Through special structural design, the structural MAMs can decrease the radar reflection cross section (RCS) and improve the impedance matching to reduce the EM wave reflection, the EM wave signal that can be detected by radar device is also reduced. To enhance the military target detection, infrared detection is applied together with the radar detection to hunt for military targets. The infrared radiation energy is closely related to the thermodynamic temperature. Most objects show higher temperature than that of the background, and the MAMs on the surface of targets generate massive heat when attenuating EM waves, which make them easily detected by the infrared detector. It seems incompatible for materials to have both good microwave absorbing performance and low infrared emissivity. While many approaches have been proposed to fabricate infrared-radar compatible stealth materials, e.g., to design multiple-layered functional coatings or to control the target's infrared radiation band out of the atmospheric window. The research on infrared low emissivity stealth material will be also discussed in this paper.

Metamaterials is also a kind of structural materials showing unnatural electric and magnetic properties (i.e. negative or ultrahigh permittivity and permeability, which is nonexistent in nature materials), which is mainly attributed to their special artificial structures. The periodically structure helps to obtain excellent microwave absorbing properties which are far beyond that of the materials can achieve, even some lossless materials can show huge microwave absorption. The efficient permittivity and permeability of MAMs can be regulated by designing unite array structure. Essentially, metamaterials reduce the EM wave reflection by improving the impedance matching between the materials and free space, and increase the absorption by electric and magnetic resonance between the arrayed units in structure. Currently, the researches on metamaterials applied as MAMs such as the invisible cloak and broadband adaptable MAMs, have attracted extensive attention. Recently, researchers are inspired by the nature creatures to design bionic structural metamaterials to obtain a wide band absorption which even cover several electromagnetic bands. Besides the traditional metamaterial without circuit analog, the advanced metamaterials such as active circuit analog metamaterial with adjustable smart performance are proposed recent years.

This overview will restrict itself primarily to the MAMs on the usage of military purpose, focuses on the military radar (frequency range of 2–18 GHz) stealth materials, involved infrared compatible (infrared-visible, infrared-radar, infrared-laser) stealth materials, and other stealth materials with multifrequency adaptability. Ultimately, the extent and complexity of this field are daunting and will require

immense amounts of global research efforts to be comprehensively elucidated. Therefore, this review is by no means an exhaustive list, we just focus it on a number of MAMs systems that we are interested in. Many systems are only superficially mentioned. The technological revolutions improved rapidly in the past one hundred years, and will probably develop in a greater speed in the further one hundred years if universal properties permit.

2. Alloys absorbent

Due to higher saturation magnetization (M_s) and stronger magnetic loss ability, alloys are one of the most commonly used electromagnetic (EM) wave absorbers, which mainly lose EM wave through eddy current loss and natural resonance in the range of GHz frequency band. At present, the commonly used alloying EM wave absorbers mainly include traditional alloys, high entropy alloys (HEAs), and composite alloy materials.

2.1. Traditional alloys

2.1.1. Fe-based alloys

1. Alloy powders

Flaky Fe-based alloy powders with nanocrystalline structure are also prepared by grinding annealed amorphous ribbons, and the aspect ratio has an important effect on its EM properties [29]. The obtained flaky $Fe_{73.5}Cu_1Nb_3Si_{13.5}B_9$ powders are sieved into two categories with different particle sizes [30]. The large flakes have larger demagnetization factor in the direction of thickness ($N_\perp$) and smaller demagnetization factor in the direction of width (N_h). According to the following shape-dependent Snoek's law (formula 8-10), a higher permeability (μ_s) and a smaller resonance frequency (f_r) can be obtained. The particle size of $Fe_{84}Co_4B_{11}Nd$ powders decrease with the extension of milling time [31]. The maximum μ' is 3.8 at 2 GHz for the sample with the particle size of 50–240 μm $Fe_{77.8}Cu_{2.39}Nb_{3.33}Si_{16.28}B_{0.62}$ alloy ribbons with nanocrystalline also get a high permeability after milling into powders [32]. To accurately measure the anisotropy energy of alloy particles have become an urgent task due to its mixed and disorderly arrangement. Magnetically aligned $Sm_{1.5}Y_{0.5}Fe_{17-x}Si_x$ flaky alloy materials are prepared by fixing the particles in epoxy resin under a magnetic field of 10 kOe [33]. The values of in-plane and the out-of-plane magnetic anisotropy fields are the field strength corresponding to 85% of the M_s for the magnetic fields parallel and perpendicular to the aligned direction, respectively. Based on the anisotropic field, M_s and initial permeability measured by experiments, the natural resonance frequency is calculated according to the Snoek formula, and it can be changed by adjusting the Si content. A maximum effective bandwidth reaches 3.7 GHz (12.7–16.4 GHz) for the $Sm_{1.5}Y_{0.5}Fe_{17-x}Si_x$-paraffine composite in thicknesses of 1.0 mm.

2. Alloy ribbons

The amorphous alloy ribbons prepared by melt spinning method have low H_c (3–24 A/m), because of no long-range periodicity and the near zero value of magnetocrystalline anisotropy in the amorphous matrix [34]. After annealing at 673 K, smaller α-FeCo(Si) nanocrystallines with size of 25 nm are precipitated in FeCoSiBNbCu alloy under the influence of Nb and Cu, which is lower than the ferromagnetic exchange correlation length (30–40 nm). All these alloy ribbons present good EMI shielding (>20 dB) in 0.2–8.5 GHz.

2.1.2. Co and Ni-based alloys

In addition to Fe-based absorbing materials, magnetic metals such as Co and Ni also have the characteristics of simple crystal structure, high saturation magnetization and low anisotropy. Many exploration attempts have also been made in the field of wave absorbing materials. Electromagnetic absorbers containing Co and Ni metals have two main research directions, including alloy powders and composite materials.

1. Pure Co and Ni based alloys

The morphology, composition, size and crystal structure of the magnetic metal or alloy are all important factors that restrict the electromagnetic wave absorption performance. Urchin-like Ni powders synthesized by Liu et al. [35] are achieve a maximum reflection loss of −43 dB at a thickness of 2 mm at 10 GHz. Electromagnetic property of the nickel chain 3D network synthesized by Cao et al. [36] show obvious temperature dependence.

FeCo alloys with different atomic ratios (3:7, 5:5 and 7:3) prepared by simple hydrothermal reduction method are successfully synthesized [37], and SEM images are shown in Fig. 1. As the Fe/Co atomic ratio increases, the alloy morphology transformed from lamellar structure to cone-shaped structure and finally the cone-shaped structure gradually become smooth. The alloy with an atomic ratio of 7: 3 had the best absorption effect: the optimal reflection loss RL (1.55 mm) reached −53.6 dB at 14.3 GHz and effective bandwidth covered the entire K_u band (11.2–18 GHz).

Huang et al. [38] synthesized FeCo alloys of different morphologies by adjusting the Fe^{2+}/Co^{2+} molar ratio, and the particle shapes showed nanocubes, nanoplates, and nanoflowers, respectively. The RL_{min} (3.4 mm) of the flower-shaped FeCo is up to −43 dB at 13.1 GHz, and the effective absorption bandwidth is 5.8 GHz (2.7–5.4 GHz and 12–15.1 GHz). CoNi nanoflowers with different sizes (0.6, 1.3 and 2.5 μm) are obtained by one-step solvothermal method, and such microstructures had obvious dependence on the concentration of precursors and surfactants. Among the three samples, the 2.5 μm CoNi nanoflower had the best RL (−28.5 dB, 6.8 GHz), while the 0.6 μm nanoflower sample had the widest effective bandwidth (6.5 GHz) [39].

Magnetic metals listed above have excellent performance in wave absorption performance, but the absorbers with a single loss mechanism often cannot meet the needs of multi-band absorption. Moreover, it is impossible to fundamentally solve the problems of high density and poor corrosion resistance of metal powders in material application only by adjusting the components and surface modification. Therefore, the proposal of composite materials also provides new ideas for solving the limitation of such absorbents.

2. Co and Ni based composites

According to the current development status of wave absorbing materials, it is difficult for magnetic metal absorbers to meet the increasing comprehensive requirements of radar wave stealth technology. The composite materials with multiple advantages have become the focus of RAM research and development. Many researchers combine magnetic metals with metal oxides, carbon materials or organic materials to obtain core-shell structured absorbing materials. This type of absorber can fully exert the synergistic effect of each component through the effective recombination between the core particles and the shell particles on the micro-nano scale, and has a relatively wide range of applications in microwave absorption.

Quan et al. [40] synthesized the porous structure Co_xNi_y/C composite material by spontaneous cross-linking reaction and calcination, and adjusted the proportion of the components through the Co^{2+}/Ni^{2+} ratio. The porous structure realizes the adjustment of dielectric constant and impedance adaptation, and achieves good electromagnetic wave absorption through multiple magnetic loss and dielectric loss mechanisms. The RL_{min} of the three samples (S1–S3) with 50 wt% fillers are all below −35 dB. The strongest reflection loss of 1.4 mm is −49.08 dB (17.36 GHz), which appears in the Co_1Ni_2/C sample. Co_1Ni_1/C shows significant effective bandwidth at various thickness intervals, and its widest bandwidth reaches 6.68 GHz at 2.2 mm.

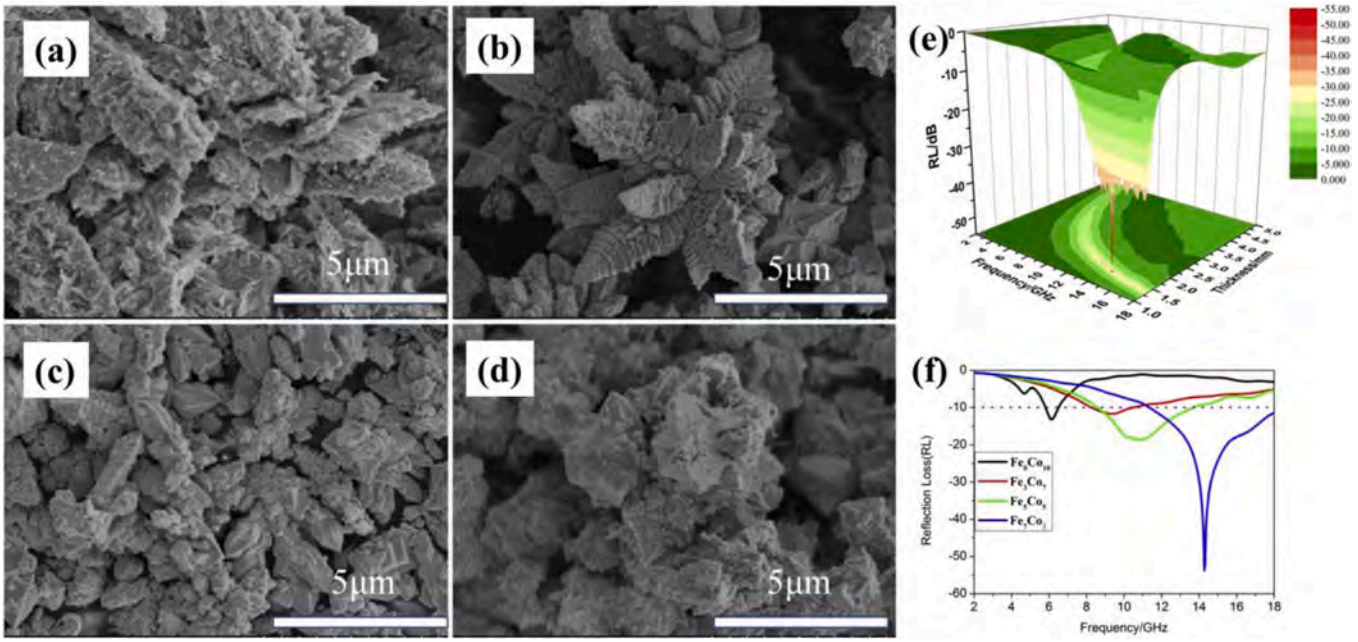

Fig. 1. (a)–(d) SEM images of FeCo alloys with different atomic radio (0:10, 3:7, 5:5 and 7:3); (e) 3D plot of RL values for Fe_7Co_3; (f) RL curves of FeCo-paraffin composites (70%) with different atomic ratio at 1.55 mm in the frequency range 2–18 GHz [37].

Zhao et al. [41] successfully prepared Ni@void@SnO_2 (Ni_3Sn_2) yolk-shell composite material through a simple two-step method. After the reaction time reached 15 h, the samples showed excellent microwave absorption performance, and the reflection loss is as low as −43 dB at 6.1 GHz. Zhao et al. [42] also proved that core-shell microspheres with Ni core and TiO_2 two-phase shells had better ability to absorb EM waves than pure nickel. The RL with thickness of 1.8 mm of Ni@TiO_2 (rutile) composite is −38.0 dB at 11.1 GHz.

The core-shell composite material type absorber greatly improves the impedance adaptability, and also obtains a small density of powder, which provides the possibility to obtain a light-bandwidth electromagnetic absorber. However, the current research is mostly concentrated in the laboratory exploration stage, and there are still many technical difficulties to achieve the goal of large-scale application. Future research needs to make continuous attempts in the exploration of cost-effective process flow, selection of core-shell materials, and verification of absorbing coatings.

2.1.3. Fabrication of alloys

1. Milling

Traditional alloys, such as carbonyl iron, FeSiAl, FeSiCr, and FeCoNi et al., have been investigated. Flaky alloy particles with large aspect ratio are desirable, and milling is the most commonly used method to prepare. Study shows that flaky carbonyl iron prepared by utilizing spherical milling medium has larger aspect ratio, complex permittivity and permeability than by cylindrical milling medium [43]. The maximum μ' can reach 7.5 at 1 GHz (85%). Therefore, in the absence of special instructions, the grinding medium is spherical. Due to the formation of larger aspect ratio alloy powder, higher complex permittivity and permeability are obtained after milling alloy powders. The improvement of EM properties can be achieved not only by increasing the aspect ratio of the alloy particles, but also by subsequent heat treatment and changing the arrangement. The complex permeability of $Fe_{76.5}Si_{21.5}Cr_2$ alloy powders increase first and then decrease with the annealing temperature increase [44]. The largest permeability appears at the critical temperature (450 °C), which corresponds to the starting formation of DO_3 ordered phase. Sphere-shaped and flake-shaped Fe_3Al particles are prepared by changing the milling environment [45]. A rotational orientation method is used to prepare the mixture of paraffin and flaky alloy particles with the same orientation. The flaky particle has a larger permeability than sphere particle, and the maximum EM parameters can be obtained for the oriented flaky sample.

2. Chemical synthesis

Due to the advantages of controllable morphology, the preparation of alloy powders by chemical synthesis method has become a popular trend in recent years, and the magnetic and EM properties can be improved significantly. P-doped FeCo microcubes are fabricated by using solvothermal method [46]. Experimental results demonstrate that the morphology and particle size of the alloy powder depend on the content of assisted agent ($NaH_2PO_2{\cdot}H_2O$), and the particles gradually change into cubes with its content increase (Fig. 2). Due to NaH_2PO_2 sticks to the [100] crystal plane, growth is impeded on this crystal plane, which results in the different growth rate between [100,111] crystal plane and the formation of cubic particles. Due to the unique morphology and the incorporation of P dopants, the saturation magnetization (M_s) increases from 164.81 emu/g to 192.62 emu/g, and the EM wave absorption performance shows the RL_{min} is −51.67 dB at 1.6 mm.

Hierarchical cobalt dendrites consisted of nanoflakes are also prepared by a hydrothermal method [47]. The reaction conditions, including the molar ratio of pyromellitic acid to cobalt chloride, the concentration of sodium hydroxide (NaOH), and the reaction temperature and time, play an important effect on the morphology, magnetic, and EM properties of the powders. Co dendrites present larger EM parameters and better microwave absorption than that of spherical and sword-like aggregates. Similar method has been used to prepare other alloy powders. Polyhedral FeCo alloy particles are synthesized by using hydrazine hydrate reduced iron and cobalt salt in highly alkaline media [48]. With the decrease of Co content, the particles change from flower shape to pyramid shape, and the permeability can reach 2.7 by adjusting the Co content. The minimum reflection loss is −52.20 dB and the effective absorption bandwidth is 6 GHz for Fe_6Co_4 sample at a thickness of 1.7 mm.

3. Other methods

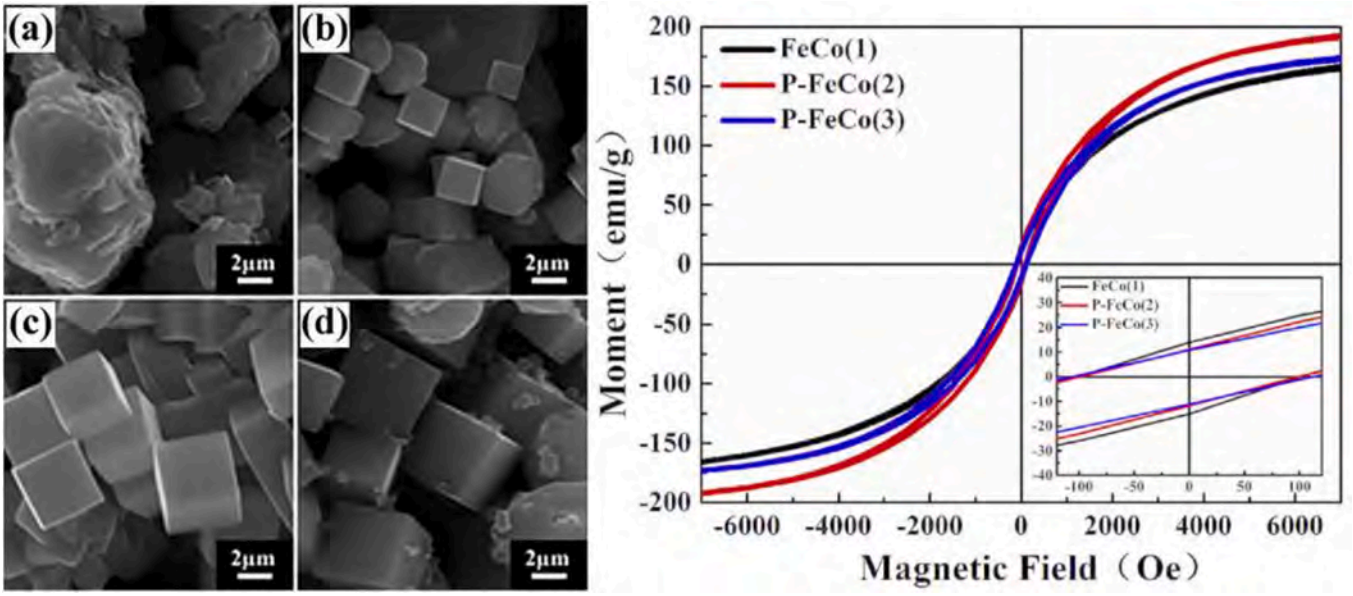

Fig. 2. SEM photographs of FeCo particles, (a) FeCo(1); (b, c) P–FeCo(2); (d) P–FeCo(3), (e) the corresponding magnetic hysteresis loops [46] .

In addition to the above milling and hydrothermal methods, other technologies are often used to prepare alloy powders. FeSiAl hollow microspheres alloy powders are prepared by two steps [49]. The precursors are obtained through twice-balling adhesive precursor method, including milling, mixing, drying, and carbonizing process. And the powders are obtained in self-reactive quenching technology, which makes the liquid powders quench quickly. Various shapes of Fe nanoparticles are prepared by changing the Al content in the anode target using arc-discharge method [50]. The presence of Al purifies the raw material and atmosphere, which makes Fe hold the polyhedral crystal habit. The absent and excessive Al interfere the growth of Fe, which promotes the formation of quasi-spherical particles. A higher EM parameters and stronger absorbing can be obtained for polyhedral alloy powder.

2.2. High entropy alloys

HEA, also known as a multi principal elemental alloy, is defined by Yeh et al. [51], which is generally composed of FCC, BCC, or two-phase coexistence. Due to the large number of components and high mixing entropy, HEA has different properties from traditional alloys, such as good mechanical properties, corrosion resistance, high temperature stability, and oxidation resistance. Recently, more and more researches have been done on the magnetic and EM properties. Research shows that M_s depends on the composition and atomic-level structures, while H_c is sensitive to microstructure, impurity, and the subsequent heat-treatment process.

2.2.1. FeCoNiCrAl

EM wave absorbing materials can be often used in harsh environment, such as alkaline or high-temperature environment. HEAs are promising as a new generation of absorbing materials due to their comprehensive properties. In recent years, researchers have begun to explore the EM properties of HEAPs. Flaky FeCoNiCrAl HEAPs are prepared by mechanical alloying method [52]. The M_s and H_c for 70 h-milling powders are 20.21 emu/g and 142 Oe, respectively. The RL_{min} is −35.3 dB at 10.35 GHz and the effective absorption bandwidth is 2.7 GHz (9.2–11.9 GHz) with a thickness of 1.5 mm. Also, $FeCoNiCrAl_{0.8}$ HEAP with crystalline structure has better EM properties than amorphous structure [53]. In addition, the increase of Cr content and annealing process promotes the increase of complex permittivity for $FeCoNiAlCr_x$ HEAPs due to the enhancement of larger particles, particle size and conductivity [54]. The as-milled FeCoNiCr alloy powders heated with a magnetic field of 10 T show a better impedance matching effect, with RL_{min} of −60.96 dB at 13.84 GHz. But the Cr content and the annealing process have little effect on the complex permeability.

2.2.2. FeCoNiSiAl

The traditional FeSiAl alloy has higher permeability and good EM absorption performance, and the magnetostriction coefficient of the FeCoNi alloy reduces after adding Si element, which promotes the FeCoNiSiAl HEA being a potential superior EM absorption material. $FeCoNiSi_{0.4}Al_{0.4}$ HEAPs are prepared via mechanical milling and melting-strip casting-milling methods [55]. Different solution and phase formation rules are founded; the former is related to crystal structure and atomic radius of elements, and the latter is determined by covalent electron concentration (VEC). The as-cast milling powders have larger aspect ratio, better elemental uniformity, and fewer defects, which leads to smaller magnetocrystalline and stress anisotropy as well as larger shape anisotropy, manifesting smaller M_s (93.6–104.4 emu/g) and larger H_c (81.5–159.6 Oe). Also, a larger μ' (varying from 1.78 to 1.90 at 2 GHz) and μ'' (up to 0.52) of the as-cast milling powders are obtained. Flaky $FeCoNi(Si_{0.6}Al_{0.2}B_{0.2})$ HEAPs are fabricated by melt-spun-milling method [56]. The aspect ratio and grain size can be tuned by changing milling time. As the milling progresses, the M_s exhibits a downtrend from 88.1 to 78.6 emu/g, and H_c also reduces from 79.5 to 63.3 Oe. The maximum μ' (1.84 at 2 GHz) is obtained after milling 50 h.

Crystal structure and microstructure have an important role in adjusting magnetic and EM properties. $FeCoNiSi_xAl_{0.4}$ HEAPs with dual-phase nano-crystalline and nano-amorphous structure, simultaneously with larger aspect ratio, are prepared by a combination technology containing arc-melting, strip-casting, and milling [57]. Due to the formation of unique microstructure and ingenious preparation technology, a small magnetocrystalline and stress anisotropy and large shape anisotropy are obtained, which leads to a less H_c (14.05–23.43 Oe) and a large magnetic permeability (2.41–2.80, 1 GHz), and the properties can be tuned by the crystallinity of HEAPs. The crystallinity of $FeCoNiSi_{0.4}Al_{0.4}$ HEAPs with same composition is tuned by utilizing the same technology [58]. Different phase proportions of milling precursor (ribbons) are obtained by changing the annealing time. A small H_c, varying from 12.97 Oe to 28.33 Oe, and a large complex permeability, varying from 2.60 to 2.30, can be obtained. The same group also reports that the

effect of Si content and annealing treatment on conductivity, magnetic, and EM parameters for $FeCoNiSi_xAl_{0.4}$ HEAPs prepared by mechanical milling [59]. The formation of $CoFe_2O_4$ phase in annealing process plays an important role in magnifying M_s and minishing H_c.

2.3. Relevant composite materials

2.3.1. Composition regulation

Magnetic loss is the main type of EM loss for alloy materials. In order to enhance impedance matching and EM loss, researchers usually combine alloy materials with dielectric and conductive materials. The EM properties of sendust/polymer and sendust/multiwalled carbon nanotube (MWCNT)/polymer composites are compared [60]. Due to the formation of conductive network by the addition of MWCNTs, the conductive loss of the composite increases, thus effectively improving the EM absorption and shielding performance. In addition, the flaky sendust particles are aligned in the same direction by a roll-milling machine at 90 °C for 10 min, and its EM properties are better than that with disorder arrangement [61]. FeSiAl/ZnO-filled resin composite coatings are prepared by mixing FeSiAl with ZnO. The increase of FeSiAl and ZnO content would lead to the increase of mixture dielectric constant, and the RL_{min} of −40.5 dB at 10.4 GHz and the effective absorption bandwidth of 3.5 GHz (8.6–12.1 GHz) are obtained.

2.3.2. Surface modification

For traditional alloys, the high real part of permittivity causes the impedance mismatch of the alloy powders. The surface treatment of the alloy powder or the preparation of the core-shell structure is often used to improve the EM absorption performance. Fe-9.6 wt% Si-5.4 wt% Al alloy powder coated with bilayer nitride shell is synthesized by surface nitriding [62]. Due to the different affinity between Fe/Si/Al and N element, selective nitride leads to the main formation of Fe_4N in the outer layer and Si_3N_4 in the inner layer. Although ε' decreases after nitriding treatment, the dielectric and magnetic loss of the alloy powder increase significantly. Excellent impedance matching promotes the strong reflection loss of −34.5 dB at 12.95 GHz and absorption bandwidth of 8.11 GHz for the nitrided composites.

In addition to nitriding, oxidation and acidification are also commonly used methods. Flaky $Fe_{87.36}Si_{8.02}Al_{4.62}$ particles are prepared by milling irregular particles, and then oxidizing the surface of the particles [63]. The EM parameters for flaky particles are larger than the irregular particles, while the complex permittivity for modified particles decreases significantly, and the complex permeability keeps unchanged fundamentally. A better match between dielectric and magnetic losses can be obtained. CoFeBSiNb metallic glass powders are treated with hydrochloric acid solution [64]. Due to the formation of a large number of loose structures and nanopores, the specific surface area increases, enhancing the interfacial polarization. The RL_{min} value of −45.2 dB at 14.64 GHz with the thickness of 2.3 mm and the bandwidth of 14 GHz (below −10 dB) are obtained.

2.3.3. Structural control

The multi-shell microstructure would provide more interface polarization for enhancing the microwave absorption performance, and magnetic@dielectric-loss type microwave absorbing composites are used to design. Due to the unique structure, the enhancement of interfacial polarization leads to the increase of the complex permittivity and the dielectric loss. Moreover, the gradient dielectric constant for the multilayer structure is conducive to the improvement of impedance matching and thus to the absorption of EM waves. Fe-cored carbon nanocapsules (Fe@C) are prepared by using microwave-metal discharge technology [65]. The coexistence of magnetic and dielectric loss and the interfacial polarization loss make the EM loss better, with the RL_{min} being −22.5 dB at 10.2 GHz for a thickness of 2.5 mm. Differently, the relationship between magnetic domain and M_s and EM properties in 3D Fe/C interpenetrating networks consist of hollow microsphere are explored [66]. The vortex domain and stripe domain inside the wall interact with each other, and positive and negative magnetic-charge localize at the two ends, thus the formation of stray field leads to a higher M_s of 340 emu/g, which is 1.55 times as that of bulk Fe. The minimum microwave absorption is up to −55 dB and the effective bandwidth (<10 dB) is 12.5 GHz (5.5–18 GHz).

2.4. Summary and prospects

Alloys, as one of the most commonly used EM wave absorbers, convert EM energy into heat energy through such magnetic loss types as eddy current loss and natural resonance. Flaky alloy particles with larger shape anisotropy can get larger permeability and better EM absorption performance. Also, the EM properties of various shapes of alloy particles have been tried to explore. HEAs are expected to be a new generation of EM wave absorbing materials due to their superior comprehensive properties, such as corrosion resistance and oxidation resistance. Alloy materials are often mixed or compounded with dielectric or conductive materials to achieve impedance matching. In addition, surface treatment is used to reduce the complex permittivity and enhance the impedance matching effect.

3. Metal oxides absorbant

3.1. MnO_2

As one of transition metal oxides with a variety of microstructures, manganese dioxide has been extensively researched due to its outstanding physical and chemical performances, such as molecular absorption, good thermal stability, easy synthesis and environmentally friendly. Manganese dioxide has been a promising candidate for microwave absorption material due to its various phases and morphologies. The basic MnO_6 octahedral units can make up α, β, γ, δ and ε-type polymorph according to different linkage ways. Different polymorphs and morphologies of manganese dioxide have different electromagnetic wave absorbing properties. As one of the microwave absorption materials, electromagnetic loss mechanism of manganese dioxide is dielectric loss with dipolar polarization.

Duan et al. [67] build the δ-MnO_2 and α-MnO_2 by hydrothermal method through trace element doping. The pure δ-MnO_2 nanosheets own the lowest permittivity whose average values of real and imaginary are 2.52 and 0.01, respectively. The Ag atom doping α-MnO_2 shows larger complex permittivity whose real and imaginary part can reach up to 15.08 to 9.57, respectively. Besides, the magnetic loss of δ- and α-MnO_2 is much lower compared to permittivity because of its dielectric-dominant character. The real and imaginary permeability of α-MnO_2 are 1.06 and 0.05, respectively. The huge difference between permittivity and permeability makes the impedance matching undesirable. Besides, the electrical conductivity of α-MnO_2 is 3.33×10^{-2} S/cm which is better than that of δ-MnO_2 which is at $\sim 0.11 \times 10^{-2}$ S/cm, which indicates the MnO_2 to be a kind of semiconductor materials. Pang et al. [68] fabricate the β- and γ-MnO_2 used as microwave absorbing materials by hydrothermal method. Through controlling the reaction condition, the crystal type of MnO_2 changes from γ to β whose morphology also changes from urchin to rectangular pyramid. Research shows that compared to γ-MnO_2 the pyramid β-MnO_2 has better microwave absorbing properties with the reflection loss reaching up to −13.3 dB. Guan et al. [69] synthesis the 1D α-MnO_2 nanorods through a low-temperature water-bathing method. Attributed to the high interfacial polarization and space charge polarization of 1D materials, the reflection loss of MnO_2 nanorods is −25 dB which is much higher than other reported MnO_2 absorbant. Nevertheless, most pure MnO_2 shows low microwave absorption and poor impedance matching, numerous strategies have been made to prepare MnO_2 composites to enhance the electromagnetic wave absorbing properties. Generally, dielectric loss not only derives from polarization, but also derives from conductivity

loss. Increase of conductivity and addition of interfacial polarization are good strategies to enhance microwave absorption property. Combining manganese dioxide with other suitable materials into a hybrid composite has been proposed to endow them with more polarization types or enhance conductivity loss, which would solve the problems of poor impedance matching and attenuation.

3.1.1. MnO_2/dielectric composites

Considerable efforts have been devoted to combining dielectric materials with manganese dioxide to form hybrid composites, which can induce multiple loss mechanism. On the one hand, the designed complex structure would bring multiple reflection and scattering, good impedance matching and multi-interface polarization. On the other hand, the addition of suitable dielectric material can further enhance the dielectric loss because of ameliorating electrical conductivity. Due to the synergy of these two aspects, the attenuation of the electromagnetic wave energy would be greatly improved.

Reasonable designed morphology would bring multiple reflection and scattering, good impedance matching and multi-interface polarization. Combination of MnO_2 with other dielectric material can further increase the dielectric loss. Due to synergy of above two aspects, the attenuation of the electromagnetic energy would be greatly improved. The electromagnetic wave absorption properties of β-MnO_2/PVDF nanocomposites have been investigated. Hybrid composite generates more surface and interfaces. The increased surface and interfaces contribute to multiple reflection and increase multi-interface polarization. The resulted β-MnO_2/PVDF nanocomposites exhibit enhanced microwave absorption properties [70]. MnO_2 nanorod loaded PVB nanocomposite is found more efficient for microwave absorption as compared to MnO_2 nanosphere. The maximum reflection loss value of −37 dB of PVB-MnO_2 nanorod composite is obtained with large bandwidth in X-band for the thickness of 2 mm. The factors such as effective permittivity, degree of EM impedance matching, antenna mechanism, and dielectric dissipation are found to depend on the morphology of PVB-MnO_2 nanocomposites. Various morphologies of α-MnO_2 nanostructures are synthesized on the surface of woven Kevlar fiber (WKF) by hydrothermal method under different reaction conditions in Fig. 3 [71].

The core-shell structure is benefited to electromagnetic wave attenuation. The special structure not only improves the multiple scattering, multiple reflections and absorption of electromagnetic wave, but also reduces the weight of materials efficiently. Besides, the presence of defects from core-shell interfaces can be easily excited under the electromagnetic field, and these defects can act as polarized centers that increase the space charge polarizations by trapping space charges, resulting in the improvement of microwave absorption ability. In addition, the core-shell structure makes the dielectric constant adjustable, which is conducive to impedance matching, and thus conducive to the attenuation of electromagnetic energy. Recently, carbon materials are performed to form core-shell nanocomposites with manganese oxide, which induced strong attenuation of microwave. The CS@MnO_2 composite shows enhanced dielectric loss [72]. The incorporation of MnO_2 nanoflaky shells with spherical carbon cores ameliorates the electrical conductivity and the impendence matching of the CS@MnO_2 composites. Polymer has also been combined with manganese oxide to form core-shell nanocomposites with strong attenuation of microwave. For example, hollow lightweight polydopamine@α-MnO_2 microspindles are synthesized with the tunable absorption frequency governed by the aspect ratio (Fig. 4) [73]. The hollow polydopamine@α-MnO_2 microspindles with optimized aspect ratio for the cavity of ~2.8 achieved strongest reflection reaches −21.8 dB at 9.7 GHz and 3 mm thickness. The dielectric polarization is regulated by different aspect ratios.

3.1.2. MnO_2/magnetic materials composites

Due to the high conductivity, excellent magnetism, and high saturation magnetization, magnetic nanoparticles/alloy/magnetic oxide, have attracted extensive attention in the field of electromagnetic attenuation. Therefore, combining magnetic materials with manganese dioxide into a hybrid composite has been proposed to improve their impedance matching performance.

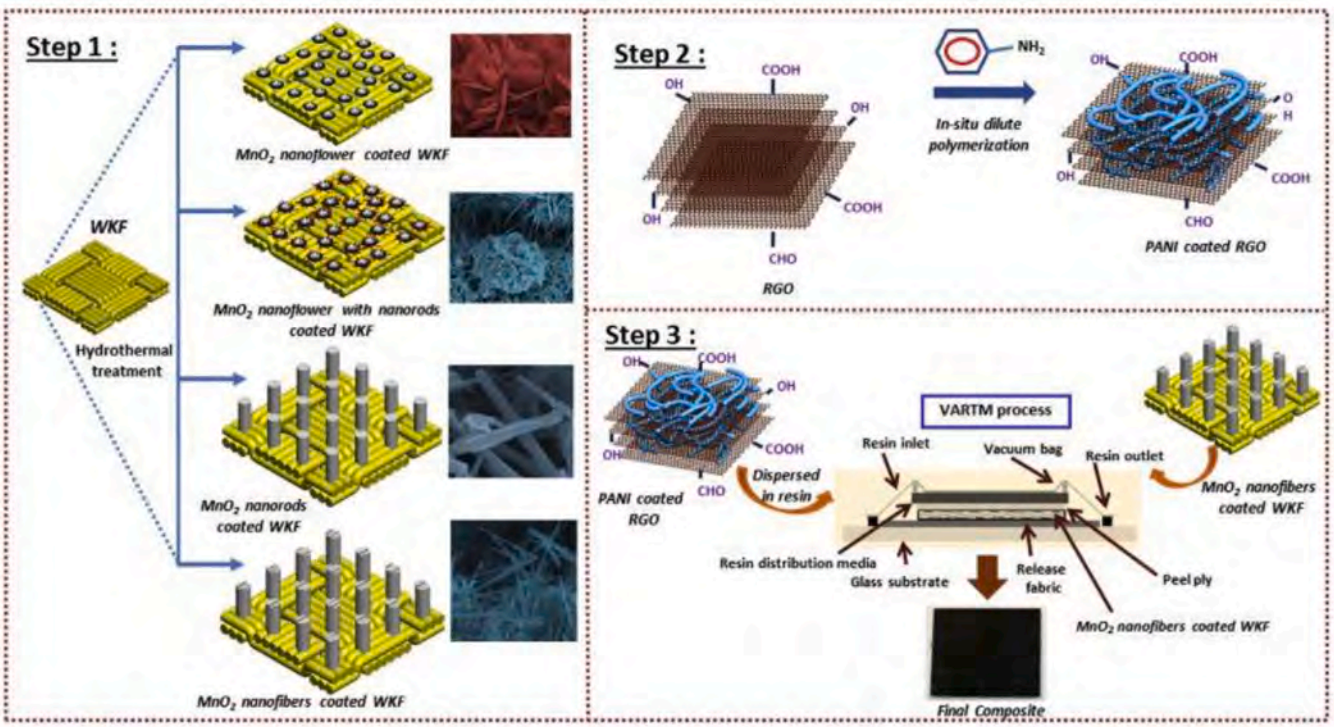

Fig. 3. Schematic diagram of the varied morphological growth of MnO_2 nanostructures on the surface of woven Kevlar fiber (WKF) and the formation of WKF/MnO_2 nanofibers/polyester (PES)/polyaniline nanofiber-reduced graphene oxide (PANI-RGO) [71].

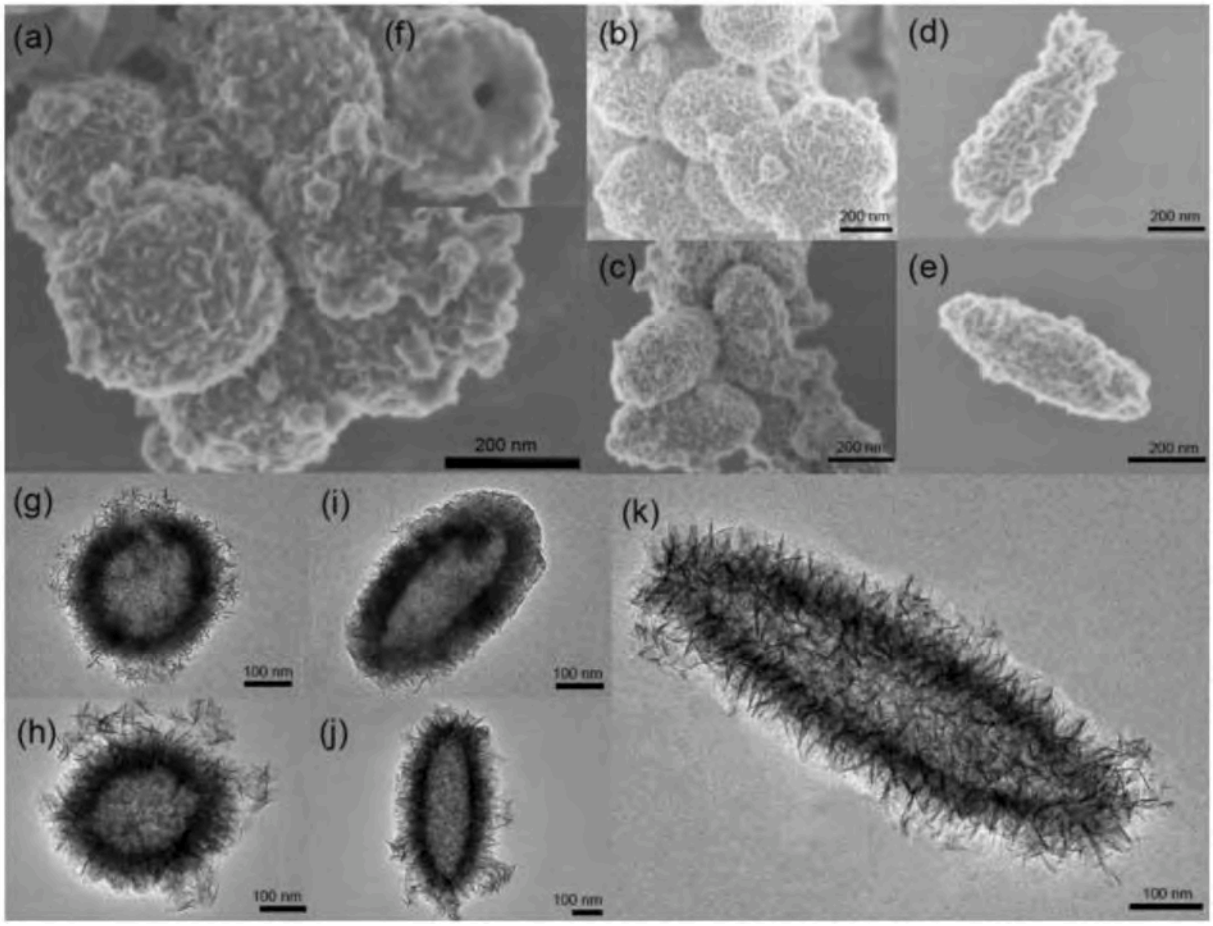

Fig. 4. FE-SEM images of microparticles with different aspect ratios: (a) HCM-1, (b) HCM-2, (c) HCM-3, (d) HCM-4, and (e) HCM-5. (f) Broken particle image of HCM-1. TEM images of microparticles with different aspect ratios: (g) HCM-1, (h) HCM-2, (i) HCM-3, (j) HCM-4, and (k) HCM-5 [73].

For examples, the carbonyl iron/MnO_2 composite with different mixture ratios is prepared by a mechanically milling method. As the weight fraction of MnO_2 increased to 30%, the maximum reflection loss of the composites reaches −39.1 dB, at 4.4 GHz with a matching thickness of 3.5 mm. The enhanced microwave absorption properties of the composites could be attributed to the good electromagnetic match and the coexistence of dielectric loss and magnetic loss. A rod-like shaped MnO_2/Fe binary composite is designed by loading magnetic Fe nanoparticles on MnO_2 rods [74]. The rod-like MnO_2/Fe material can form the conductive loss network, benefiting to dielectric loss ability and EM transfer properties. By controlling the mass ratio of Fe, the EM transfer properties are tunable.

Core-shell Fe_3O_4@MnO_2 composite microspheres with three different surface architectures, namely mushroom-, honeycomb- and corolla-like morphologies, have been synthesized through a facile two-step method. Both mushroom-like and corolla-like Fe_3O_4@MnO_2 composite microspheres have very broad absorbing bandwidth in the frequency range of 2–18 GHz, and the corolla-like composites exhibit the strongest absorbing capability with the maximum reflection loss value of −48.5 dB (11.2 GHz) [75]. Electromagnetic energy absorption mainly derives from matching impedance, conductive loss, multiple scattering and absorption in the cavities, and interfacial polarizations between Fe_3O_4 cores and MnO_2 shells in the composites.

3.1.3. *MnO_2/magnetic-dielectric materials composites*

Benefitting from the excellent properties of two or more magnetic-dielectric coupling materials, their hybrid composites have displayed outstandingly performed. Simultaneously integrating carbonaceous material and magnetic material into MnO_2 is a promising method to achieve excellent electromagnetic performance.

Hierarchical structures of graphene@Fe_3O_4 nanocluster@carbon@MnO_2 nanosheet arrays are prepared by a multi-step route by combining the in situ hydrothermal reaction thermal, subsequent treatment process and finally in situ redox replacement reaction [76]. The resultant hierarchical graphene@Fe_3O_4 nanocluster@carbon@MnO_2 nanosheet array composites exhibit significantly enhanced microwave absorption properties compared with graphene@Fe_3O_4 nanoclusters, which originates from the unique hierarchical structure and larger surface area. The watermelon-like Fe_3O_4@C@MnO_2 hybrid is synthesized via a typical two-step solvothermal method [77]. The excellent performance of this hybrid can mainly be attributed to its ideal matching of magnetic loss and dielectric loss, large specific surface area, interfacial polarizations and some other causes. A novel kind of Ni-based foam that modified by MnO_2 nanosheets (denote as Ni@MnO_2 NS foam) are synthesized by a facile hydrothermal reaction [78]. The excellent electromagnetic wave attenuation could be responsible for magnetic loss natural resonance of Ni frameworks and dielectric loss of interface polarization and dipole polarization.

Meanwhile, core-shell structure and other structures are constructed to boost microwave absorption. Cubic hollow Co/N/C@MnO_2 structure is synthesized via a self-templated and eco-friendly route in Fig. 5, where polydopamine (PDA) acts as carbon source and hierarchical MnO_2 nanosheets are incorporated for improving impedance mismatch by introducing hierarchical MnO_2 sheets and modulating filler loading for regulating the excessive permittivity in Co/N/C [79,80].

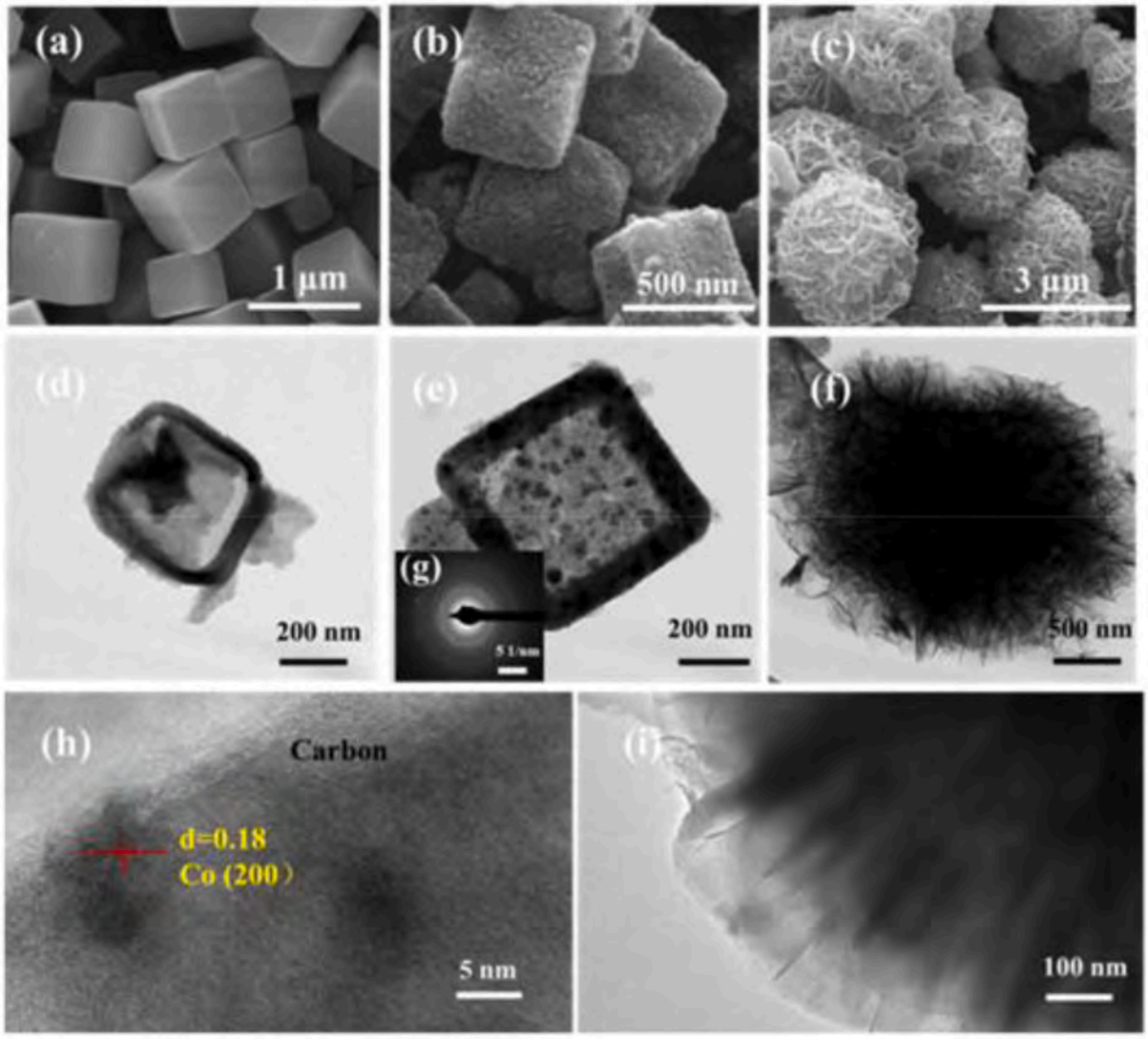

Fig. 5. FESEM images of (a) ZIF-67 nanocubes, (b) Co/N/C nanoboxes, (c) hierarchical Co/N/C@MnO_2. TEM images of (d) ZIF-67@PDA yolk-shelled structure, (e) Co/N/C nanoboxes and (f) hierarchical Co/N/C@MnO_2. (g) the corresponding SAED pattern. (h) high-resolution TEM images of Co/N/C and MnO_2 sheets, respectively [79].

Co/N/C@MnO_2 composites display maximum reflection loss of −58.9 dB and a broad bandwidth of 5.5 GHz. The excellent microwave absorption properties are attributed to synergetic effects of excellent impedance match, and dramatic electromagnetic wave attenuation ability arising from multiple helpful constituents, abundant interfaces, and extraordinary hollow structure. A hierarchical hollow core-shell $ZnxFe_{3-x}O_4$@porous MnO_2 spheres for loading on graphene nanosheets are synthesized by multistep solvothermal reaction progresses [81]. The ternary composites show excellent electromagnetic wave absorption performance in both reflection loss and bandwidth. The maximum reflection loss of −50.6 dB occurs at 8.96 GHz and effective bandwidth below −10 dB could shift from 3.6 to 18.0 GHz with a thickness of 1.5–5.5 mm. The excellent electromagnetic wave absorption properties of rGO/hollow$ZnxFe_{3-x}O_4$@porous MnO_2 composites are attributed to strong impedance matching, high attenuation, good λ/4 cancellation foundation, eddy effect, natural resonance, multi-interfacial polarization, and multiple reflections/scatterings. A three-layered CoFe@C@MnO_2 hierarchical nanocube is designed by consisting of CoFe nanoparticles embedded within porous carbon and the growth of MnO_2 nanoparticles on the nanocubes. The magnetic losses of the CoFe alloy nanoparticles, dielectric loss of carbon and MnO_2, interfacial polarization between the CoFe alloy, carbon shell, and MnO_2 nanoparticles are contributed to good matching condition and superb electromagnetic wave performance. Due to these structural and compositional features, the as-synthesized CoFe@C@MnO_2 nanocubes achieves maximum reflection loss of −64 dB at 15.6 GHz with a thickness of 1.3 mm and effective absorption bandwidth achieves 9.2 GHz with a thickness of 1.6 mm [82]. The enhanced microwave absorption property derives from the synergistic effects of the magnetic loss and the intrinsic dielectric losses, which facilitates multiple interface polarization and appropriate impedance matching. The flower-like MnO_2/RGO nanocomposites are prepared by a facile hydrothermal method. The introduction of RGO nanosheets in MnO_2 improves the electrical conductivity, contributing to the microwave propagation on the material surface. And the special framework and synergistic effects between flower-like MnO_2 and RGO nanosheets endows remarkable microwave absorption performance in 8–12 GHz. The maximum reflection loss achieves −37.1 dB at 10.8 GHz when the matching thickness of 2.0 mm [83]. Conductive network formed by RGO, multiple dipole polarization and defects polarization relaxation on the surface of RGO nanosheets, as well as interfaces polarization between flower-like MnO_2 and RGO improve the impedance matching, and enhanced electromagnetic wave

scattering and absorption. The yolk-shell Fe_3O_4@carbon@MnO_2 microspheres are synthesized via a series of processes including coating, carbonization and etching in Fig. 6. The MnO_2 shell plays significance role in restricting the electrical polarization between the carbon shells and meanwhile improving the impedance matching condition of the composites. The yolk shell Fe_3O_4@carbon@MnO_2 composite samples exhibit that the maximum reflection loss value is −58.25 dB at 5.56 GHz with the thickness of 4.2 mm [84]. The excellent electromagnetic wave absorption performance is contributed by the hollow yolk-shell structure, and the effective complementary between Fe_3O_4 core and the carbon@MnO_2 double-layer shells, which results in multiple reflection, strong polarization loss and conduction loss.

3.1.4. Summary and prospects

Integrating two or more kinds of materials with MnO_2 is a useful strategy to achieve outstanding absorption performance, which has been devoted to tuning the electromagnetic parameters and adjusting the impedance matching characteristics. The network composed of many nanoparticles could increase the specific surface area of the material and improve the conductive loss. The multiphase heterostructures could modulate the electromagnetic wave response, including dipole polarization, interfacial polarization, and magnetic resonance. These varieties of electromagnetic wave absorption factors endow these nanocomposites with good electromagnetic wave absorption abilities. It is believed that these challenges will be solved continuously with the joint efforts of scientists around the world. In the future, MnO_2-based nanocomposites will still be the most competitive candidates for microwave absorbers.

3.2. Ferrite absorbent

In terms of chemical composition, ferrite is a composite metal oxide composed of iron group ions, oxygen ions and other metal ions. Classified by crystal structure, ferrite materials can be divided into three types: spinel, garnet and pyrrhotite ferrite. Among the choices for MAM, ferrite materials have been widely applied due to its high crystal magnetic anisotropy, permeability, and magnetic resonance frequency. Their microwave absorption mainly contributes to magnetic loss mechanism including self-polarization, hysteresis loss, domain wall resonance and natural resonance. Although the ferrite absorbing materials have the advantages of strong absorption loss, high abrasion resistance, thin coating and low price, but the performance of narrow absorption band, high weight and poor thermal stability still limits their application. In order to improve the comprehensive properties of ferrite absorbing materials, researches are focusing on the following two direction. On the one hand, other materials are introduced to form composite materials which shows increased dielectric loss and optimized impedance matching. On the other hand, the elements doping and microstructure designing are used to increase the attenuation of EM waves and improve its absorbing performance.

3.2.1. Pure ferrite

Spinel ferrite crystal has high symmetry, small magnetic anisotropy and good soft magnetic properties, which can be used as EM waves absorbing materials. For example, $NiFe_2O_4$ has a minimum reflection loss of - 16 dB at X-band [85]. $BaFe_2O_4$ has a minimum reflection loss of -30.67 dB at 11.14 GHz [86]. However, due to its low permittivity and permeability and poor impedance matching, its application frequency is

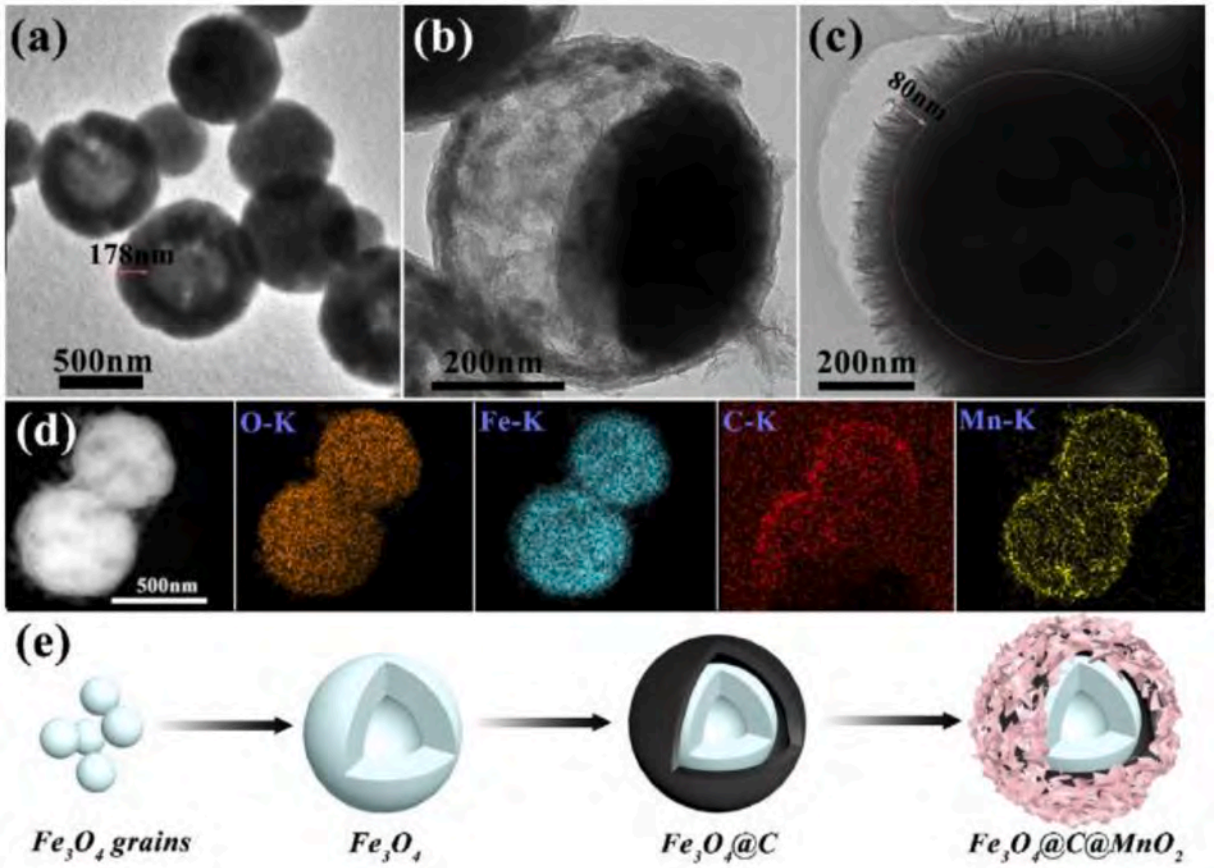

Fig. 6. (a) The TEM images of hollow Fe_3O_4 microspheres; (b) the TEM images of yolk-shell Fe_3O_4@carbon microspheres, (c) the SEM images of yolk-shell Fe_3O_4@carbon@MnO_2microspheres, (d) HADDF-STEM image and element mapping of yolk-shell Fe_3O_4@carbon@MnO_2 microspheres. (e) Schematic illustration of the synthesis process of yolk-shell Fe_3O_4@carbon@MnO_2 microspheres [84].

limited. The research of spinel ferrite is mainly to improve its absorbing effect by nano and composite. At present, M-type ferrite ($BaFe_{12}O_{19}$) and W-type ferrite ($BaFe_{16}O_{27}$) are most widely used as microwave absorbant research directions [87,88]. Compared with pure ferrite, doping and substituting can change the magnetic anisotropy and enlarge the absorption bandwidth. For example, $BaFe_{12}O_{19}$ prepared by coprecipitation method has weak electromagnetic wave absorption performance, while the doped $BaZn_{0.5}Co_{0.5}ZrFe_{10}O_{19}$ has obvious improvement in electromagnetic wave absorption performance, with a reflection loss of −14dB [89].

3.2.2. Ferrite composites

To overcome the disadvantages of high density, poor thermal stability, and low impedance matching of pure ferrite materials, the research on ferrite composite materials is particularly attractive in improving the comprehensive characteristics to satisfy the multiple requirements in the microwave absorption application [90,91].

1. Ferrite/metal composites

The microwave absorbing properties of ferrite can be improved by atom doping and replacement in the microstructure. Metal-ion replacement in ferrite can improve the electromagnetic loss, further improve the attenuation and microwave absorption performance of the material. The magnetocrystalline anisotropy in hexagonal ferrite is caused by the obvious axial component of ion at 2B site. When Ni^{2+} is added, it will occupy the B site preferentially, which increases the aggregation of the main chain of ferrite colloid, leading to the loss of mesoporous network structure. The resistivity of the sample is high and decreases with the increase of temperature. With the increase of Ni^{2+}, the ferromagnetic region increases, the paramagnetic region decreases, and the saturation magnetization of ferrite increases. In addition, the addition of Zn^{2+}, Zr^{4+}, Cd^{2+} and Sr^{2+} ions also improved the magnetic properties of the materials. For example, with the increase of Ru^{2+}, the absorption performance of $SrFe_{12-x}Ru_xO_{19}$ increases gradually. When x = 1.5, the minimum reflection loss is −33.3 dB [92]. However, when non-magnetic Mg^{2+} is added to the ferrite lattice, it occupies the B site firstly, which reduces the magnetization of the B site and the exchange effect. It is not conducive to the improvement of the absorption performance.

Adding metal powder into ferrites is another effective way to fabricate the composite materials with a superior microwave absorbing performance. Due to the existence of metal powder, the dielectric loss of the material is increased, and the disadvantage of low absorption efficiency of ferrite in low frequency band is made up. Thus the frequency range of the absorbing material is widened. Spinel ferrite grows on the surface of metal powder and forms the interface of metal ferrite. The interface polarization effect increases with the increase of material surface. The absorption property of ferrite is improved. For example, combine carbonyl iron flakes and $ZnFe_2O_4$. YC-100 sample at 1.5 mm has a RL_{min} value of −47.0 dB [43].

2. Ferrite/carbon composites

Due to their good conductivity and low density, adding carbon into ferrite composites can increase the dielectric loss, reduce the weight, improve the impedance matching, and finally broaden the absorption bandwidth [93].

The combination of ferrite and graphene increases the dielectric loss of ferrite and further improves the comprehensive microwave absorption performance [94]. The reduced graphene oxide/-$Ni_{0.4}Zn_{0.4}Co_{0.2}Fe_2O_3$ (rGO/NZCF) nanocomposites are prepared by uniformly dispersing the nano-NZCF particles on the rGO nano sheet. The eddy current caused by electromagnetic field produces additional magnetic field, which can eliminate the external magnetic field. Compared with the pure NZCF and rGO, the rGO/NZCF nanocomposite has more excellent electromagnetic performance [95]. $Co_{0.33}Ni_{0.33}Mn_{0.33}Fe_2O_4$ is prepared by introducing a large number of polar groups –COOH and –OH on the surface of graphene. The residual defects and groups in graphene can cause polarization relaxation and electronic dipole relaxation, which can further improve the absorption of EM waves [96]. The addition of carbon material can also prevent the agglomeration of ferrite nanoparticles, and effectively improve the dielectric loss of the composite. In addition, the special physical structure can also improve the absorbing properties of the composite. The porous microspheres are assembled on the surface of the multilayer graphene to form $Bi_2Fe_4O_9$/rGO composite. When the thickness of the coating is 2 mm, the absorption loss value at 13.8 GHz is −71.88 dB. It is much better than that of ferrite/graphene composite [97]. The fancy structure formed by coating $CoFe_2O_4$ nanoparticles in graphene sheet effectively reduces the aggregation of graphene and enhances the interface polarization between $CoFe_2O_4$ particles and graphene. The impedance matching of the material is further improved [98]. The 3D network structure also increase the electromagnetic loss by increasing multiple reflection and scattering of EM waves.

3. Ferrite/conductive polymer composites

In the microwave band, the small adjustable range of dielectric constant of ferrite leads to small dielectric loss, which limits the improvement of absorption performance and the broadening of absorption band. Conducting polymer has high conductivity and dielectric stability. The combination of ferrite and conducting polymer increases the dielectric loss, improves the impedance matching and microwave absorption performance. In addition, the double-layer composite structure has stronger interface effect. Polyaniline (PANI)/Ba ferrite (BF) bilayer chiral composite is prepared by using L-camphorsulfonic acid as chiral inducer. PANI improves the impedance matching between BF and air. The maximum absorption loss of the composite is −30.5 dB at 33.25 GHz, the effective absorption bandwidth is 12.8 GHz, covering the whole Kα band [99,100]. For $Ni_{0.5}Zn_{0.5}Fe_2O_4$(NiZn ferrite)/polyaniline (PANI) nanocomposites, the interaction between polyaniline chain and ferrite particles improves the thermal stability of the composite. Compared with single-layer composite, double-layer composite has better impedance matching performance and interface effect.

3.2.3. Atom doping and morphology controlling

The rare earth ions doped in ferrite will replace the smaller-radius metal ions to increase the lattice constant which leads to the increase of lattice distortion and dielectric loss. At the same time, the doping of rare earth ions will also increase the magnetocrystalline anisotropy field and coercive force of ferrite crystal, thus increasing the hysteresis loss. La^{3+} doping can improve the microwave absorption performance of ferrite [101]. La^{3+} ions partially replace Fe^{3+} ions, resulting in the conversion of Fe^{3+} ions into Fe^{2+} ions. The saturation magnetization decreased and dielectric constant increased. With the increase of La^{3+}, the overall magnetic interaction and magnetic loss of the sample decrease, the dielectric polarization and dielectric loss increase. The difference between ε" and μ" decreases, and the impedance matching and absorption properties are improved.

The microwave absorbing property of ferrite also depends on its microstructure. The common ferrites are needle like, rod-shaped, flaky, and fibrous. In recent years, ferrite nanofibers have been successfully prepared. In the $Ni_{0.4}Co_{0.2}Zn_{0.4}Fe_2O_4/BaTiO_3$ composite fiber prepared by electrospinning, the distribution of NCZFO and BTO particles along the fiber axis reduces the magnetic coupling between NCZFO particles. It promotes the resonance absorption of magnetic particles [102]. In addition, the coercivity of $BaFe_{12}O_{19}$ hollow fiber prepared by electrospinning is far less than that of the common fiber, which shows strong coercivity, soft magnetic property and high saturation magnetization.

For the composite structure, the core-shell structure can effectively improve the EM waves absorption capacity. The core-shell structure

provides more paths for the refraction and reflection of EM waves and increases the attenuation of EM waves [103], as shown in Fig. 7. In the core-shell Fe_3O_4@C composite, the presence of Fe_3O_4 microspheres improves the graphitization degree of carbon shell. The coating of Fe_3O_4 microspheres on carbon shell improves the composite dielectric constant and impedance matching [104]. For the core-shell of nano--$Mg_{0.96}Tb_{0.04}Fe_2O_4$@polypyrrole, terbium ions successfully enter the ferrite nano lattice, and change its electromagnetic parameters, enhancing the coupling effect between $Mg_{0.96}Tb_{0.04}Fe_2O_4$. The saturation magnetization and coercive force of the composite increase with the increase of $Mg_{0.96}Tb_{0.04}Fe_2O_4$ content, which improves the absorbing property of the composite [105]. In addition, the thickness of the shell also has a certain influence on the absorbing properties of the composite.

3.2.4. Summary and prospect

The microwave absorbing properties of ferrite are improved by the preparation of ferrite composite and the morphology control. Firstly, when the interface of composite materials is increased, which leads to the increase of interface polarization effect, as well as the dielectric loss. Secondly, a higher dielectric constant is obtained in the composite materials to make up for the low dielectric loss of ferrite. Thirdly, in the core-shell structure, there are multiple reflections and scattering of EM waves, which increases the consumption of EM waves. Fourthly, increasing the impedance matching of ferrite is beneficial to the EM waves entering into the material. Fifth, reducing the density of materials can meet the lightweight requirements in application. Besides, in order to develop a ferrite absorbing material with wide absorption band, strong absorption capacity, good environmental and temperature stability, innovative research must be carried out to meet the increasing requirements.

4. Conductive polymers absorbant

Conducting polymers (CPs) present high sensibility to modificaitons, controllability in micromorphologies, especially the flexibility in dielectric and electrical properties. Due to the enormous advantages compared with metals and semiconductors, many typical conducting polymers including polyaniline (PANI), polypyrrole (PPy), and polythiophene (PTh) are widely used as effective dielectric loss-type absorbing components. Therefore, extensive applications have been obtained in the fields of microwave absorption and electromagnetic interference (EMI) shielding. However, according to free electron theory, high permittivity resulting from high conductivity and huge gap between permittivity and permeability of conventional pristine CPs always lead to poor impedance matching and absorbing performance. Therefore, researches on CPs absorber most focus on the impedance matching improvement which can be realized by decreasing conductivity and permittivity, or increasing permeability through properly design on microstructure and composition.

4.1. Structure regulation

Among the numerous CPs, PANI and PPy are the most welcomed for their versatile morphologies with significant differences and resulting various conductivities and dielectric performances affected by plenty of parameters, especially for PANI, such as types of doped acid (macromolecular or protonic acid), chemical oxidation processes (rapid mixing, interfacial or electrochemical polymerization), different types of oxidants and temperatures. Therefore, "there are as many different types of polyaniline(s) as there are people who make it", stated by Alan MacDiarmid [106].

Due to the high conductivity and resulting impedance mismatch, conventional PANI nanorods [107] only exhibit a minimum reflection loss (RL) of −9.85 dB at 7.33 GHz, and do not have effective absorption bandwidth (EAB, RL value < -10 dB). Small irregular self-assembly porous PANI microspheres [108] show better impedance match level, whose minimum RL and EAB values reach −26.5 dB and 4.1 GHz, respectively. By constructing nanoring-shaped morphology [109], this PANI NRs porous structure contributes to enhanced reflection and refraction of incident EM wave, then continuously consumed their energy, ensuring excellent microwave absorption property with minimum RL reaching −39.10 dB at a thickness of 2.00 mm and EAB reaching 4.75 GHz (11.80–16.55 GHz).

The optimum conditions of conventional PPy are investigated [110],

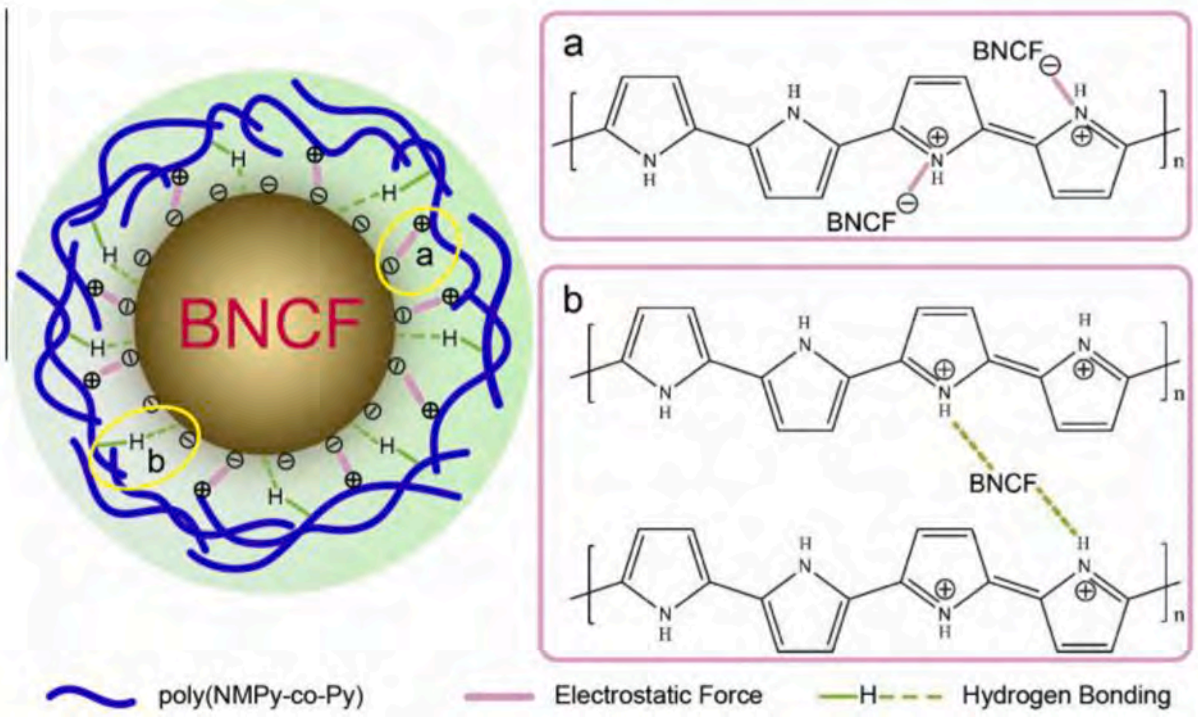

Fig. 7. The structure schematic of poly (NMPy-CO-Py)/BNCF composite and the possible interaction [103].

taking account of reaction time, reaction temperature, types of doping agents and the molar ratio of initiator (APS) to pyrrole (Py) monomer on the electrical and dielectric properties. The PPy sample with 2 mm thickness has a minimum RL value of −19.68 dB at approximately 16 GHz and an EAB of 6.2 GHz in the range of 8–18 GHz. While the helical nanostrutures [111] exhibit striking microwave absorbing performance, attributed to their high aspect ratios and especially increased circular polarizations, even under low filler loadings and excellent EMI shielding efficiency (SE) at relatively high filler loadings, indicating their tunable EM protecting abilities. The EAB of L-MDGA templated helical PPy nanofibers (LHF-PPy) can reach 7.04 GHz (10.6–17.64 GHz) only under a filler loading ratio of 7 wt%. Both L-MGA templated helical PPy nanotubes (LHT-PPy) and LHF-PPy are effective MAMs for both X (8–12 GHz) and Ku (12–18 GHz) bands. For EMI shielding, the SE higher than 10 dB covers a frequency range from 2 to 18 GHz only at a thickness of 1 mm.

According to the Faraday's law of electromagnetic induction [112], when EM waves irradiate on helical structures, an inductive current can be induced in this helical structure. Meanwhile, circular polarization also takes place and polarizes to form right-handed and/or left-handed circular polarized waves. While, the speed of circular polarized waves is not equal to that of the incident EM waves, resulting in significant increased attenuation compared to nonchiral materials. In addition, circular polarization greatly increases the polarization relaxation of p-electrons or defects, and further improves the attenuating ability [113]. Hence, helical structures can be a promising structure for novel MAM.

4.2. Composition strategy

4.2.1. Introducing wave-transparent or magnetic components

According to the concept of impedance matching, the characteristic impedance of the absorbent should be close to Z_0, the impedance of free apace, to realize that much more EM waves can incident into absorbents and achieve zero reflection at the interface between the free space and absorbents. Actually, an overly large gap between the complex permittivity ε_r and permeability μ_r is not expected [114]. As the relatively high dielectric performance resulted from the high conductivity and the nearly negligible magnetic loss characterization, the impedance matching level and microwave absorbing performance of pristine CPs are not promising. Hence, effective efforts to minish the large gap between ε_r and μ_r have been made by means of compositing with wave-transparent and/or magnetic components, or other components to restrain the conductive network of pristine CPs.

Numerous traditional magnetic materials, Fe, Co, Ni and relevant alloys and compounds for instance, have been widely investigated to composite with CPs for significant dielectric-magnetic synergistic effect, enhanced magnetic loss performance and better impedance matching. Highly regulated core–shell Fe_3O_4@PPy microspheres [115] with adjustable PPy shell thickness from 20 to 80 nm by regulating the relative ratio of pyrrole to Fe_3O_4 can reach as much as −31.5 dB (>99.9% absorption) reflection loss at 15.5 GHz with a matching layer thickness of 2.5 mm. Nano-stick shaped Fe_2O_3-PPy conducting ferromagnetic polymer nanocomposites [116] are simultaneously equipped with high electrical conductivity of the order of 10^{-2} S/cm and saturation magnetization (Ms) value of 35 emu/g. PPy nanocomposite having weight ratio [pyrrole]/[Fe_2O_3] = 1:3 shows microwave absorption as high as SEÃ22.5 dB (>99% attenuation) in the frequency range of 12.4–18 GHz (Ku-band). The Ms, remnant magnetization (Mr) and coercivity (Hc) of cobalt ferrite hollow microspheres with protrusions/polythiophene (CFHMP/PTh) [117] composites are 566.4 Oe, 40.8 emu/g and 17.6 emu/g, respectively. Contributed to the dielectric-magnetic synergistic effect, the dielectric property of CFHMP/PTh composites is better that of pristine CFHMP, while the magnetic property is worse. CFHMP/PTh composites exhibit strong electromagnetic dissipation ability (RL = −33.8 dB at 9.5 GHz) and the EAB is 3.1 GHz (8.2–11.3 GHz) at a thickness of 3.0 mm.

Typical wave-transparent components and other semiconductor components, such as graphene oxide (GO) and SiO_2, SnO_2 and MnO_2 are employed to restrain the conductive network of CPs, then improve the impedance matching. Sanghamitra Acharya et al. [118]reported fabrication of a novel microwave absorbing material through one port chemical reduction of graphene oxide (GO) in presence of magnetic inclusion of nano-strontium aluminium ferrite $SrAl_4Fe_8O_{19}$ (SAF) to make ternary composite films in Poly (Vinylidene) Fluoride (PVDF). The microwave shielding ability as well as absorbing nature of both as prepared films are found to be excellent, RGOSAF21PVDF is found to be more efficient shielding material as compared to other. Well-ordered core/shell/shell-like Fe_3O_4@SiO_2@PPy microspheres with prominent electromagnetic microwave absorption performance are obtained [119]. The tailored shell thickness can be tuned from 20 to 60 nm (including SiO_2 layer) via changing the molar ratio of Fe_3O_4@SiO_2 to Pyrrole. The minimum RL reaches −40.9 dB at 6 GHz with the coating thickness of 5 mm. The EAB could reach 6.88 GHz from 11.12 to 18 GHz, completely covering the whole K (12–18 GHz) band. SnO_2 nanoparticles@polypyrrole hybrid aerogels [120] display excellent electromagnetic wave absorbing performance. Only with 10 wt% of nano-SnO_2 filler loading in wax, the EAB of the hybrid aerogel can reach 7.28 GHz. Through the regulation of sample thicknesses, effective electromagnetic wave absorption at lower frequencies can also be achieved.

4.2.2. Constructing interfaces and pores for composites

Constructing interfaces and pores plays an important role among the development of MAM, because the resulting huge specific surface area can facilitate the propagation and multiple scattering and enhance the interfacial polarization of the incident EM waves, which provides more opportunities for interaction between absorbents and the EM waves. Constructing interfaces and pores not only enhances the EM wave attenuation, but also decreases the bulk density of the absorbents. Hence it has been an efficient route to meet the demands of strong absorption intensity and broad effective bandwidth coverage with thin width and light weight of MAM.

1. 0-D core-shell structure

Investigations on the mechanism of microwave absorption indicate that interfacial polarization at the interface between core and shell contributes to the dielectric loss significantly, which is of benefit to create well matched characteristic impedance in core-shell composites, then produce strong RL. Highly uniform core-shell PPy@PANI composites [121] as shown in Fig. 8, whose PANI shells can be well controlled from 30 to 120 nm by changing the weight ratio of aniline and PPy microspheres, display excellent microwave absorbing performance, especially for PPy@PANI-0.8 and PPy@PANI-1.2, whose

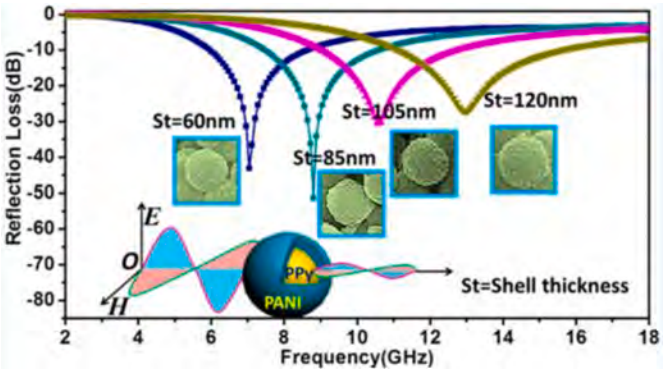

Fig. 8. Calculated RL of core-shell PPy@PANI with adjustable PANI shell thickness (St) from 60 nm to 120 nm in the frequency range of 2–18 GHz [121].

minimum RL values can reach −43.1 dB at 7.1 GHz and −51.3 dB at 8.8 GHz with thicknesses of 4.0 and 3.0 mm. The core/shell/shell-structured Ni/SiO_2/PANI hexagonal nanoflakes possessing in-plane [111] easy magnetization and out-of-plane interfacial polarization are synthesized by a three-step liquid chemical method [122] . As a result, the H–V-oriented composite achieves the best electromagnetic impedance matching and absorption with a broad absorbing bandwidth of 4 GHz, a wide thickness range of 7–10 mm, and a minimal RL of −41.5 dB in the Ku (12–18 GHz) band.

2. 1-D nanotube or nanofiber structure

PANI nanorods with tunable chirality [123] are grew on helical carbon nanotubes (HCNTs), a typical nanoscale chiral structure. The experimental results show that the hierarchical hybrids (PANI@HCNTs) exhibit distinctly dual chirality and a significant enhancement in EM losses compared to those of either pure PANI or HCNTs. The minimum RL of the as-prepared hybrids can reach −32.5 dB at 8.9 GHz. Further analysis demonstrates that combinations of chiral acid-doped PANI and coiled HCNTs with molecular and nanoscale chirality lead to synergistic effects resulting from the dual chirality.

Massive multiple interfaces existing in polydimethylsiloxane/multi-walled carbon nanotubes (PDMS/MWCNT) nanocomposites constructed by the incorporation of cotton fibers (CTF) make EM waves efficiently attenuated by the wave reflection at the multiple interfaces and then absorbed at the interfaces of PDMS/CTF and CTF/MWCNT. The EMI shielding effectiveness values of the PDMS/MWCNT nanocomposites with 2.0 and 3.0 vol% MWCNT increase from ~16 to ~30 dB, ~20 to ~41 dB by adding 15 vol% CTF, respectively [124].

3. 2-D vertical arrays on sheet

PANI/GN hybrid [125] prepared by in situ intercalation polymerization shows a minimum RL and EAB reaching −36.9 dB and 5.3 GHz (8.2–13.5 GHz) at the thickness of 3.5 mm. However, the ribbon-like PANI nanofibers and large-scaled GN layers can be clearly recognized under TEM and SEM. Improved Debye relaxation process [126] is found in the sandwich-like PANI-GN-PANI structure compared to pristine PANI and GN, and increases the RL and EAB to 45.1 dB and ~8 GHz with a thickness of 2.5 mm. J. Liu et al.

4. 3-D porous structure

Conductive thermoplastic composites containing both MWCNTs and PANI doped with para-toluene sulfonic acid (PTSA) are formulated using two different methods [127]. In the first method, PANI-PTSA-coated MWCNTs are synthesized and processed into an insulating matrix. The second method involves mechanical mixing of separate synthetic PANI-PTSA and non-coated MWCNT solids into an insulating matrix. Microwave absorption measurements at X-band frequencies (8–12 GHz) indicate that the former composites are poor absorbers, while the latter are good absorbers and showed stronger absorption than composites containing only PANI-PTSA or MWCNTs. 3D polypyrrole/poly (3, 4-ethylenedioxythiophene) (3D-PPy/PEDOT) composite is prepared via a self-assembly method [128]. The composite consisting only 5 wt% 3D-PPy/PEDOT in a wax matrix exhibites an EAB of 6.24 GHz at a thickness of 2.5 mm, and highest EABof 6.28 GHz can be reached. Dielectric carbon nanotubes@polyaniline (CNTs@PANi) hybrid microwave absorbeents [129] are synthesized via an interfacial modulation strategy and the CNT nanocore structure is optimized. The heterogeneous interfaces from PANI and CNTs can be well regulated by longitudinal unzipping the multi walls of CNTs to form 1D CNT-and 3D CNT-bridged graphene nanoribbons and 2D graphene nanoribbons. By controlling the oxidation peeling degree of CNTs, their interface area and defects are enriched, thus producing more polarization centers to generate interfacial polarization and polarization relaxation, and also introducing more PANI loadings.

4.3. As precursors for nitrogen-containing carbon materials

Carbon materials, such as carbon black, carbon fiber, carbon nanotube, graphene, etc. have been widely studied as MAM, and details are demonstrated in Chapter 4. Recently, heterogeneous atom-doped carbon materials are expected to be promising candidate as microwave absorbents, especially the N atoms, which can donate electrons to the carbon conjugated system and lead to enhanced dielectric loss contributed to its larger electronegativity. N-containing conjugated CPs, like polyacrylonitrile (PAN), PANI and PPy are widely used precursors by means of high temperature carbonization. It is demonstrated that morphology diversity can be inherited to N-doped carbon materials, because carbonization process does not destroy the complicated morphologies of the polymer precursors [130]. Hence, equipped with enhanced dielectric loss capacity, morphology (interfaces and pores) diversity and reduced conductivity, N-doped carbon materials obtained from N-containing CPs precursors have a great potential for development of MAM.

Thanks to the emergence of the special heterostructure and associated significant interfacial polarizations, carbonized hydrochars/ZnO nanocrystals (CH/ZnO) composites [131] are endowed with the optimized RL achieving −49.24 dB with the thickness of merely 1.24 mm, and EAB ranging from 13.2 GHz to 16.6 GHz.

Accordingly, the existence of the surface amorphous carbonized layer can effectively improve the impendence match and alter both the interfacial and dielectric loss. Barium haxe-ferrite nanoparticles coated with amorphous carbon layers, carbonized from PANI ranging from 10 to 30 nm thickness [132], display a minimum RL reaching −35 dB at 15.5 GHz and EAB reaching ~2.0 GHz (ranging from 14.4 GHz to 16.4 GHz) thickness of 5.5 mm. Unique hierarchical configuration of core-shell FeCo@C nanoparticles encapsulated in polydopamine (PDA)-derived carbon nanocages [133] show strongest RL located at −67.8 dB at 15.8 GHz, and the EAB covering 11.0–16.3 GHz with the thickness of 2.00 mm.

4.4. Summary and prospects

In summary, composition strategy for dielectric-magnetic synergistic effect and better impedance matching, as well as structure design by constructing interfaces and pores to enhance interfacial polarization and multiple scattering, are the two dominating routes to broaden the application of conducting polymer-based MAM. Superior environmental stability, morphology and physicochemical property diversities and really low synthesis cost will endow CPs and relevant composites a strong vitality as MAM and also other applications. In addition, the theoretical calculation of CPs-based composites MAM is to be explored.

5. Carbon absorbent

Carbon materials, including carbon black, carbon fiber, carbon nanotubes, graphene, etc., are one of the most widely used MAM due to their high electrical conductivity, low density. The conductive loss attributing to its high electrical conductivity is the main microwave absorbing mechanism for carbon materials. However, no magnetic loss leads to a poor impedance matching which results in a high reflection and low absorption of EM wave. The fabrication of carbon-based composites is an effective way to improve the impedance matching and microwave absorbing performance. The current researches on carbon-based composites are mainly focusing on the following two designs: adding dielectric material (manganese oxide, zinc oxide and silicon carbide) into carbon to decrease the electrical conductivity and microwave reflection, and adding magnetic materials (alloys and oxides of Fe, Co, Ni, and etc.) to increase the permeability and introduce magnetic loss mechanism. Carbon based composites can satisfy the multiple requirements of light weight, thin thickness, wide frequency bands and

enhanced properties of MAM in changeable circumstance.

5.1. Traditional carbon absorbent

5.1.1. Carbon black

Carbon black (CB) is a kind of amorphous carbon. It has good EM wave absorption characteristics in the high frequency range, and also has stable and lasting conductivity, good dispersion, low density and low price [134]. The high conductivity of CB results in a strong reflection of EM waves when CB is used alone. According to the absorption mechanism, the impedance matching can be improved by uniting carbon black absorbent with the permeable material. For instance, a double-layer absorbing material is designed using the quartz glass fiber reinforced polyimide (SiO_2f/PI) composite as a matching layer and CB as an absorption layer [135], thus achieved better absorption.

In addition, carbon black can enhance dielectric loss performance by compounding with dielectric loss materials, resulting in improved impedance matching. It is found that the epoxy resin (EP) matrix composited with tetrapod-like ZnO whiskers (T-ZnO) and carbon black as absorbent has porous structure and adjusted complex permittivity as shown in Fig. 9. The dispersion distribution of ZnO whiskers in the epoxy resin matrix leads to interface electronic polarization, while the whisker needle leg has a stronger electronic polarization, which can greatly increase the effective absorption of EM waves [136]. The carbon black/reduced graphene oxide (CB/RGO) composites with enhanced absorbing properties are synthesized via freeze-drying and reduction processes [137]. The significant enhancement is mainly due to the unique local conductive network structure formed by introduced graphene sheets. The loss mechanism of the enhanced dielectric properties covers the local conductive networks, electron hopping, interfacial polarization and relaxation loss. Besides, CB is often introduced to magnetic material to obtain both magnetic and dielectric loss mechanism, such as the coating of CB-based carbonyl-iron powder (CIP) or ferrite absorbent.

5.1.2. Carbon fiber

Carbon fiber (CF) is a multi-functional material with high strength, high modulus, low density, small coefficient of thermal expansion, corrosion resistance and excellent electrical properties [138]. Because of these advantages, CFs are being widely used as reinforcement phase in the ceramics, metallic and polymeric matrices. CF is a kind of conductive loss material, which is easy to form a large continuous conduction current under the action of electromagnetic field, and resulting a strong reflection of radar waves. Generally, CF is scarcely used as a wave absorbing material alone. The surface modification and structural design of carbon fiber are carried out to meet the requirements of new wave absorbing materials.

Compared to the common solid CFs, hollow carbon fibers (HCFs), porous carbon fibers (PCFs), hollow porous carbon fibers (HPCFs) and carbon nanofibers (CNFs) possessed the superior properties because of the large surface area, low density and multiform framework. Their microscopic morphology is shown in the Fig. 10. Research has shown that introducing a hollow or porous structure are both beneficial to the strong absorption [139]. Hollow structures could accelerate the increasing rate of the real part of complex permittivity while lowering that of the imaginary part, while porous structures enhance multiple reflections and scattering. As a kind of nanomaterials, CNFs have surface effect and quantum size effect. The size of CNFs-based composite materials is controlled in the nanoscale is beneficial to improving absorbing property and lowering matching thickness.

In a general way, magnetic loss absorbent such as magnetic metal and metal oxides, carbonyl iron, etc., are combined with carbon fiber to prepare low density and strong absorption composite materials. By chemical doping or surface modification on the surface of carbon fiber, a layer of magnetic powder is deposited to improve its magnetic permeability, so as to obtain excellent absorbing performance. For example, abundant interfaces brought by Fe_3O_4 coated on the surface of the carbon fiber and the synergistic effect between dielectric/magnetic components contribute to the enhancement of impedance matching and dominate the mechanisms of attenuation ability. In order to further improve the absorbing property of carbon fiber composites, on the basis of magnetic surface modification, the dielectric material such as manganese dioxide and reduced graphene oxide is used to enhance the dielectric property to attenuate EM waves. Moreover, the dielectric material can be also decorated on the carbon fiber surface, such as silicon carbide.

5.2. Nano-carbon absorbent

Currently, there are mainly three categories of nanostructures for carbon materials: carbon nanotubes (CNTs), graphene, and other special carbon nanostructures. Compared with traditional carbon materials such as CB and CF, carbon nanomaterials have larger specific surface area, smaller size effect, higher ratio of surface atoms and more surface hanging bonds due to their size advantages at the nanoscale. Hence, carbon nanomaterials have attracted much attention from researchers in recent years. However, carbon nanomaterials such as graphene and carbon nanotubes have the same poor impedance matching as

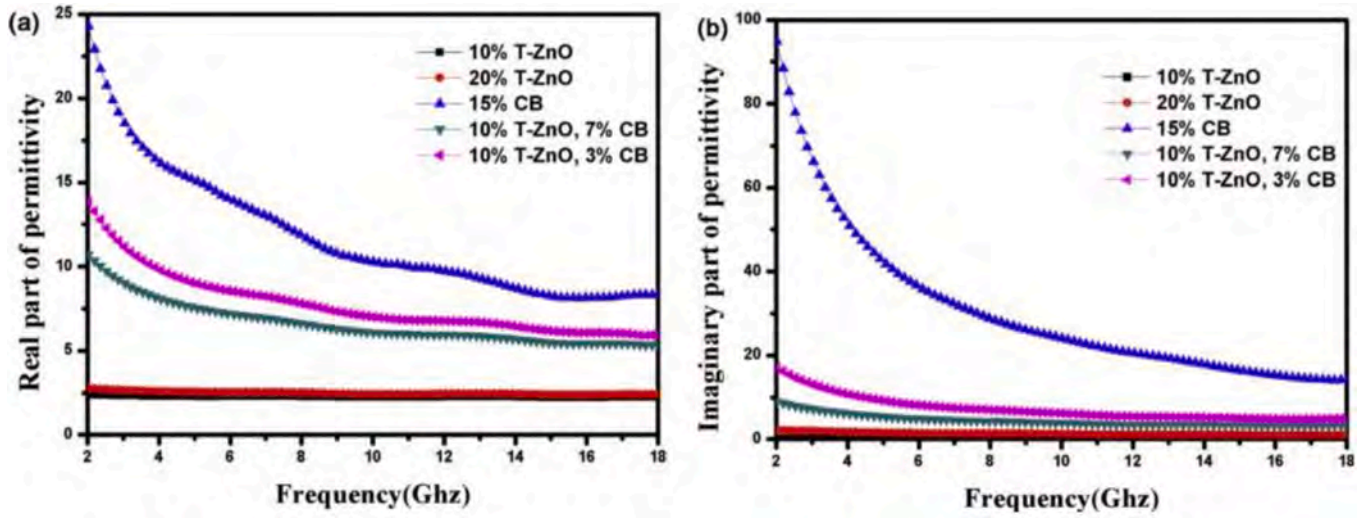

Fig. 9. The frequency dependence of complex permittivity of pure T-ZnO, pure CB and CB/T-ZnO/EP composites [136].

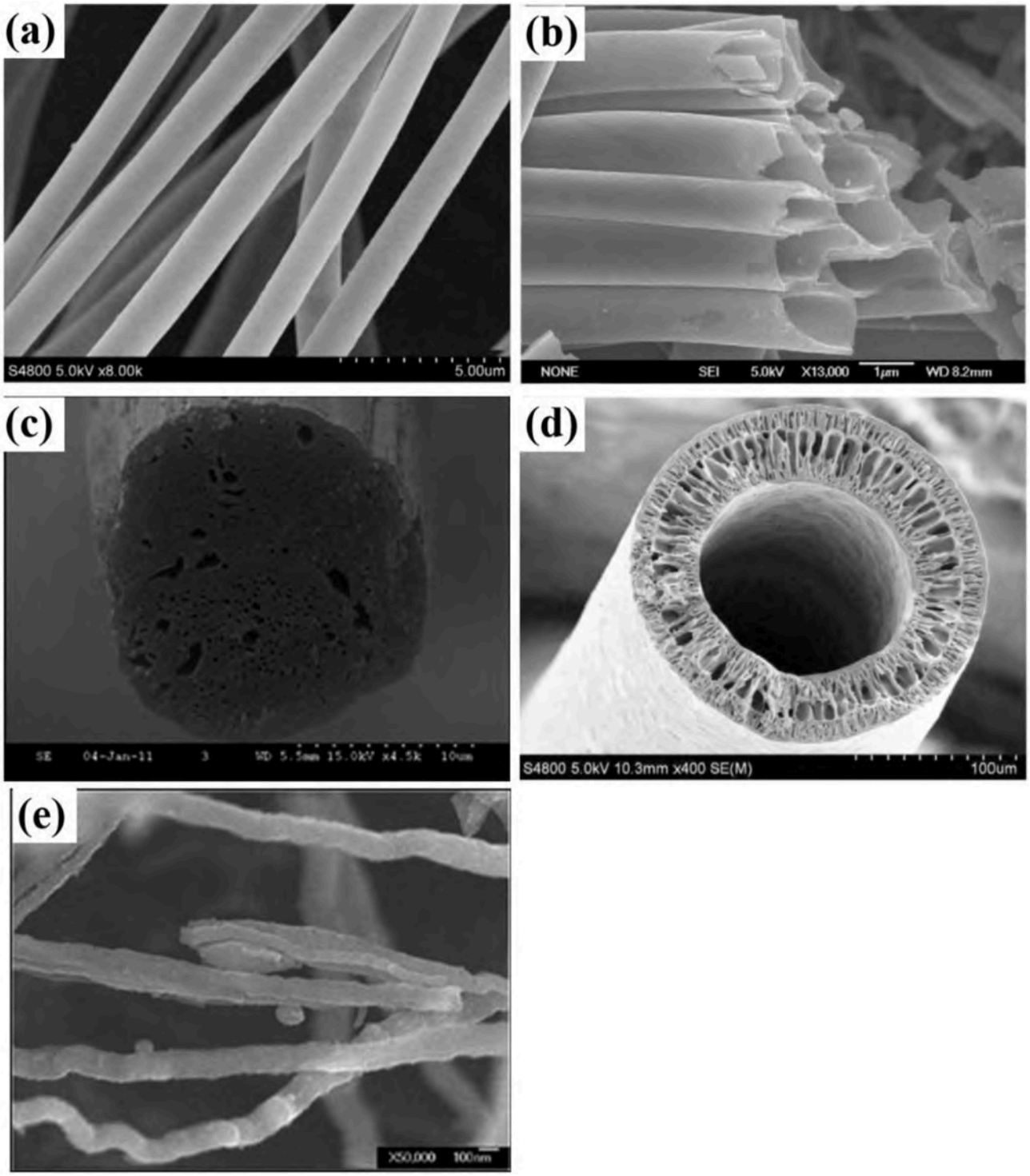

Fig. 10. SEM images of (a) common CFs, (b)HCFs, (c)PCF, (d)HPCF and (e)CNFs [139].

traditional carbon materials. Besides, they are more prone to agglomeration. Therefore, carbon nanomaterials are generally used after composite with magnetic loss materials or dielectric loss materials, which can not only improve impedance matching to enhance microwave absorption, but also effectively solve the confusion of agglomeration.

5.2.1. Graphene composites

Graphene, like other carbon materials, faces the problem of poor impedance matching and easy agglomeration, which can be improved by compounding with other materials [140,141]. In situ synthesis by simple hydrothermal reaction is a common method for the synthesis of rGO-based composites. Some oxygen-containing functional groups, such as carboxyl and hydroxyl groups, and some specials structural defects will generate on the surfaces of rGO. They can provide reaction sites for the precipitation process. The ions are fixed to the rGO surface by electrostatic interactions with the functional groups. And then the desired crystal in situ crystallize. Aunique structure of rGO/starlike-ZnO is constructed with the minimum RL reaching −77.5 dB and the maximum effective bandwidth reaching 6.9 GHz. The starlike ZnO hinders the aggregation of rGO, and the ZnO nanocrystals on rGO sheets

effectively improve the interface of the heterostructure and the impedance matching of rGO [142]. Similar methods are also used to prepare $NiFe_2O_4$-rGO, MoS_2/rGO and other complexes. In brief, hydrothermal synthesis is a mature method to prepare carbon nanocomposites.

The composite components in graphene-based composites have varieties of morphologies. This can also affect the microwave absorption performance of composites to a certain extent. For example, the cubic crystal $ZnSnO_3$ particles in the $ZnSnO_3$/rGO hybrid material (Fig. 11) can be regarded as a scaffold to support the layered graphene to increase the surface area [143]. A larger surface area can cause multiple reflections and provide more active points for energy to escape, and microwave energy can be converted into other forms of energy over a longer propagation period. Then, floral Co_3O_4 is implanted on the surface of rGO [88]. Flower-shaped Co_3O_4 with a capacitor structure can induce multiple interfaces and dipole polarization due to its large number of interfaces and pores. In particular, the pore structure of Co_3O_4 petals produces a large number of defects and functional groups, resulting in a great dipole polarization. Furthermore, the core-shell structure of carbonyl iron/SiO_2 decorated reduced graphene oxide (CI/SiO_2/RGO) is fabricated [144]. The core-shell structure of CI/SiO_2 can generate additional interfacial polarization, space charge polarization and multiple scattering, which are also conducive to EM wave absorption. The wave transparent medium SiO_2 as the shell improved the impedance matching and attenuation capacity of the absorber. By growing CuS nanosheets on magnetically modified graphene, a hybrid nanocomposite with microwave absorption enhancement is still designed [145]. When the electromagnetic wave penetrates CuS nanoflakes, it can be subjected to multiple reflections and diffusions caused by the relatively large surface area and high pore volume of the internal pore space.

Doping of rGO with heteroatoms has been regarded as an effective approach to tailor the electrical properties of rGO. It is expected that doping elements into graphene may produce more defects, which is beneficial for microwave absorption. Especially, nitrogen doping in the crystal lattice of rGO could not only enhance the defects or dipole polarization and conduction loss capacity, but also optimize the impedance matching condition. Enhanced microwave absorption performance had been achieved in CoNi/nitrogen-doped graphene hybrids, nitrogen-doped reduced graphene oxide/nickel-zinc ferrite (NRGO/$Ni_{0.5}Zn_{0.5}Fe_2O_4$) composite, Fe_3O_4 nanocrystals anchored on nitrogen-doped graphene nanosheets, γ-Fe_2O_3 nanoring/porous nitrogen-doped graphene (γ-Fe_2O_3 NR/PNG) composites and so on.

5.2.2. CNT composites

1. CNT

The arrangement of carbon nanotubes will affect their microwave absorbing properties. By changing the angle of intersection of carbon nanotube films when stacking, a remarkable reflection loss of −47.66 dB is achieved by stacking four aligned CNT sheets with an intersectional angle of 90° between two neighboring ones. The propagation of electromagnetic wave can be affected by adjusting the angle between adjacent CNT film layers, thus affecting the absorption performance. Carbon nanotubes can composite with dielectric materials like TiO_2, ZnO, manganese oxide to improve impedance matching [146]. These dielectric oxide particles decorating on the surface of the carbon nanotubes lead to the formation of polarizations and capacitor-like structures at the interfaces between MWCNTs and the dielectric material. The capacitor-like structure at the interfaces could attenuate the power of

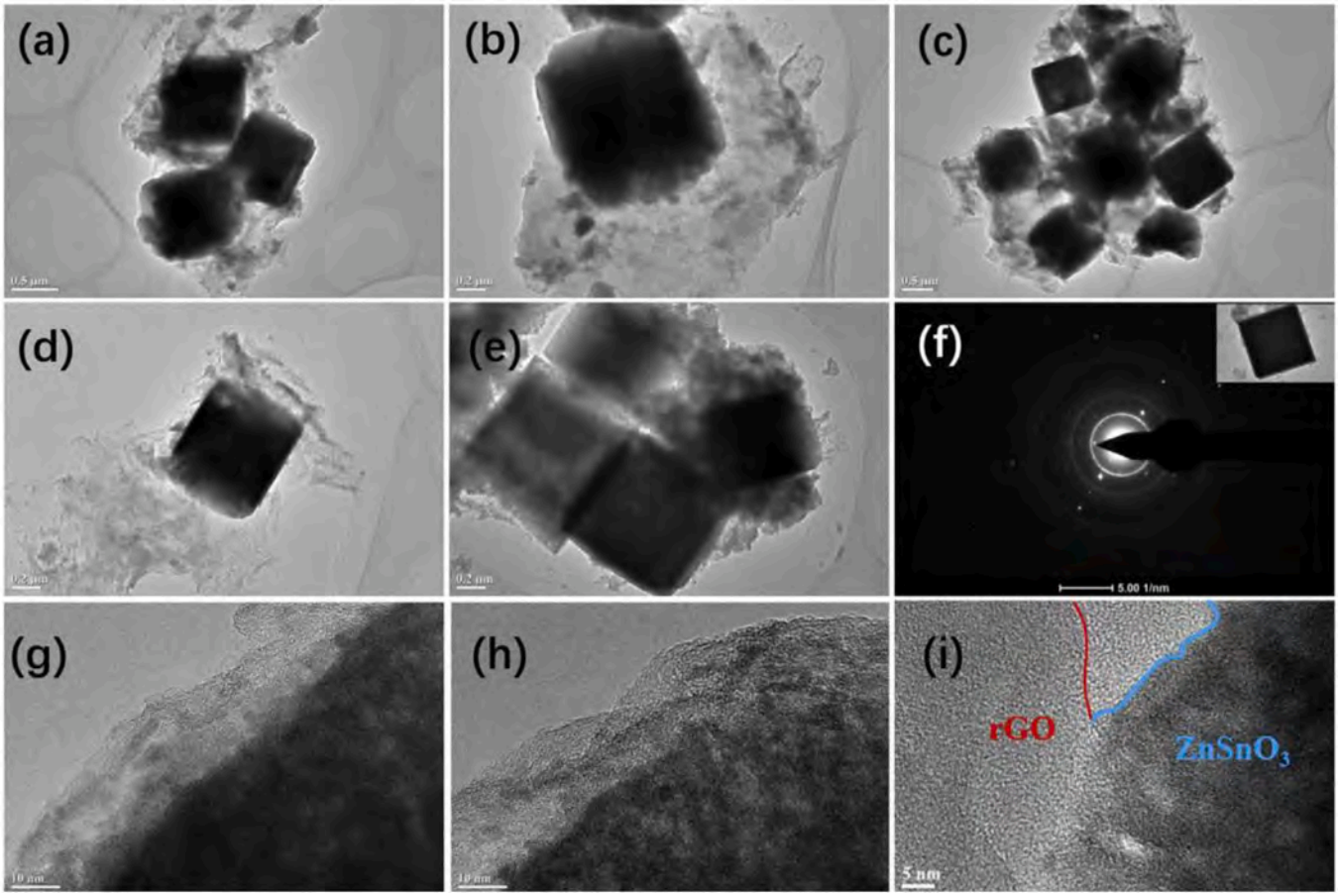

Fig. 11. The TEM images of the $ZnSnO_3$/rGO [143].

incident microwaves by aligning the polar bonds or charges in the alternating electromagnetic field. A simple, room-temperature water bath method came forward to prepare crystalline manganese oxide and CNT-MnO_x nanocomposites at atmospheric pressure [147]. Altering the pH of the reaction solution allows better control over the phases of the composite product, which can be either CNT–MnO_2 or CNT–Mn_3O4 [148,149].

Except for composite dielectric materials [150], the other way is to increase magnetic loss through composite CNT with magnetic materials including Fe, Co, Ni metals, alloys, and their oxides, etc. The addition of magnetic loss materials made up for the low permeability of CNTs, and realized the dual attenuation of EM waves with conductivity loss and magnetic loss. For instance, Fe_3O_4 nanoparticles coated on the CNT surfaces result in high incidence probability, multiple reflection and absorption of microwaves, and effective complementarities between the dielectric loss and the magnetic loss. Carbon nanotubes are easy to form conductive networks in composites due to their large aspect ratio. Such a conductive network is hard to convert the electromagnetic energy into thermal energy, owing to the ultralow resistivity which always results in strong inverse radiation, as shown in Fig. 12. In order to reduce inverse radiation, tunable graphitized amorphous carbon layer block the directly contact between MWCNTs and Fe layers [151]. This amorphous carbon layer played a key role on suppressing inverse radiation, eddy current and simultaneous boosting efficiently conductivity loss ability.

5.3. Microstructure regulation

5.3.1. Core-shell nanostructure

Many scientists have shown their interests in constructing core-shell structures to improve the chemical homogeneity and enhance the functionality of carbon-based composites. The multiple reflections between the core and the shell can improve the dielectric loss of the composite material, thus significantly improve the wave absorption of the composite materials. For example, a novel Fe_3O_4@C@MnO_2 hybrid is successfully synthesized with core-shell structure [152]. The introduction of MnO_2 nanosheet is beneficial to increase dielectric loss. Besides, the space formed by MnO_2 nanosheet can effectively enhance the reflection loss by interface reflection. Due to the polar interface between MnO_2 and carbon, other ways such as interface relaxation, interfacial polarizations and eddy current loss can also enhance the hybrid's reflection loss.

Owing to high specific area and special porosity structure, metal-organic frameworks (MOFs) using magnetic metals (Fe, Co, Ni or bimetallic) as metal center can be directly pyrolyzed to design metal/C nanocomposites with porous carbon and magnetic constituents for high-efficient EMW absorbers due to the synergy effect between magnetic loss and dielectric loss [153]. Multi-interfacial Ni@C@ZnO composites [154] with optimized yolk-shell structure are synthesized by involving the initial bimetal Ni–Zn MOF precursor and a subsequent pyrolysis under Ar_2 atmosphere. It creates unique "Schottky contact barrier" in the MOF-derived hierarchical magnetic-dielectric system. It can be shown in the Fig. 13, reduced metallic nickel nanocrystals/clusters catalyze the formation of graphitized carbon matrix, which provides electron transportation path and increases the conductivity loss. Meanwhile, the core-shell Ni@C micro-unit assembly into a magnetic 3D hierarchical microsphere, inside which the thin dielectric loss ZnO flakes are embedded. The Schottky barrier at the Ni@C–ZnO boundaries intensify the local electric field and thus improve the interfacial polarization.

5.3.2. Other special nanostructure

There are some other carbon materials with special microstructures that are also conductive to the microwave absorption such as porous carbon, carbon nanofiber, nanorod, nanosheet, nanowires, etc [155–159]. Porous carbon (PC) materials demonstrate great potential in EM wave absorption due to their ultralow density, large surface area, and excellent dielectric loss ability. 2D hierarchically laminated Fe_3O_4@nanoporous carbon (NPC)@rGO magnetic/dielectric nanocomposites is developed [160]. It is found that the high-density magnetic stray field located around the laminated nanocomposites, which

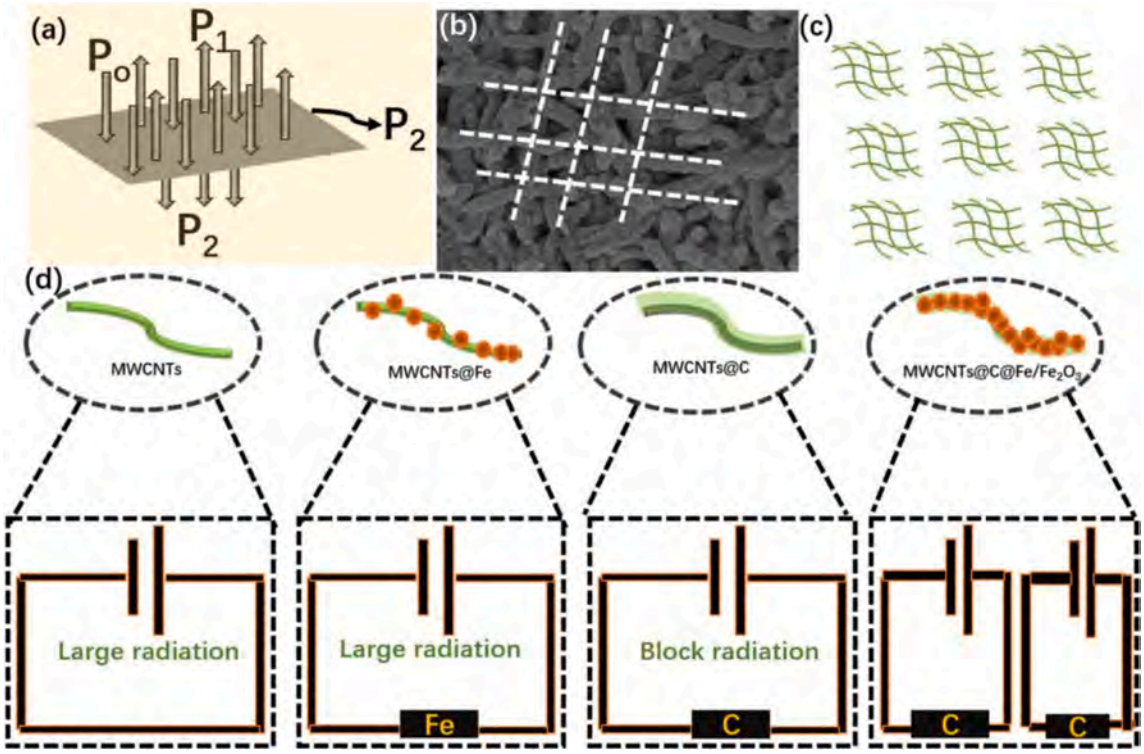

Fig. 12. Schematic illustration of (a) electromagnetic wave propagation route and (b) conductive network in MWCNTs-related composites; (c–d) micro-current loss mechanism for MWCNTs-related composites [151] .

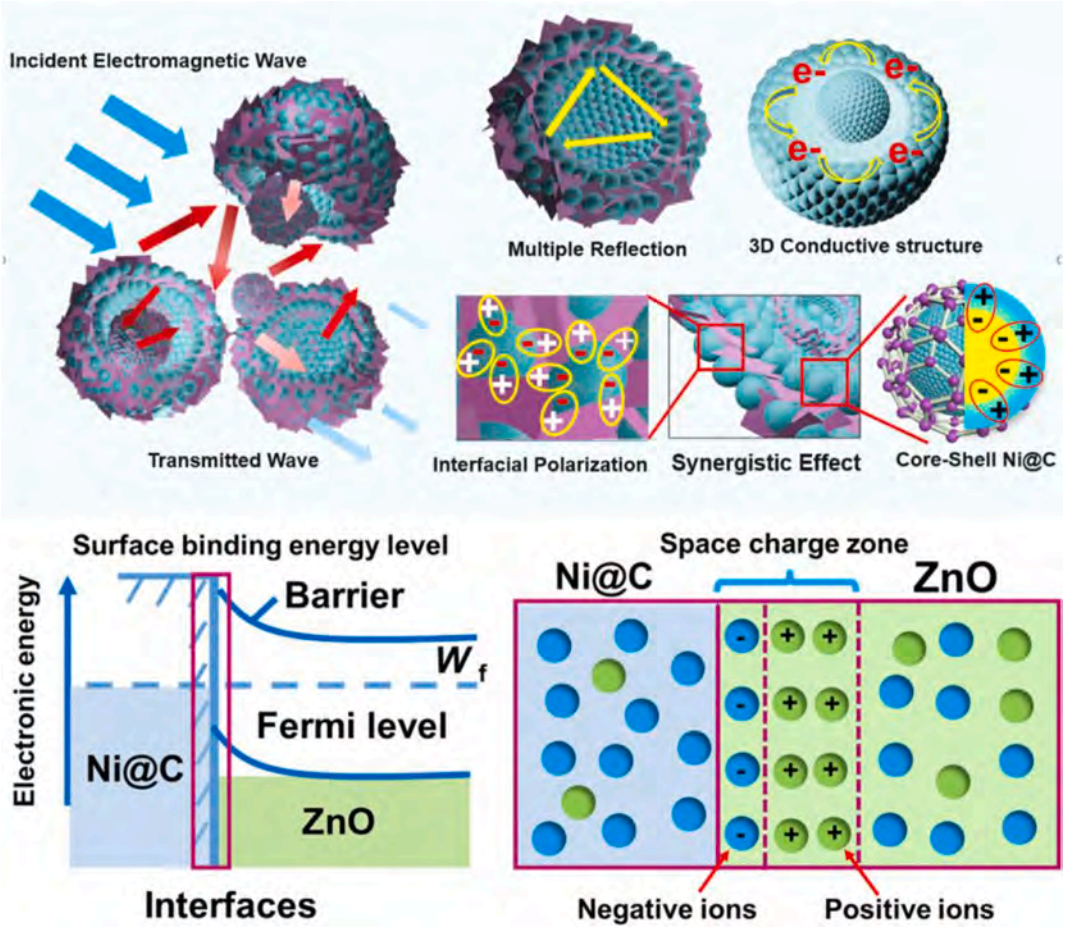

Fig. 13. The microwave absorption mechanism of yolk-shell Ni@C@ZnO absorber [154].

confirmed the micron-scale 3D magnetic coupling network in the laminated composites which is helpful to the enhancement of magnetic loss and the optimization of impedance matching. Two-dimensional Co/C nanosheets by directly carbonizing ZIF-67 nanosheets is synthesized [161]. As expected, the as-fabricated two-dimensional C/Co composites exhibited excellent performance for microwave absorption on account of increased dielectric loss by providing effective pathway for electron hopping and migration and multiple reflection. Unique peapod-like Cu/C core-shell nanowires (CSNWs) are specifically designed and prepared [162]. The outer carbon shells can improve the chemical stability of Cu core. The gap between Cu nanorods/nanoparticles is filled with air with low permittivity, which can tune impedance matching. Modulation over the composition and aspect ratio of Cu nanorods/nanoparticles encapsulated by carbon shells can control dielectric loss and conductivity.

5.4. Summary and prospects

In this section, the recent advanced developments of carbon-based composites including CB, CF, graphene, CNT, and other microstructure carbon material for microwave absorption are comprehensively introduced and summarized. The combination of carbon materials with other loss materials (conductive polymer, magnetic metal, ferrite and ceramic, etc.) can improve the impedance matching characteristics of carbon-based materials, introduce more loss mechanisms (such as magnetic loss, more kinds of polarization loss, etc.), and effectively improve the absorbing performance of materials. In addition, the morphology and structure of the absorbing material will also affect the conductive loss, magnetic loss, dielectric relaxation, interface polarization and impedance matching of the material, and then have a certain impact on the absorbing. In conclusion, carbon and its composites show excellent EM wave absorption properties. However, there are many challenges of multicomponent carbon nanostructures composites such as the balance of broadband and strong absorption, the combination of structure and function and clear EM wave absorption mechanisms for carbon nanostructures. It is believed that these challenges will be solved continuously with the joint efforts of scientists around the world. In the future, carbon nanocomposites will still be the most competitive candidates for microwave absorbers.

6. Ceramic absorbant

The electrical conductivity and dielectric properties of ceramic materials such as SiC and $BaTiO_3$ can be tuned by controlling the defects, morphology, structure, etc. Ceramic materials also show high strength, excellent high temperature resistance, outstanding chemical stability and low density. These characteristics make them as one of promising candidates used as MAMs. At present, researches of ceramic absorbant mainly focus on the microstructure controlling and composition designing. Their composites consist of carbon materials, magnetic materials or others have been widely studied.

6.1. SiC

6.1.1. Pure SiC

When pure SiC is used as absorbing agent, the influence of morphology and structure on absorption efficiency should be considered. At present, SiC nanowires, nanotubes, nanoribbon, nanohollow

spheres and other structures have been successfully synthesized. Literatures have confirmed that SiC structures with low dimension exhibits better microwave absorption performance than bulk SiC materials. Therefore, the nanowires and nanotubes with high aspect ratio attract more attention in microwave absorption field. Dielectric materials with a large length-diameter ratio present better conductive properties. With the length increasing, SiC nanowires (SNW) connect with each other to form a conductive net and present a low resistance. The conductive net consisting of SiC would have large complex permittivity and polarization loss. The SiC containing more stack fault (SF) are benefit to dielectric loss. SFs inside the SiC crystal structure can disrupt the balance of the electric charge distribution, create a large number of interfacial dipoles, oppose the EM field and induce energy dissipation. The SiC with the highest density SFs [163] shows largest permittivity. Besides, the materials owing better absorption performance need to satisfy both of the loss ability and impedance matching. Hollow SiC microspheres (HSS) (Fig. 14) with the thin shell and air cavity have better impedance matching and microwave absorption properties [164].

6.1.2. SiC composites

The absorption performance of pure SiC is undesirable in the low frequency band. Numbers of methods have been performed to improve EM wave absorption performance of SiC materials, including atom doping, defects regulation, surface modification and preparing composites [165,166]. Carbon materials and polymers with lower density, high electric conductivity is widely used to prepare SiC-based composite materials. In C-doped SiC ceramic nanocomposites [167], the amorphous carbon and graphite uniformly coat on the SiC matrix. The dielectric properties of the nanocomposites can be tailored via changing the C contents.

As known, the net-like structure is beneficial to EM wave absorption due to the excellent impedance matching and multiple reflections. The net-like C skeleton often derives from polymeric and biological materials. For example, the C skeleton originates from pyrolysis of melamine foam, then thin SiC coating is fabricated on the skeleton [168](Fig. 15). SiC/C-900 °C has high attenuation constant and multiple polarization due to the existence of defects and interfaces. Carbon materials such as carbon fibers (CFs), carbon nanotubes (CNTs), graphene shows excellent conductive attenuation on microwave. But the physical properties, such thermal stability and mechanical properties are inferior to the ceramic materials. As reported, when SiC nanowires coating on the outside surface of graphene, The yield strength and Youngs modulus increase rapidly [169]. In addition, SiC nano wires have a major contribution to the improvement of thermal stability of graphene aerogels. The hydrophobicity of graphene aerogel-SiC nanowires is also improved owing to the microscopic roughness of macropores in SiC layer. The graphene aerogel-SiC can exhibit a better absorbing property whose minimum RL value is 54.8 dB at 5.3 GHz.

Universal transition metal oxides containing MnO, NiO, Fe_3O_4, etc. are introduced into SiC-based absorption materials, due to their special magnetic properties. It is worth noting that structure, morphology, crystallization, content of transition metal oxides would make much influence on electromagnetic properties of the composite. MnO/SiC composites shows better absorption performance than SiC [170]. The better impedance matching and loss performance of MnO/SiC are the main factors to increase the microwave dissipation compared to the pure SiC. Antiferromagnetic materials such as Fe_3O_4 and NiO are also widely used for microwave absorption. The microwave absorbing performance of SiC/Fe_3O_4 hybrid nanowires [171] is adjusted by changing the weight ratios of Fe_3O_4. The huge interfaces between SiC and Fe_3O_4 particles are beneficial to the polarization loss. The coercivity and residual magnetization of all the SiC/Fe_3O_4 nanowires is zero which implied that the hybrid nanowires are superparamagnetic at room temperature. As the ratio of Fe_3O_4 increases, the magnetic saturation and permeability rises which lead to an excellent microwave absorption. According to the research, compared to the ferromagnetic materials, the influences of antiferromagnetic component on magnetic properties are very limited. The Fe, Co, Ni forming composites with SiC is worth expected. However, ferromagnetic particles always forming Si–O-metal bonding with SiC due to the existence of the silica layer between SiC and magnetic metal. This not only influence the magnetic properties but also the electrical conductivity.

6.2. $BaTiO_3$

$BaTiO_3$ is a kind of typical perovskite ferroelectric oxide. It is widely applied in harsh condition such as high-temperature and corrosive environments. Meanwhile $BaTiO_3$ is a kind of dielectric materials which makes it a strong candidate as microwave absorbing materials.

6.2.1. Atom-doped $BaTiO_3$

The microwave absorbing properties is undesirable for the pure $BaTiO_3$. Element doping is beneficial to improve the microwave attenuation. The doped ion can change the particle size and electromagnetic properties of $BaTiO_3$. The average particle size of Fe doped $BaTiO_3$ nanocrystals [172] decreases after Fe doping. The doping ions are located on particle surface and inhibite the particle growth during the nucleation process. Zhang et al. [173] synthesized a series of novel Ag doped $BaTiO_3$ ($Ba_{1-x}Ag_xTiO_3$) nanocomposites. Compared with the pure $BaTiO_3$, there are peaks of permittivity and permeability at high frequency for doped $BaTiO_3$. Rare earth element La doped $BaTiO_3$ [174] shows the reflection loss of −41.0 dB at 9.8 GHz and effective bandwidth (below −10 dB) of more than 1.7 GHz when La^{3+} content is 0.6%. Especially, the oxygen vacancies of $BaTiO_3$ also have huge influence on the dielectric properties. The accumulation of charges around oxygen vacancies slows down the motion of domain wall and increases the polarization loss.

6.2.2. $BaTiO_3$ composites

$BaTiO_3$/C composites can take both advantages of conductive loss and polarization loss. Cui et al. [175] fabricate the core-shell $BaTiO_3$@C microspheres, hollow carbon shells (HCS), and $BaTiO_3$(BTS) for

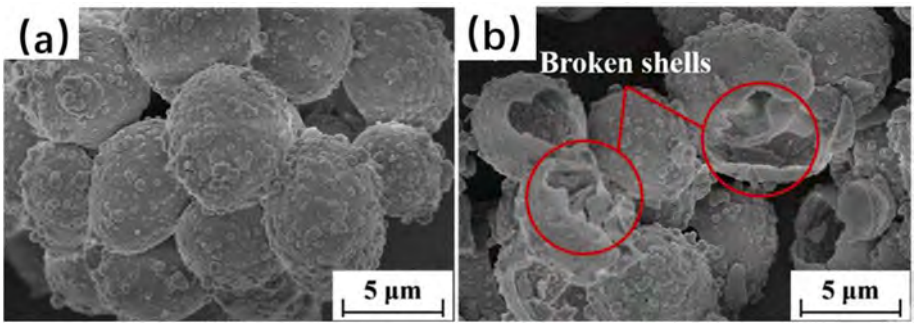

Fig. 14. SEM of Hollow SiC microspheres [164].

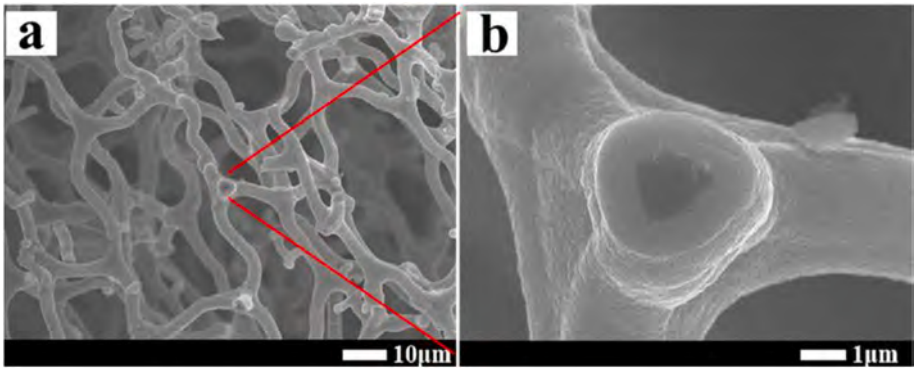

Fig. 15. Pyrolysis and CVD preparation process of SiC/C foam and SEM of SiC/C foam [168].

microwave absorption. It is found that individual BTCs or HCSs possess very low ε′ and ε″ values. The relative complex permittivity and dielectric loss capability of mixed BTCs and HCSs are much higher than those of pure BTCs and HCSs, but lower than those of $BaTiO_3$@carbon. This indicates that the interfacial polarization between BTCs and HCSs contribute to microwave absorption. The loss mechanism is shown in Fig. 16. For the $BaTiO_3$/reduced graphene oxide (RGO)composites [176], the $BaTiO_3$ nanotube has high aspect ratio. Multiple phase heterostructure materials have huge interfaces that may capture space charges due to the different conductivity which will enhance the microwave attenuation.

$BaTiO_3$ shows excellent polarization properties, but poor impedance matching because of its low magnetic properties. Their composite with ferromagnetic materials exhibits excellent electric polarization and strong magnetoelectric coupling at room temperature which potentially contribute to microwave attenuation. Composites consisting of dielectric and magnetic materials shows good impedance matching and excellent microwave absorption due to the strong polarization around the interfaces. Magnetoelectric coupling between the ferromagnetic and ferroelectric phases could also effectively enhance the ferromagnetic and dielectric polarization. The $BaTiO_3$ coated Ni nanocomposites synthesized by Shi et al. [177] present significantly enhancement on microwave absorption compared to the pristine Ni nanoparticles. The ε′ and ε'' of Ni@$BaTiO_3$ are higher than those of Ni in the frequency range of 1–18 GHz. The u' and u'' values of Ni@$BaTiO_3$ nanoparticles are slightly lower than those of Ni in low frequency but higher in high frequency. Huang et al. [178] investigates the microwave absorbing properties of Fe_3O_4–$BaTiO_3$ composites in the frequency range of 1–18 GHz. All the composites have larger ε′ and ε'' compared to those of pure $BaTiO_3$ and Fe_3O_4 materials.

6.3. MXenes

MXene is a kind of 2D ternary ceramic material with very high aspect ratios, abundant natural defects and special metallic features, whose thicknesses is corresponding to a few atomic layers. T_X denotes the functional groups on surface such as –OH, =O, and –F. Its extraordinary structure endow it special electromagnetic performance which makes it

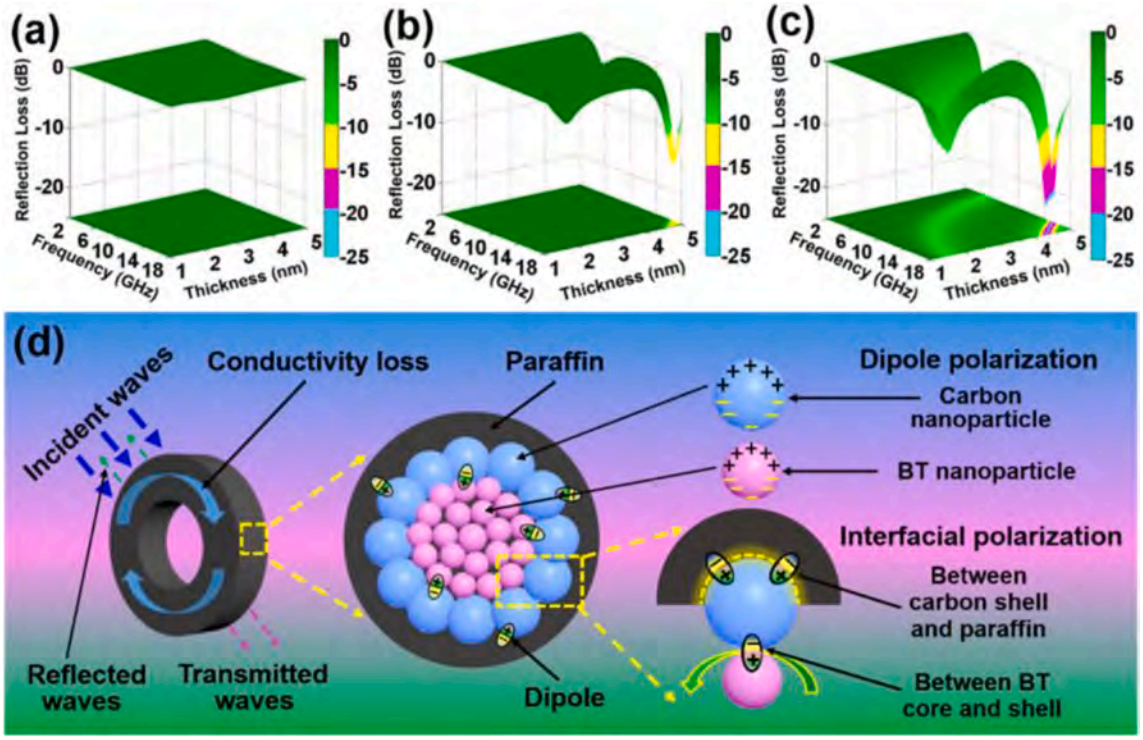

Fig. 16. Three-dimensional maps of calculated RL values of BTCs (a), HCSs (b), and BTCs/HCSs (c) with varying absorber thicknesses in the frequency range of 2.0–18.0 GHz. Schematic illustration of microwave-absorption mechanisms in BT@carbon microspheres [175].

widely applicated as microwave absorbing and shielding materials [179–182]. As one of the most important family members, $Ti_3C_2T_x$ has been extensively researched as microwave absorbant. Liang et al. [183] design a dielectric RGO/$Ti_3C_2T_x$ aerogel anchored with magnetic Ni nanochains through directional-freezing method and hydrazine vapor reduction process. The addition of MXene helps improve the attenuation constant due to its high electrical conductivity and high active groups numbers. Besides, the heterogeneous dielectric/magnetic interfaces and oriented cell structure both contribute to the absorption performance by improving the impedance matching, electric-magnetic coupling effects and multiple polarizations. In particular, the 2D MXenes-based composite is much lighter than metal materials. Yin et al. [184] use $Ti_3C_2T_X$ MXenes as dielectric mediator to obtain RGO/$Ti_3C_2T_X$ hybrids foam for the first time. The composites are of hollow core-shell architectures and tunable dielectric attenuation. The prepared RGO/$Ti_3C_2T_X$ foam shows excellent microwave absorbing property which is better than other reported foam-based counterparts. The abundant charges can migrate and hop under the alternated EM field between conductive $Ti_3C_2T_X$ spheres and RGO flakes through defects and heterointerface which will form huge field-induced microcurrents and give rise to conductive attenuation. Yin et al. [185] also fabricate f-$Ti_3C_2T_X$/SiCnws hybrid foams with ultralow density. The absorption performance is enhanced with the increasing content of $Ti_3C_2T_x$ in composite, which is because of the increasing conductive loss. The combination of conductive $Ti_3C_2T_X$ and dielectric SiCnws makes the impedance better matched with free space and efficiently decreases the microwave reflection. The layered $Ti_3C_2T_X$ also contributes to the formation of hierarchically porous structure in composites which can not only results in low mass loading but also contributes to the microwave dissipation. The micro current between the nanosheets contributed by defects and interface under EM field also enhance the conductive a lot. The extraordinary 2D structure of MXenes plays a crucial role in their excellent electromagnetic property. The 2D materials, such as graphene and layered transition metal dichalcogenides (LTMD) are widely used as microwave absorbing materials attributed to their defined dimensionalities, exotic electronic properties, high specific surface areas and polymorphism. MoS_2 is a widely known LTMD material consisting of S–Mo–S triple layers which are bounded by weak van der Waals forces. Ning et al. [186] fabricate few-layered MoS_2 nanosheets by top-down exfoliating from bulk MoS_2 used as dielectric dominant microwave absorbing materials. Its microwave absorbing properties are first reported. By comparing the MoS_2 nanosheet and bulk materials, the dependency of dimension on dielectric properties and microwave absorption are further studied. Research shows that the dielectric attenuation capacity (imaginary permittivity) of MoS_2 nanosheet is twice as high as that of bulk materials. The main attenuation mechanism is dielectric polarization loss arising from Mo and S defects and the high specific surface area. Ning et al. also reports their researches on MoS_2 nanosheets encapsulated hollow carbon spheres [187] and MoS_2-linear 2H/1 T dual-phase materials [188]. The 1T/2H phases in MoS_2 sheet help to rearrange the inhomogeneous charge distribution so that to facilitate electrons behavior. The 2D MoS_2 nanosheet can endow abundant interfaces between 2H and 1 T phases to boost impedance matching and EM wave absorption. These works present facile strategies for designing transition metal sulfide absorbant used for microwave absorption in practical application.

6.4. Summary and prospects

Most ceramic materials such as SiC, $BaTiO_3$, basalt, MXenes etc, can be used as microwave absorption materials due to their excellent dielectric and conductive attenuation properties. While the pure ceramic materials can not satisfy requirement, it is necessary to fabricate ceramic based composite materials with carbon, magnetic materials (ferromagnetic or antiferromagnetic materials), and conductive polymers, etc. The conductive loss, multiple polarization, and magnetic loss mechanisms can be enhanced by fabricating composites. Besides ceramic materials show outstanding mechanical properties, high-temperature resistance and corrosion resistance, which will satisfy the requirement of harsh application condition.

7. Absorbent with high temperature resistances

The harsh working environments like high temperature and corrosion atmosphere requires MAMs have not only wide and strong absorption but also good mechanical properties and high resistance to oxidation, corrosion, and high temperature. In terms of high temperature resistance, there are still many problems to be solved. Currently, most people use ceramic materials and carbon materials to explore and optimize high temperature dielectric properties. Some progress has been made. However, improving the magnetic properties at high temperatures is also important to get a good impedance matching. The main reason limiting the application of magnetic materials at high temperatures is their low Curie temperature. Materials will lose magnetism if it exceeds the Curie temperature. Therefore, raising the Curie temperature of the magnetic material and improving the high temperature soft magnetic properties of the magnetic material are the urgent and effective to increase the absorption at high temperature. In addition, the composition controlling, material modification and structure optimization can be used to improve the impedance matching and high temperature microwave absorption performance.

7.1. Temperature-dependent dielectric materials

7.1.1. Temperature-dependent conductivity

Due to good oxidation resistance and dielectric properties at high temperature, carbon and ceramic materials are widely used for high-temperature wave absorption research [189]. Both the real and imaginary part of the dielectric constant of carbon and ceramic materials increases with temperature increasing (Fig. 17). The increase of the real part is due to the shorter relaxation time in high temperature, while the increasing imaginary part is because of the increasing conductivity.

In order to improve the high-temperature absorbing performance of the dielectric absorbing materials, many researches focus on increasing the high temperature conductivity. Carbon materials can form conductive networks, their high temperature conductivity can be increased by increasing the concentration of carbon materials. By combining multi-walled carbon nanotubes (MWCNT) with silica [190], the reflection loss of the entire X band in the range of 30–600 °C can be less than −10 dB (wave absorption rate reaches 90%). Besides carbon materials, ceramic materials also show good high temperature conductivity, and their conductive loss can be enhanced by atom doping and structure modifying. For example, Ni doped SiC has a higher conductivity loss than that of pure SiC, which is due to the electronic transition between Ni nanoparticles. Doping SiC with Fe particles can change the crystallinity [23]. The special structure consisting of SiC particles as electromagnetic (EM) absorbers and SiO_2 as transparent matrix has a high dielectric constant at high temperature. The minimum reflection loss (RL) at 500 °C is −32 dB, which can be effectively absorbed the microwave in entire X band. Through simple mixing, cold pressing and sintering, SiO_2 matrix composites reinforced by TiC nanowires are prepared. As the content of TiC increases, a conductive network is formed and the conductivity of the material increases. When the thickness is 3.0 mm at 200 °C, the minimum reflection loss RL at 9.1 GHz is −61.0 dB.

7.1.2. High-temperature oxidation resistance

The oxidation resistance will affect the dielectric properties, thereby affecting the high temperature microwave absorption performance. The oxidation behavior of bulk Ti_3SiC_2/cordierite composite ceramics are studied [191]. The result shows that the composite ceramics have excellent oxidation resistance at 800–1000 °C. When the temperature increases from 800 to 1000 °C, due to the oxidation of the Ti_3SiC_2 filler surface, the complex dielectric constant will decrease in the initial

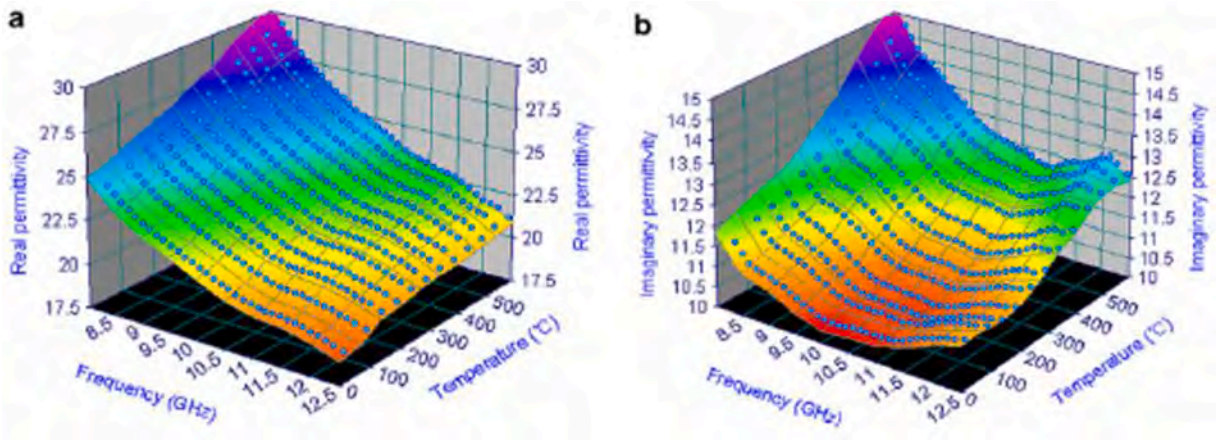

Fig. 17. (a) The real part and (b) the imaginary part of the permittivity vs. frequency and temperature [189].

oxidation stage, but it will remain stable as the oxidation time increases. $BaTiO_3$ and $MgAl_2O_4$ composite ceramics are synthesized by traditional solid-state sintering method [21]. As the temperature increases to 473–573K, the real part of the dielectric constant of the material increases significantly. As the temperature further rises to 873 K, the real part of the dielectric constant gradually decreases. Ceramic coating are prepared by atmospheric plasma spraying [192]. The sample is very stable at high temperature and can be repeatedly processed in the temperature of 300 K–1173 K without flaking. At the same time, ceramic coatings with a thickness of 1.5 mm shows considerable microwave absorption in the range of 8 GHz–18 GHz at temperature of 673–1173 K. A single-layer radar absorption structure are fabricated by combining conductive carbon black (CB) with $SiC_f/AlPO_4$ [193]. Oxidation experiments show that the material has good strength after being oxidized in air at 1273 K for 50 h, and the complex dielectric constant is not much different from that before oxidation. By simulation, the effective absorption bandwidth for the RL < -10 dB for o $SiC_f/AlPO_4$ composites can be more than 3 GHz.

7.1.3. Temperature coefficient of dielectric constant

The stability of the dielectric constant at high temperature is very important for materials that work at high temperature. In order to study the temperature stability of the dielectric constant at high temperature, dielectric constant temperature coefficient τ_ε is defined. The dielectric constant temperature coefficient τ_ε represents the relative average changing rate of the dielectric constant during unit time when the temperature rises by 1 °C. When τ_ε is close to 0, the dielectric constant of the material has good temperature stability. The τ_ε is related to the density of the material. $(Na_xLi_{1-x})_{0.5}Nd_{0.5}TiO_3$ is synthesized by solid-state reaction [137]. By adjusting x, the material density can be changed, and the dielectric constant increases from 9.65 to 10.15, and τ_ε decreases from 112 to −36.4 ppm/°C. When x is 0.6, the τ_ε of prepared composite substrate is close to zero (−0.9 ppm/°C). The three-layer structure $NiSnTa_2O_8$ ceramics are prepared using traditional solid state methods [194]. The sample has good dielectric constant temperature stability. The microwave dielectric properties of $TaNiSnTa_2O_8$ ceramics are: $\varepsilon_r = \sim 21.04$, $\tau_\varepsilon = -2.63$ ppm/°C (1425 °C). In addition, as the temperature increases, there will be crystal transformation and pyrolysis which will change the dielectric properties greatly. The microwave dielectric properties of five pyrolusite-biomass mixtures are measured by resonant cavity perturbation technology [195]. The results show that as the temperature increases, the dielectric properties of these mixtures show similar variation: increase firstly, then decrease sharply, and finally increase. That trend is mainly attributed to the crystal transformation of amorphous MnO_2 and the reduction reaction of pyrolusite caused by biomass pyrolysis.

7.2. Temperature-dependent magnetic materials

7.2.1. Magnetic properties influenced by temperature

To obtain a high M_s at high temperature, the curie temperature T_c need to be improved. For iron-based amorphous alloys, high curie temperature T_c and high temperature soft magnetic properties can be obtained by changing the element content or doping elements to change the crystallization temperature and crystallinity of materials. For $(Fe_xCo_{1-x})_{73.5}Cu_1Mo_3Si_{13.5}B_9$ amorphous and nanocrystalline alloys [196], replacing Fe with Co atoms reduces the initial crystallization temperature of the material and increases the secondary crystallization temperature, thereby increases the Curie temperature of the material. Replacing Fe with Co reduces the magnetic permeability at room temperature, but it has better soft magnetic properties at high temperature. The initial permeability at 10 KHz can be maintained at about 600 °C. The nanocrystalline FeAlSiBCuNbGe alloy shows good thermal stability and high initial permeability at high temperature [197]. Doping Ge in the alloy will reduce the activation energy, thereby reduce the amorphous forming. When Ge is added to the alloy, the average grain size increases and the thickness of the intercrystalline amorphous layer decreases. This will increase the curie temperature of the amorphous phase and significantly improve the high temperature soft magnetic properties. By changing Al content of the $(Fe_{0.5}Co_{0.5})_{73}.5Nb_3Si_{13.5}Cu_1B_{9-x}Al_x$ alloy, the curie temperature of the aluminum alloy containing amorphous phase is lower than that of the aluminum alloy free phase, but the high temperature magnetic flexibility is improved [198]. The addition of other elements can change the magnetic properties such as the coercive force H_{Cl}, saturation magnetization M_s, the curie temperature and permeability.

Compared to traditional alloys, high entropy alloys have better corrosion resistance, high temperature resistance, and oxidation resistance. Therefore, high entropy alloys are a strong candidate as high temperature absorbing materials. As the temperature increasing (Fig. 18), the saturation magnetization M_s and coercive force H_{Cl} of the high entropy alloys gradually decrease. As the temperature increases, the arrangement of magnetic domains saturation trend to be disordered which makes the decrease of magnetization M_s. The magnetocrystalline anisotropy constant K_1 decreases with increasing temperature that makes coercive force H_{Cl} gradually decreases. Both of the above factors contribute to the increase of initial permeability u_i when temperature increases [199].

7.2.2. Magnetic properties regulated by heat treatment

By annealing, ultrafine crystals forms and the crystallinity increases which will improve the high temperature soft magnetic properties. Nanocrystalline $(Fe_{0.65}Co_{0.35})_{78.4}Si_9B_9Nb_{2.6}Cu_1$ alloy [200] is annealed for 0.5 h at different temperature between 460 °C and 640 °C to obtain a

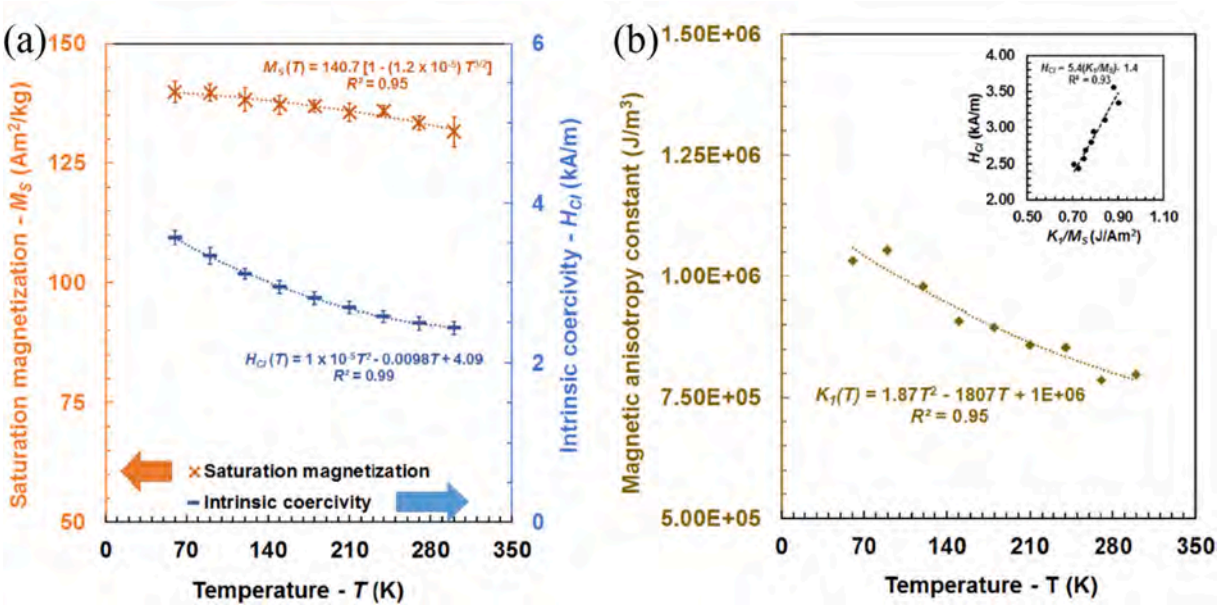

Fig. 18. (a) Variation of M_S and H_{CI} from 300 K to 60 K. (b) Variation of magnetic anisotropy constant ($K1$) from 300 K to 60 K [199].

two-phase nanocrystalline structure composed of amorphous matrix and FeCo. As the annealing temperature increasing, the volume fraction of crystals increases which results in an increase of saturation magnetization M_s. However, when the annealing temperature is 640 °C, the saturation magnetization decreases due to the formation of the boride phase [200]. The high temperature soft magnetic properties can be improved by annealing to change the crystal volume fraction and thickness of the intercrystalline amorphous layer. Fe–Si–Cr alloy has three steps phase transformation under heat treatment [44]. As the locality of the 3d electrons decreases, the ultrafine magnetic field increases after the A_2 phase is formed. This contributes to better soft magnetic performance. However, as the temperature continues to increase, the formation of the DO_3 phase will reduce the soft magnetic properties. Therefore, Fe–Si–Cr alloy with high magnetic permeability can be obtained by heat treatment at the critical temperature when DO_3 phase forms.

7.3. Summary and prospects

In summary, conductance loss is the main mechanisms of dielectric loss and the conductivity at high temperature, and it can be improved by element doping, phase modifying, and constructing conductive network. In addition, high temperature absorbing materials must have good structural stability, oxidation resistance and dielectric constant temperature stability. The studying on high temperature magnetic properties is mainly focusing on Fe based amorphous alloys and high entropy alloys. The curie temperature T_c of Fe based amorphous alloy can be increased by adding other elements to change the crystal structure and crystallinity. In addition, for iron-based amorphous alloys, annealing can be used to increase the crystal volume fraction, reduce the thickness of amorphous layer, strengthen the exchange coupling effect, and form ultrafine crystals to improve high temperature magnetic properties.

8. Theoretical calculation for microwave absorbant

8.1. First-principles calculation for metal oxides and carbon materials

First-principles calculations have become a powerful method to supplement experiments to predict and explain the atomic-scale electromagnetic phenomena. In this section, we will discuss the theoretical modeling of materials based on density functional theory (DFT). Depending on the situation, the exchange-correlation functional has been considered. Through analyzing the results of electronic structure calculation, the basic information, such as the charge distribution, density of states, Muliken population can be obtained. The absorbing properties of materials are predicted indirectly from these results of computation.

8.1.1. MnO_2

The first-principles calculations are firstly used to reveal the relationship between electronic structure and absorbing performance by Duan Yuping Group [201,202]. In the atomic structures of MnO_2, the point defect are considered as substitutional doping. The bond length of metal atoms-O become shorter and the bond strength enhanced after Fe doped. The increasing bond strength would reduce the dielectric loss. While considering the Ni doped MnO_2, the charges of Ni enter into the conduction band, which can enhance the conductivities of MnO_2 and contribute to the conduction loss. At the same time, the Ni-doped MnO_2 shows magnetic characteristic [203]. Considering the feasibility of heteroatomic doping, the results shows that under the O-rich growth condition, Mn atom is easier to be displaced by Al atom rather than Al insertion reaction [204]. In the Al-doped model, as the increasing doping concentration of Al, the conductivity of α-MnO_2 is gradually improved, because the Al ions provides more electrons for α-MnO_2, contributing to the improvement of conductivity of α-MnO_2 [205]. In short, for α-MnO_2, doping strategy shows positive effect on conductivity and can enhance the conductive loss.

The study on Co-doped β-MnO_2 showed the similar results [206]. The weak bound electrons enter into the conduction band, which contributes to the loss-free displacement polarization process, so that increase the real part of complex permittivity. The defects effects on conductivities can observe in particular plane or area, while the bulk material often shows electric insulation characteristic. The defects have limited improvement in bulk conductivities.

By analyzing the electronic polarizations of Co doped δ-MnO_2 models, both the Co defects and Mn, O vacancy are considered [28]. The defective formation energies (DE) of the defective models are calculated to value the possibility of forming the relative samples. According to the results, the DE of two Co-doped is lower than 0, which mean the process synthetic process is thermodynamic spontaneous process. While for Mn and O vacancies, the DE is positive, which means the non-spontaneous process. Considering the process of synthesizing substitutional Co and

the lowest DE of institutional Co system, the institutional sites are the prefer sites for Co ions to dope.

Different from the Fe ions effect on α-MnO_2, after Co doped into δ-MnO_2, the bond strength of Mn–O get weaker and band length gets longer, which indicate the stronger dielectric response. To calculate the electron density distribution of the system, it uncovered that the defects can influence the distribution of the electrons, the electron clouds in the conductive band can contribute to dielectric conductivity and enhanced the dielectric response properties. Depend on this situation, the vacancies have been researched deeply in other types of MnO_2. Compared the density of states (DOS), the effects of doping ion have limited influence than the vacancy situation. The reduced band gap can contribute to the conductivities and enhance the conductive loss. The pure MnO_2 β-MnO_2 perform the antiferromagnetism [207]. According to these researches, the defects in MnO_2, including heteroatoms and vacancies, both can bring the magnetic characteristic. However, in the experiments they can barely exhibit magnetic performance much less magnetic loss [208].

8.1.2. Carbon material

The ideal CNTs owns the high conductivity and no band gap. As shown in Fig. 19, the effect of vacancies on the energy gap ($E_G = E_L$-E_H) of CNTs is calculated [209], where E_L and E_H are represent lowest unoccupied molecular orbital and highest molecular orbital, respectively. As the increasing of the vacancy concentration, the band gap increases firstly and then decreases, which indicates controlling vacancy can adjust the conductivity of CNTs and then affect the conductive loss. While, the terminal function group –H and –OH increase the band gap of CNT from 0 eV to 0.813 eV and 1.018 eV respectively, which lower the conductive loss [210].

8.1.3. Other defective structures

For SiC structure, the formation of Si vacancy is more difficult than C vacancy, according to the defective formation energies. And the C vacancy system exhibit lower band gap than intrinsic SiC, which contribute to improving the conductive loss [211]. As shown in Fig. 20, the effect of Co doped in SiC mainly attributes to two aspects [212]. Firstly, doping breaks the periodic charge distribution and causes vacancies in the crystal to increase the numbers of dipoles. Secondly, the bandgap gets narrow after doped so that the number of conductive carriers arise to increase the conductive loss. In conclusion, the dielectric loss has been improved after Co doped.

Introducing Fe ions into SiC, from DOS curves, there are carriers show at Fermi level in $Fe_3Si_{105}C_{108}$, while there is obvious a band gap in SiC. These results indicate that Fe doping can increase the charge carriers and change the system to a half-metallic material. Therefore, the electric conductivity has been increased through Fe doping and further enhance the conduction loss [11]. The effect of the rare earth ions the perovskites materials are studied. The strong forces between the rare earth ions influence the polarization. Combining the results of experimental characterizations, La/Nd doped $BiFeO_3$ shows rhombohedral structure and La/Nd replaced the Bi sites [213] . The asymmetric distributions mainly occur on the Bi sites. The study of Gd-doped $BiFeO_3$ shows that the cell volume increase after doped [214]. The net charge of Gd is positive which indicate that the charge transfer from the Gd to surrounding atoms. And the band gap decreases after Gd doped, which can improve the conductivity of the system.

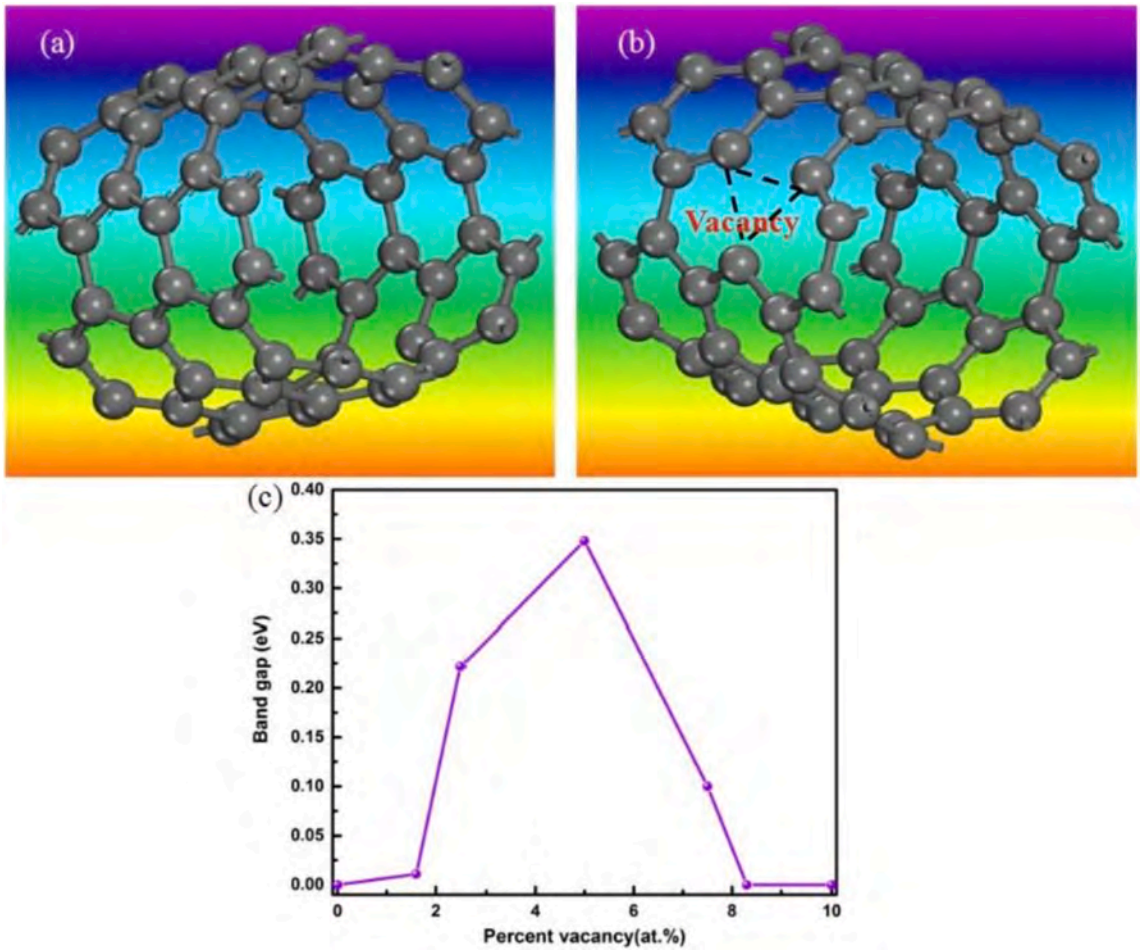

Fig. 19. (a) The ideal CNTs, (b) CNTs with vacancy defects, (c) the plots of vacancy concentrations versus band gap [209].

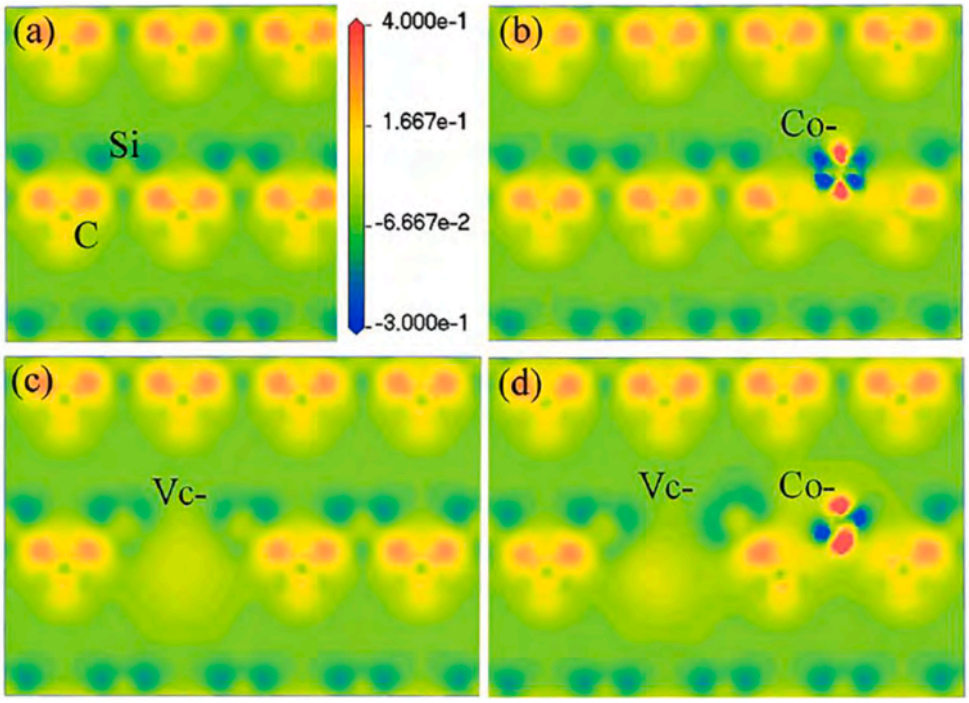

Fig. 20. Electrons distribution of (a) SiC, (b) Co doped SiC, (c) SiC with C-vacancy, and (d) Co doped SiC with C-vacancy [212].

8.1.4. Relevant composites

For composites, it is hard to establish the crystal structure that used to do the calculation. There are two examples of the applications of first-principles calculations. For the composites Co/CoO, to investigate the effect of two phases proportion on the microwave absorption property, the modeling is based on CoO crystal, and gradually increase the reduction degrees of CoO, which is the path from CoO crystal to Co crystal. And then calculated the relative properties to explain the composites absorption behaviors [215]. The band gap of CoO is 0.75 eV, while adding Co, the band gap reduces to 0. As the Co amount is gradually increased, the electrovalent bond of Co–Co is increased, and the electrical conductivity is enhanced, affecting the dielectric properties of the products.

The electronic structure of $BiFeO_3$ Nanowire- RGO Nanocomposite is explored [216], in which the structure of sample is simplified into $BiFeO_3$ (BFO) added a monolayer graphene (G) with 15 Å vacuum space. After relaxing and optimizing, the superlattice structure used to calculate is shown in Figure (a). The banding energy between BFO and G is −5.4 eV. From the electron density mapping and difference charge density, on the G sheet, the distribution of charges is imbalance, accumulating on the C atom that close to Fe. And there is no band gap in the BFO-G structure, which mainly contribute from C 2p orbitals. The strong hybrid interaction is observed between O 2p and Fe 3d, which is considered the origin of ferroelectricity of BFO-G and has positive effect on electronic polarization.

8.1.5. Summary and prospects

According to these researches, the application of first-principles calculation on absorbing materials mainly focus on the explanation the variations of dielectric performance between the defective model and the origin model. There are two significant conclusions from these researches:

(1) Introduction of defects can improve the dielectric response. Compare to the perfect model, the existence of defects will break the symmetry in the localized microstructure and bring the asymmetrical charge distribution, which are the origin of electric dipole that contribute to dielectric loss.
(2) The defects can change the electronic structures, according to DOS, generally can increase the conductivities of materials. In some cases, after introducing defects, the materials alter from insulator or semiconductor to half-metallic materials. The increased conductivities point to the enhanced conductive loss.

However, there is few studies about predicting the magnetic loss, which waits for further studies to break through. Generally speaking, even though the modeling cannot represent the materials completely, it can explain the micro absorption behaviors to some degree. The explorations of the theoretical research are well conformed the experimental results, which confirm the availability of the application of first-principles calculation in the studies of absorbing materials.

8.2. First-principles calculation for alloys

First-principles calculation based on the density functional theory (DFT), performed through Vienna Ab-initio Simulation Package (VASP) on powerful calculation, are one of the most widely used method to analyze the energy, electronic properties, magnetic properties, structure information, microparticle interactions, etc. DFT calculation and phonon calculation can help analyze the phase transition assisted twinning by estimating the stacking fault energies, temperature-dependent phase stabilities of different structures. In addition, first-principles calculations can also be used to evidence the result of other computational methods or experimental data. In this section, the recently research on first-principles calculations for magnetic materials including traditional alloys, Heusler alloys, High Entropy alloys (HEAs) and some other alloys are presented. The influence mechanisms on the magnetic properties are also revealed.

8.2.1. Traditional alloys

As ferromagnetic elements, Fe, Co and Ni alloys show excellent magnetic properties and widely used as MAMs. The magnetic properties of materials are obviously dependent on the composition and

microstructure, the influence mechanisms can be further revealed by analyzing the density of states (DOS) and magnetic moments information through first-principles calculation.

Atomic magnetism can be affected by neighboring atoms. Researchers report that the magnetism of Co atoms is very sensitive to the Fe atoms around them, and Fe atoms could provide different magnetic moments in different sites of $Al_{13}Fe_4$ alloy [217]. It can be proved by the changes of the magnetic properties in M_xPt_{1-X} (M = Co, Ni and V) [218]. The main contribution of total DOS comes from the hybridization of M-3d and Pt-5d states, which can effectively enhance the spin and orbital magnetic moment and then improve the magnetic properties. CoPt alloy has larger total magnetic moment of $4.31\mu_B$ and higher magneto-crystalline anisotropy than NiPt and VPt alloys, whose total magnetic moment are $1.86\mu_B$ and $0.80\mu_B$, respectively.

In spite of the structure of alloy, the concentration of special atoms is also a necessary factor which can make great changes in alloy magnetism. It is found that the magnetic properties of $Mn_{13-n}Co_n$ clusters are strongly depended on the concentration of Co, especially for those with n = 0,1,3 and 4, whose magnetic moments increased greatly with the addition of Co. This is because of the decrease of antiferromagnetic coupling of Mn atoms which are on the surface of cluster via increasing the concentration of Co [219]. Moreover, the calculations of the magnetic properties of $Hg_{1-x}Mn_xTe$ alloys show that the change from anti-ferromagnetic to ferromagnetic could result in a metal-insulator transition at higher Mn concentrations [25].

8.2.2. Heusler alloys

Although Cr and Mn atoms are antiferromagnetic elements, in specific structure they may provide considerable magnetic moments, thus enable the systems to exhibit great magnetic properties. The magnetic property of ferromagnetic Mn_2MoAl Heuslar is reported. The total magnetic moment of Mn_2MoAl is $1.04\mu_B$, which is mainly from Mn ($0.70\mu_B$), while the magnetic moments of Mo and Al are $-0.28\mu_B$ and $-0.01\mu_B$, respectively [220]. And in other types of Mn based Heusler alloys such as Ni_2MnX (X = Ge, Sn, Sb) Heusler alloys, Mn atoms have the largest magnetization density which result in the largest magnetic moment. The total magnetic moment of Ni_2MnSn reached $4.110\mu_B$, among that the magnetic moment of Mn is $3.486\mu_B$ [221], as shown in Fig. 21.

In some alloys, the magnetic properties of materials are also affected by the external factors. The changes in lattice constant can also cause changes on the magnetic properties of atoms. First-principles calculation can help to obtain the required material properties through component design and structural optimization. The spin polarization and Fermi level are two essential parameters to evaluate the material properties. As reported, spin polarization and Fermi level are tuned by using Co atoms to replace the Mn sites in Mn_2VIn alloy [222]. With the increase of the concentration of Co (0.25–1.75), the spin polarization raised from 15.38% to 93.60%, but the total magnetic moments decreased because of the decreasing magnetic moments of Mn atoms. Moreover, by calculating the magnetic moment, the magnetic information of the material can also be obtained [223].

8.2.3. High (medium) entropy alloys

High (medium) entropy alloys (HEAs/MEAs) show excellent comprehensive performance because of its cocktail effect which takes advantages of all the element components. Regulating the composition and content of component in alloy helps control on the magnetic properties of high entropy alloys. Research shows that CoFeMnNiAl alloy has better soft magnetic properties than CoFeMnNiGa and CoFeMnNiSn, while CoFeMnNiCr shows a paramagnetism behavior. The First-principles calculation showed that the total electron density of states (DOS) of CoFeMnNi and CoFeMnNiCr are more symmetric, while the spin-up distribution of CoFeMnNiAl is higher than that of spin down,

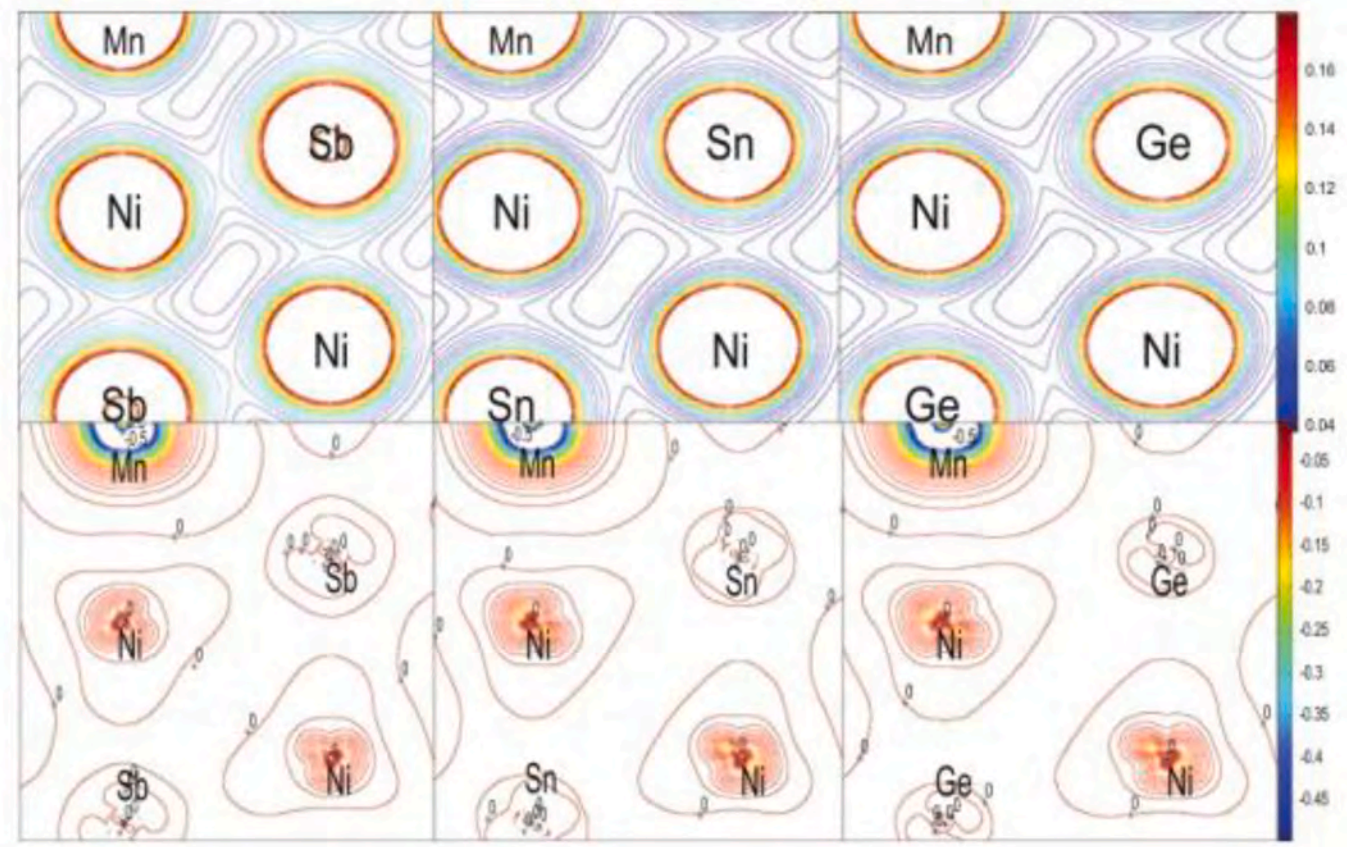

Fig. 21. The calculated charge (upper panel) and magnetization (lower panel) density distributions of Ni_2MnX (X = Ge, Sn, Sb) in the (110) plane [221].

which makes Mn provide large positive magnetic moment. Therefore, with the addition of Al, BCC phase is obtained and the antiferromagnetic properties of Mn are suppressed, which promote the magnetic property of the alloy [224]. In the high entropy alloy, the calculation of the first principle reveals the micro mechanism of the magnetic change resulting from the element doping and phase transformation, which would be a very useful for the design of magnetic absorbing materials.

8.2.4. Other magnetic materials

Besides the alloys mentioned above, some other magnetic materials such as polycrystalline materials, coating materials and amorphous alloys show favorable magnetic properties because of the magnetic moments provided by the transition element atoms. The magnetic properties for a single Fe atom chain wrapped in the armchair (n,n) boron nitride nanotubes (BNNTs) ($4 \leq n \leq 6$) are analyzed using the density functional theory [225], as shown in Fig. 22. The magnetic moment of Fe will increase by increasing the diameter of Fe nanotubes. With the increasing Fe concentration at Cr sites, the total magnetic moment and ferrimagnetic transition temperature (T_C) increase [226]. Another investigation report that the magnetic susceptibility of $Co_{68}Fe_4B_{15}Si_{13}$ amorphous alloy has a positive correlation with the cluster size and fraction of metal atoms, while it shows a negative correlation with the fraction of metalloids. With the increase of boron and silicon atoms in the cluster, the magnetic susceptibility decrease obviously [227].

8.2.5. Summary and prospects

First-principles calculations helps further understand the changing mechanisms of magnetic properties. For the metals consisting of transition elements, the interaction and orbital hybridization between those elements are the main factors that determine the magnetic moment of materials. Thus, the rational utilization of first-principles calculations based on density functional theory (DFT) will help analyze the electronic behaviror and magnetic properties of materials.

9. Microwave absorbing coatings

Microwave absorbing coating is the mixture composed of absorbents and resin. It is coated on the surface of aircraft, ships and other structural parts to attenuate the power of scattered electromagnetic wave and help realize electromagnetic stealth. Generally speaking, researchers have two ways to improve the microwave absorbing performance of coatings. On the one hand, by the design of composition, microstructure of absorbents the electromagnetic absorption can be regulated. On the other hand, the structure of coating in wavelength scale can also significantly influence the microwave loss capability of coating. In addition, embedding the frequency selective surface into coating and introducing corresponding electrical resonance and magnetic resonance into coating is also an effective way to broaden the effective absorption bandwidth of coating.

9.1. Composition design

9.1.1. Coatings filled by dielectric absorbents

It is difficult for dielectric material to possess multiple loss mechanisms simultaneously, so mix different dielectric materials to enhance the microwave absorbing performance is performed. For example, compared to $BaTiO_3$/epoxy resin coating, the nanocrystalline carbon black/$BaTiO_3$/epoxy resin composite coating exhibits a higher absorption at a thinner thickness. The significant increase in the imaginary part of the dielectric constant indicates that the addition of carbon black effectively increases the conductivity loss and enhances the electromagnetic wave loss efficiency per unit volume of coating. Although carbon black can adjust the dielectric properties of coating to a large extent, it trend to be agglomerated, and the density difference from other materials is large, which cause an uneven distribution of carbon black in coating [8]. Therefore, some researchers use metallic materials (Fe, Cr, FeCrAl) or aluminum oxide to increase the conductive loss of coating. The uniform dispersion of two materials in coating not only effectively improves conductive loss of coating but also enhances interface polarization between the different particles.

Adding particles with high conductivity into coating can efficiently control the microwave absorption properties. Heat treatment and morphology control on absorbent are two common methods to control the dielectric constant of coating. When ZnO/Al_2O_3 composite coatings are annealed in vacuum, there will be a higher concentration of oxygen vacancies and higher electrical conductivity of ZnO particles. In addition, the increased crystallinity and elimination of internal stress during annealing process also help to improve the complex permittivity of absorbers. At the same time, the microwave absorption performance of the coating has also been adjusted [228,229].

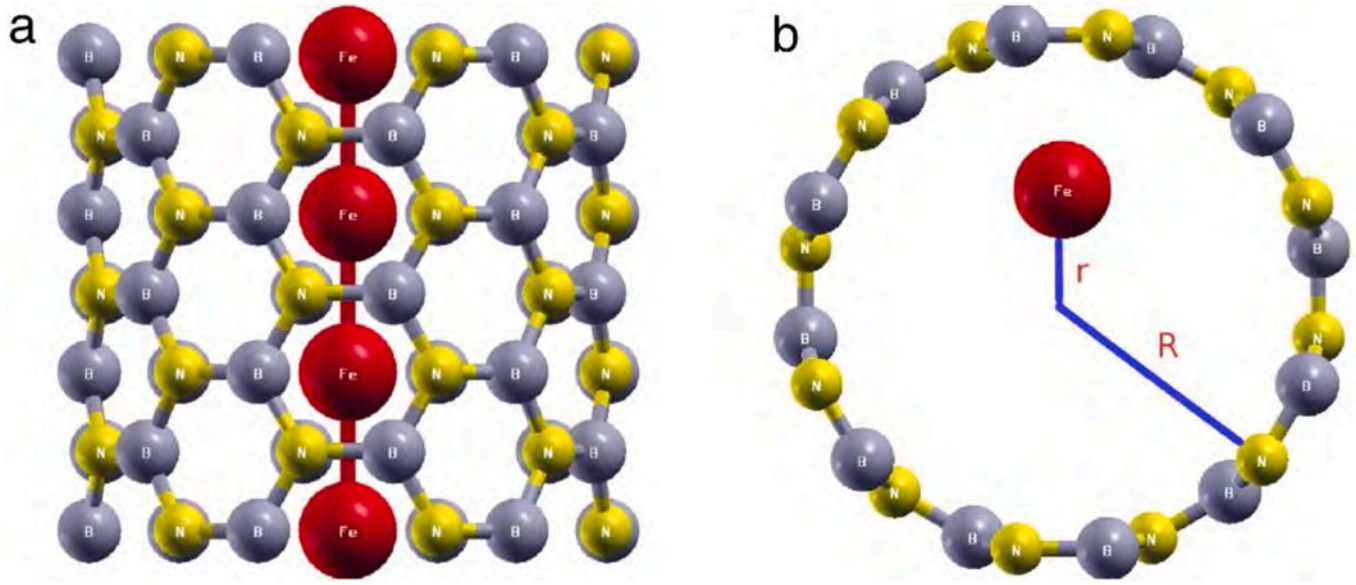

Fig. 22. The model of a linear Fe atom chain bound in the armchair (6, 6) BNNT [225].

9.1.2. Coatings filled by magnetic absorbents

Microwave coatings with wider absorption bandwidths and less thicknesses are required. Compared with dielectric materials, magnetic absorbers have higher loss efficiency per unit thickness, so introducing magnetic absorbers into coating can effectively reduce the thickness of coating. Although the coating has a certain microwave absorption capacity at low thickness, the Snoek's limit indicates that the spherical iron carbonyl cannot obtain high permeability in the microwave band. To break this limitation, Zhao et al. [43] transform spherical carbonyl iron into flake carbonyl iron by ball milling. The plate morphology endows the carbonyl iron a higher magnetic permeability and the corresponding reflection loss reaches to −7.5 dB in the range of 8–18 GHz. Adjusting the grain size of magnetic absorbers on the basis of appropriate morphology can further improve the electromagnetic wave absorption. You [230] et al. change grain size by changing annealing conditions. Results prove that an appropriate increase in grain size is beneficial to reduce the number of disordered domains, improving the magnetic loss ability of absorbers and enhancing the microwave absorption to −43.4 dB. These changes in morphology and grain size of absorber are significant to the improvement of the microwave absorption performance of coating, but the above changes may also cause a substantial increase in the permittivity, which may cause the impedance mismatch. Therefore, some researchers add both spherical and flake carbonyl iron to coating, which can effectively prevent the permittivity from being too large [231].

9.1.3. Coatings filled by dielectric-magnetic composite absorbents

A single dielectric material or magnetic material usually cannot meet the impedance matching. Therefore, dielectric-magnetic composite absorbent is widely used. Adding different dielectric loss absorbents to carbonyl iron can effectively improve the microwave absorption performance. Carbon material is one of the widely used absorbents because of its multiple electrical loss mechanisms. Adding CB into CIP can increase the conductivity loss and interface polarization [232]. Multi-walled carbon nanotubes (MWCNTs), as one-dimensional material, have large aspect ratio, which have less aggregation than the 1D carbon materials such as CB. A better dispersion of absorbents and better impedance matching than pure MWCNTs and CIP materials improve microwave absorbing properties [233,234]. Besides, graphene, SiO_2, $CuSiO_3$, Ti_3C_2 MXene/flake iron carbonyl are also widely used with magnetic materials to improve the impedance matching and increase microwave attenuation mechanisms.

9.2. Structure design

9.2.1. Coatings with special structure

Besides the absorbent, the coating thickness and structure can also influence the microwave absorption performance of coating. The multilayer structure coating can reflect EM waves many times and attenuate their power during this process. The structure design such as multi-layer and "island" discontinuous structure can help to improve the impedance matching and enhance microwave absorption.

Multi-layer coating can also help to break through the restrictions on material selection. By fabricating multi-layer structure, each layer of coating can be systematically designed. Double layers coating consisting of cobalt flakes with high shape anisotropy can cover 4.17–12.05 GHz with the thickness of 2.66 mm [235]. Two-layer coating with the top layer of CNTs/epoxy and bottom layer of graphite/epoxy is prepared. The absorbing bandwidth (RL < −5.0 dB) achieves 2.4 GHz [236]. Flexible double-layer coatings is fabricated using carbon-coated nickel nanoparticles and carbon nanotubes as the matching and loss layer, respectively, which achieve a RL of −30.78 dB [237]. Apart from simple multi-layer structure, novel honeycomb sandwich structure coating is fabricated to effectively enhance the properties. FeCo, Tb and epoxy resin composites are sprayed onto the honeycomb sandwich core. The nano titanium powder is dispersed in a hydrogenation acrylonitrile-butadiene rubber using as the matching layer [238]. The absorbing bandwidth (RL < −5 dB) of the above structure reach 2.6–18 GHz.

In order to balance the absorbing properties and mechanical properties of coating, some fiber materials are applied to the structural design. A new sandwich structure, coating-carbon fiber-coating, is designed by Asif Shah et al. [239] The addition of carbon fibers can not only improve the flexural properties of the Fe nanoparticle/epoxy coatings but also adjust the microwave absorption performance of the coating. When the carbon fibers' array is vertical to the direction of incident microwave, a strong reflection of microwave will inwardly form, which is conductive to the attenuation of EM wave by absorbent. On the basis of the above research, those research team also prepares nanocomposite plate using similar materials. Arrayed carbon fibers and gradient dispersion of Fe nanoparticles not only provide structural resonance but also good impedance matching. Based on these advantages, some researchers further optimize the coating into a pyramidal multilayer structure. Compared with traditional multi-layer microwave absorption coating, this pyramidal structure takes advantages of insensitivity for EM incident angle and ultra-wide absorption band. The carbonized cotton/wax mixture is used as absorbent to fabricate a polymeric patterned shell which provides shape support and mechanical robustness [240]. The pyramid structures not only greatly broaden the effective absorption bandwidth, but also show stable reflection loss when the incident angles changing from 5° to 60°as shown in Fig. 23.

9.2.2. Frequency selection surface coating

Multiple-layer structural coatings have shown strong microwave absorption properties. However, coatings with such structures always have a large thickness, which limits their application. In order to get desirable microwave absorption properties with less thickness, some researchers embed the frequency selection surface (FSS) into coating. There will be electrical and magnetic resonance between frequency-selective surface and EM waves which will effectively increase the microwave absorption without increasing the thickness. The FSSs used in coatings are commonly square loops, circular metal sheet, cross metal sheet, split ring resonators, and rectangular sheet, etc. Different FSSs can make the coating exhibit different microwave absorption characteristics. For example, multiple square loops with multiple resonance peaks in a wide frequency band are often used to broaden the effective microwave absorption bandwidth. Cross pattern can effectively enhance the microwave absorption in low frequency range. In order to further improve the microwave absorption performance without increasing the weight, some researchers fabricated the inhomogeneous substrate coating such as nesting FSS, which can absorb a broadband microwave from low to high frequency bands.

9.3. Summary and prospects

Microwave absorbing coating has been developed for decades. Through composition and structure design researchers aim to fabricate the thin and lightweight coating with broadband and strong absorption. But the increasing requirements such as compatibility of radar and infrared, self-healing and self-cleaning characteristics, high-temperature resistance, self-adaptive and other multi-functional integrated coating are to be satisfied for the future research on microwave absorbing coating.

10. Infrared stealth materials

Precision and resolution of infrared detection have been greatly improved in recent years. Infrared detection has become one of the most important detection and tracking method in modern war. Therefore, improving low infrared emissivity materials to protect devices from infrared detection becomes an urgent topic in stealth field. In most cases, the temperature of people and devices is higher than that of the

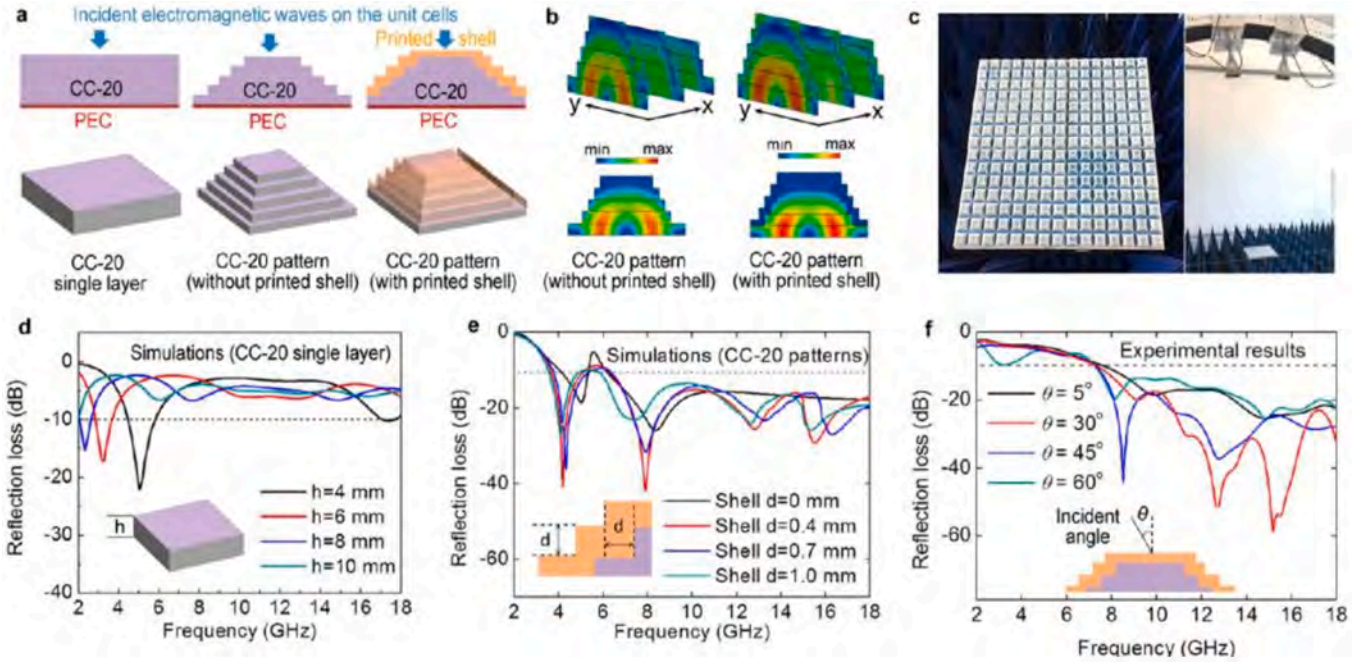

Fig. 23. Effects of 3D printed patterned shell on the electromagnetic absorption performance [240].

background. There are three main ways to achieve infrared stealth. The first, use low infrared emissivity coatings to reduce the infrared emission of the object surface. Secondly, control the temperature of the object and reduce the radiation energy. Thirdly, reduce infrared radiation in the atmospheric window wavelength range. For now, researchers are focusing on searching or synthesizing efficient low infrared emissivity materials, designing multiband compatible stealth coatings, and developing coatings that can be applied at high temperatures.

10.1. Low infrared emissivity materials

The application of low infrared emissivity materials is the most efficient way to realize infrared stealth. According to Stefan-Boltzmann's law, one of the important means is to prepare low infrared emissivity surface. In recent years, a variety of low emissivity materials such as metals, alloys, composite, multiple-layer low emissivity materials, and photonic crystals have taken large effect in infrared stealth, which show great research potential.

10.1.1. Metals and alloys

The initial research on low infrared emissivity materials focuses on the exploration of low emissivity pigments. Some metals, such as Au, Ag, Zn, Cu, Fe and Al, have been widely studied due to their low emittance and easy availability. Considering the cost, Ag and Au are generally used in composite materials. Cu and Al are also widely researched because of their abundant storage, mature metallurgical process and low cost. By spraying 50 μm Al/epoxy resin coating onto tinplate, the effects of size, shape, and Al content on the infrared emissivity of the coating are studied [241]. The result shows that the flake aluminum powder pigments with micron size particles have the lowest emissivity. The lowest infrared emissivity can be 0.16. Directional distribution of numerous flaky Al powder on the surface increases the effective reflection area and makes infrared radiation difficult to enter the coating.

Compared to pure metals, alloys have better corrosion resistance. An epoxy-polyurethane (EPU) and bronze low infrared emissivity coating is prepared by a spray technique. It demonstrate that the EPU/bronze composite coatings with 40 wt% bronze have the lowest infrared emissivity and the best corrosion protection compared to PU/Cu, PU/(ball-milled) Ag–Cu and PU/Al coatings [242]. The reflection area, roughness, microscopic energy band, crystal structure will have obvious effect on metal infrared emissivity. $La_{0.8}Sr_{0.2}MnO_3$ samples with rhombohedral, orthorhombic, and monoclinic structures are prepared [243]. The Kirchhoff's law and theory of wave optics are used to explain the influence of grain size, morphology, and lattice parameters on the infrared emissivity. The result shows that the orthohombic $La_{0.8}Sr_{0.2}MnO_3$ which has the smallest particle size has the lowest infrared emissivity. But the honeycomb structure of orthohombic sample results in repeated reflection and scattering, which increases the infrared emissivity. The research has promoted the progress of low emissivity metal system.

10.1.2. Composites and multiple layers

Changes in chemical bond, structure, and atomic or molecular distribution result in a change in performance. Interaction between the functional groups and interface of each component is beneficial to the low emissivity materials. Surface modification is a simple and effective method to improve the performance of coatings. Flux-capping method is used to coat polyethylene wax on Cu and Al powders, then use the modified Al and Cu powders to prepare low emissivity coatings [244,245]. The simple linear chain structure and great liquidity of polyethylene wax can effectively decrease the emissivity of coatings. The coating prepared by the modified powders has lower infrared emissivity. A facile vacuumed hot-pressing method is used to synthesize silver particles modified (SMCNP)/glass fiber reinforced polymer [246]. The addition of a small amount of silver particles greatly increases the conductivity of the carbon nanotube paper. The infrared emissivity of the modified carbon nanotube paper composite in 2–14 band is inferior to raw material and the relative radiation energy is lower, as shown in Fig. 24. In the meantime, the polymer possesses thin, lightweight, admirable mechanical properties and can integrate with engineering matrix material successfully. It means the composite material can perform well in practical infrared stealth application.

Multilayer structure is also widely used to reduce the infrared emission. A three-layer core-shell composite [247] which is SiO_2/Ag/-TiO_2 'sandwich' composites with SiO_2 in the center, Ag in the middle, and TiO_2 in the surface is synthesized. The addition of silver increases the reflectivity of the material. Meanwhile, during the deposition of Ag on SiO_2 particles, disorder of the elementary dipole decreases the

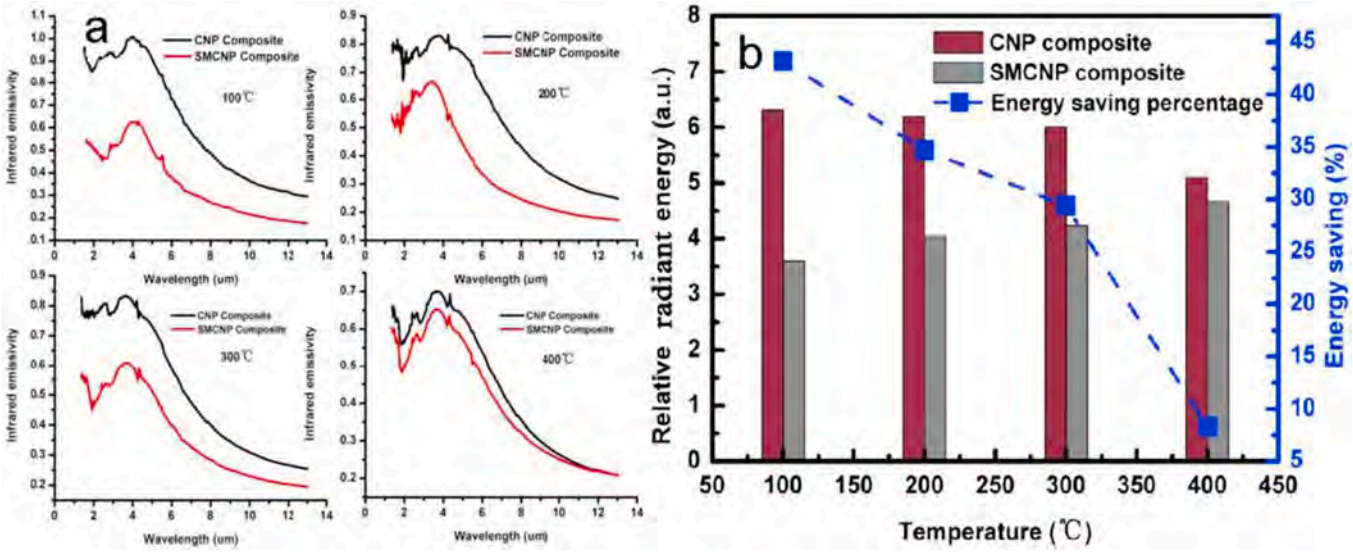

Fig. 24. Infrared emissivity and relative radiant energy of SMCNP/GFRP and CNP/GFRP composite at different temperatures [246].

infrared absorption. Furthermore, infrared emissivity of anatase TiO_2 with less lattice distortion after heat treatment is lower than amorphous TiO_2 without heat treatment. The infrared emissivity of particles is reduced to 0.558. But it is difficult to design multi-layer pigments because of the complicated preparation process. In contrast, multilayer coating has a better application prospect.

Multilayer coatings not only have good infrared stealth performance but also possess other excellent properties. Layers with different properties can supplement each other to improve the practicability. Layer-to-layer interactions, such as addition of electron migration networks and formation of chemical bonds will influence the electrical properties. TiO_2/Si/Ag(Cr)/TiN_x multilayer thin films with low infrared emissivity values and high transparency are obtained by using RF and DC magnetron sputtering on soda-lime glass [248]. Fig. 25 illustrates how the structure works. On the one hand, multilayer thin films have good electrical conductivity, therefore the films can prevent most infrared rays from entering. On the other hand, after absorbing the energy, the wetting angle between the coating and water can be reduced. In addition, heterojunction film composed of wide bandgap semiconductor and narrow bandgap semiconductor can prompt the hydrophilicity of the coating.

10.1.3. Photonic crystal

In traditional coatings, more than 50% of the compositions in coating are organic resin, which has poor stability at high temperature. The photonic crystals make up for these disadvantages. Since Yablonovitch and Tohn proposed the concept of photonic crystals, researchers have done a lot of work on developing photonic crystal materials with controllable electromagnetic properties.

Photonic crystal is a kind of metamaterial, and it has band gaps for some photons with specific wavelengths which can has a selectivity characteristic on the electromagnetic wave. High vacuum electron beam coating technology is used to prepare Ge/TiO_2//Si/SiO_2 one-dimensional heterostructure photonic crystal (1DHPC) (Fig. 26). The test result indicates that for the microwave with wavelength of 3–5 and 8–14 μm, the infrared emissivity of prepared 1DHPC is as low as 0.060 and 0.239, respectively. in wavelength range of 5–8 μm, the as-prepared 1DHPC has higher infrared emissivity of 0.562. the Ge/TiO_2//Si/SiO_2 one-dimensional heterostructure photonic crystal has obviously infrared spectrally selective characteristic [249]. In recent years, infrared emissivity can be controlled by applying external voltage to photonic crystal such as the intelligent photonic crystals with low infrared emissivity. However, although scientists have improved the preparation technology of photonic crystals, its complicated fabrication still limits its

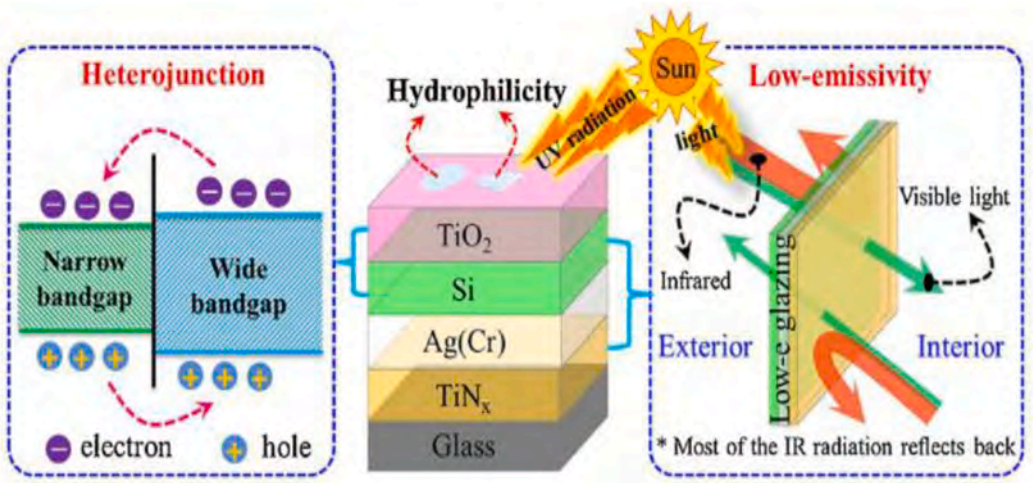

Fig. 25. Interaction between multilayer coating and electromagnetic wave and hydrophilicity of the structure [248].

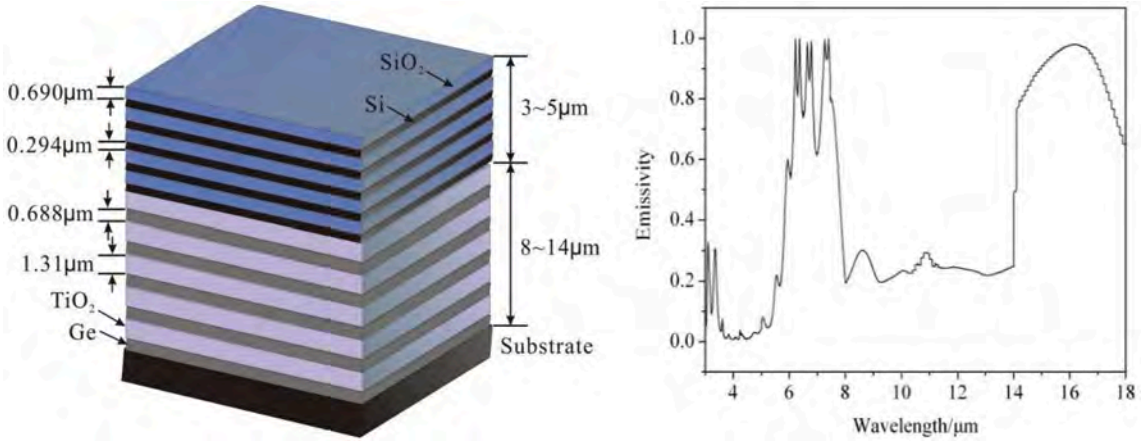

Fig. 26. Structural model and infrared emissivity of $Ge/TiO_2//Si/SiO_2$ [249].

application. Therefore, simplifying the preparation of photonic crystals is an urgent problem to be solved in the future research.

10.2. Multi-band infrared stealth materials

The low emissivity infrared stealth coatings of single traditional pigment have high reflection to electromagnetic wave, what means they are cannot camouflage under the detection of electromagnetic wave in other bands. The compatible stealth has become a major challenge to scientists.

10.2.1. Infrared-radar compatible stealth material

The absorption mechanism of radar wave such as dielectric loss and magnetic loss can be introduced by adding absorbing materials into the materials with low infrared emissivity. Researchers from Dalian University of Technology [250] find that when the composition ratio of the surface layer is Al: PU: ZnO = 0.6: 1: 0.6, the infrared emissivity of the coating can decrease to 0.504 while radar wave can be effectively absorbed in 11–18 GHz. Cavities forming during the surface modification can help to increase the impedance matching. At the same time, the interface polarization between different layers improves the absorbing property of the low emissivity materials. Al/MWCNTs (multi-walled carbon nanotubes) composite shows good compatibility [251]. Al sheets intersects among the MWCNTs, forming a cavity and resulting in electromagnetic resonance. Oxygen-containing groups introduced by multi-walled carbon nanotubes conductive networks and defects between Al coatings lead to the molecular polarization and dipole polarization of the material under the effect of an external electromagnetic field. The highest reflection loss is −39.2 dB in the wavelength range of 9.2–12.24 GHz and the infrared emissivity is 0.67 [252]. Some surface modification materials can also form a conductive network to absorb electromagnetic wave. Surface metallized perovskite type La0·7Ba0·3MnO3 powders are used to prepare Ni–P/$La_{0.7}Ba_{0.3}MnO_3$ composite. The infrared emissivity of the surface modified powder decreases by 0.2. The formed conductive network increases the value of imaginary parts of the permittivity. Meanwhile, Ni has a strong magnetic loss ability, which increases the value of real and imaginary of the permeability. The synergistic effect of dielectric and magnetic loss broadens its effective absorption bandwidth. The study provides an approach for making infrared-radar compatible stealth material. Some researchers have also made infrared and radar-compatible camouflage by designing the structure of the coatings.

10.2.2. Infrared-visible light compatible stealth material

Low emissivity materials always have high reflectivity for visible light. How to reduce the brightness of low infrared emissivity materials is a new problem for researchers. The surface modification on materials with high reflectivity is used to reduce the specular reflection by increasing the surface roughness and diffuse reflection, to get low brightness. For instance, researchers coat MnO_2 and Co_3O_4 on the surface of Al by ball milling. Low infrared emissivity multilayer coatings have been widely used as multifunctional coatings. An excellent infrared-visible light compatible stealth performance is obtained from OMO materials (oxide–metal–oxide structure) [253]. The metal layer shows low infrared emissivity, and the dielectric layers regulate the brightness and color. The $TiO_2/Cu/TiO_2$(TCT) coated polyester fabric has controllable color with different sputtering time of Cu. The infrared reflection of the TCT coated polyester fabric changed from 5% to 30% compared with untreated polyester fabric.

10.2.3. Infrared-laser compatible stealth material

An efficient method of synthesis composite with infrared and laser stealth materials is proposed to get infrared-laser compatible stealth materials. Similar to infrared-visible light stealth, low infrared emissivity materials are surface modified to increase the scattering and diffuse reflection to reduce the laser reflection intensity. Al powder is coated with antimony-doped tin oxide (ATO) to obtain an infrared-laser compatible stealth materials [82]. The Al/ATO composites exhibited optimal infrared-laser compatible stealth performance with the infrared emissivity of 0.708 and the reflectivity of 43.4%. Besides surface modification, researchers also propose grating structure [254]. The composed structure contains two-dimension polar crystals SiC grating and Ag/ZnS multilayer films substrate. The former excites surface phonon polariton and gets high absorption at specific wavelengths, while the latter works for high reflection in the infrared band. According to simulation results, the structure absorbs around 90% of the electromagnetic wave at the wavelengths of 1.06 and 10.6 μm. At the same time, the reflection in the infrared band is 95%, and the average transmission in the visible band is 75%.

10.3. Infrared stealth material with high temperature resistance

Based on Stefan-Boltzmann's law, the infrared energy emitted by an object is proportional to the fourth power of the temperature. The infrared detector uses the difference of infrared radiation energy between the object and the background to image, and temperature is one of the most important factors. It is imperative to study the high temperature performance of stealth materials because many devices work at high temperature. However, oxidation of metal materials and cracking of binder in high temperature cause failure of stealth materials. The research on the improvement of thermal stability is required.

Adhesive is the weakest part of coatings at high temperature. Addition of Si can effectively strengthen the heat resistance of binder. Si–O–Si groups form when the coating is sintered. The net structure can

prevent the diffusion of combustible degradation products. The Al powder is add into epoxy-siloxane to prepare high temperature resistance with low emissivity composite coatings [255]. The lowest infrared emissivity value of coatings is 0.15 in the wavelength of 8–14 μm when the Al concentration is 40%. Emissivity stays in the low level when temperature below 500 °C. Meanwhile, the composite coatings exhibit high thermal stability and good thermal shock resistance. $Cr_{39}Ni_7C$ powders are used to prepare heat-resistant low emission coatings, and the inorganic silicate is used as binder [256]. The Si–O–Si bands and high crystallinity improve high temperature resistance of the coatings. As the temperature rises to 600 °C, infrared emissivity can be further reduced to 0.55. Inorganic silicate is one of the stable adhesive at high temperature. Besides, ZnO is an insulating semiconductor filler with low infrared emissivity. ZnO with flake, flower and acicular morphologies have different properties at high temperature [257]. The flake ZnO powders have the lowest emissivity in the wavelength of 3–5 μm at 500 °C. The Drude model can be used to explain infrared reflection properties of ZnO with different morphologies. Researchers also analyze their behavior at high temperature from electron average scattering time and lattice vibration.

At present, there are few systematic researches on high temperature resistant infrared stealth materials. By looking for stable pigments and adhesives at high temperatures, or by developing new coatings through structural design, the application of low infrared emissivity materials at high temperature is feasible.

10.4. Summary and prospects

The infrared stealth materials in the future require light weight, thin thickness, and wide coverage of microwave band. Metals and their oxides, conductive polymers, semiconductors, composites, and photonic crystals exhibit excellent low infrared emission properties. However, there are few studies on the theories of low emissivity, and the interaction mechanism between various materials is not fully researched. To further reduce the emissivity and improve the comprehensive properties of materials, the theoretical research is required.

11. Microwave absorbing metamaterials

11.1. Bionic microwave absorption metamaterials

The microwave absorption metamaterials also could be inspired by natural models, such as biological evolution of animals, plants, insects, seashells et al. There are “natural meta-atoms” on the body surface of these creatures, and could play a role in absorption or self-adaptivity of EM waves. However, the natural models are always act in visible light frequency range, whose wavelength is much less than microwaves. Thus, the “natural models” used for microwave absorption that need to be re-analyzed and re-designed.

In order to escape visual detection of natural enemies, biologies have been evolved and possessed the specific photonic structures, and they are not work through microscopic structures like atoms and molecules, but they are ordered by “functional units” that are orders of magnitude larger than molecules and atoms. Chameleons are typical natural models that could dynamic regulate EM waves, there are non-close-packed array of guanine nanocrystals on their body surfaces which construct a natural photonic crystals and that could control the photonic band gap from spacing of guanine nanocrystals. The models of chameleons could avoid the absorption restrict from the band gap. Along the route of dynamic color conversion by this photonic model, the non-close-packed of silica particles could embedded in the elastomer matrixs, the different elongation or compression of the elastic photonic film exhibits a structural color shifts from red to blue.

In addition to chameleon, octopus and cephalopods in oceans also have adaptive ability to EM wave. There are any central chromatophore pigment cells ringed by muscle cells on the squid skin, and the chromatophore pigment cells expanded and contracted through the mechanical action of the muscle cells, thus absorb or reflect visible light within corresponding wavelength. Encouraged from the mechanism, researchers have translated the function from visible light to infrared spectrum, and developed an adaptive and camouflage material in infrared frequency regime. And the dynamic concepts could apply in many fields and frequency range. Some plant also has the self-adaptive ability that is the phototropism, a phenomenon in which the growing organs of plants are bent by the irradiation of one direction of light, such as sunflower. The nano cylinders are constructed by photothermal and mechanical materials, which could make the cylinders bent under incoming light, and track the light from beginning to end. The principle behind the concept and mechanism also could inspire the MAM, which realize self-adaptability and broadband absorption.

In addition to self-adaptive models, moth-eye micro structure is a typical model in EM waves anti-reflection within visible light frequency range. There is a sub-wavelength structure of gradual refractive index unit, which have significant eliminates reflections of visible light. The micro structure of moth eye surface is arrayed hexagonal hump [258], and a glass fabricated a bionic moth eye structure by Langmuir-Blodgett deposition technique and oxygen plasma treatment, and the treated glass revealed an excellent antireflective function, as well as a hydrophobic properties is displayed by the bionic structure [258]. The similar moth eye structure also could be found in Rosa petals and cicada wings, the researchers inspired by these structures to fabricate bionic materials, also demonstrate the antireflection ability.

The butterfly also has regulating abilities of EM wave, which stem from the microstructure on their body surface. Only some specific butterflies’ micro structures are suit for microwave materials. The wings of butterfly could realize transparent within whole frequency range of visible light [259], moreover, in the report, the ability could maintain even for large view angles of 80%. The property is like moth eye model, but the micro structure is novel, which is small nanopillars. This functional structure and concept could apply in microwave absorption materials, to enhance the impedance matching between the absorption material and free space. Some butterfly wings reveal as black, researchers have been found that there is nano hole micro structure on these butterfly wings, and it cooperate with the black pigment in their bodies, could realize effective absorption within whole visible light band, as shown in Fig. 27. This concept and structures also could be used in the MAM, and it could make the materials realize broadband absorption [260].

Some beetles have particular ability to manipulate light polarization, which derived from the gyrotropic chiral structures on their carapace, this chiral structure also could be found in some plants. When the EM waves with line polarization enter into the helix chiral materials, its polarization is rotated to circular type, this property of chiral structure has been demonstrated in many studies [261,262]. But there is EM waves loss when polarization rotation, this loss effect could be used in microwave absorption metamaterials to enhance absorption.

To date, researchers have used the natural models to enhance the performance of microwave absorption metamaterials, and have been demonstrated it is a feasible design route. E.g. inspired by the microstructure of the moth eye [263], the broadband absorption at deep sub-wavelength thickness and the 8.04–17.88 GHz absorption bandwidth at 1 mm thickness are realized, which demonstrated that anti-reflection ability of natural model also could be used in microwave frequency range, and through the multilayer and multiscale structure constructed by the moth eye model, the multi-band adaptability and hydrophobicity are realized, constructing a superior stealth, ultraviolet shielding, hydrophobic model. The chiral structure of jeweled beetles also successfully enhanced the property of MAMs [264], as shown in Fig. 28. The fibers of the beetle’s carapace show a spiral chiral structure, which could rotate the polarization of EM wave, and corresponding loss. In this work, the loss effect is used in microwave absorption materials, bionic chiral metamaterials are prepared and realized enhanced

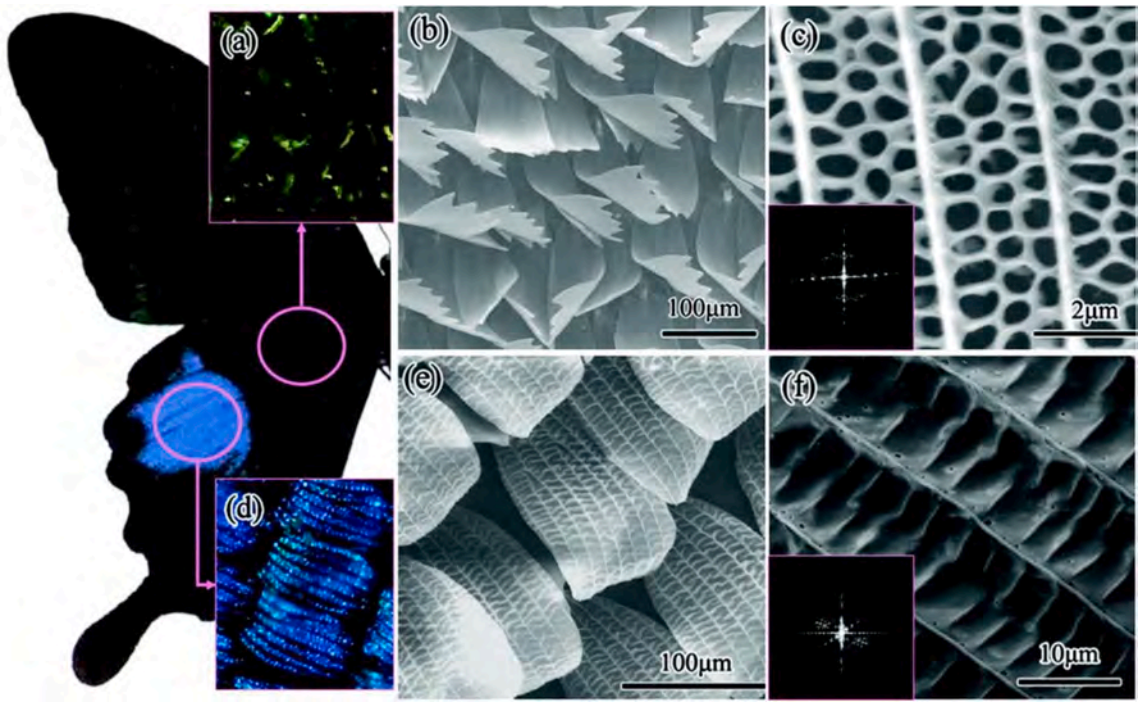

Fig. 27. Micro structure of butterfly wings [260].

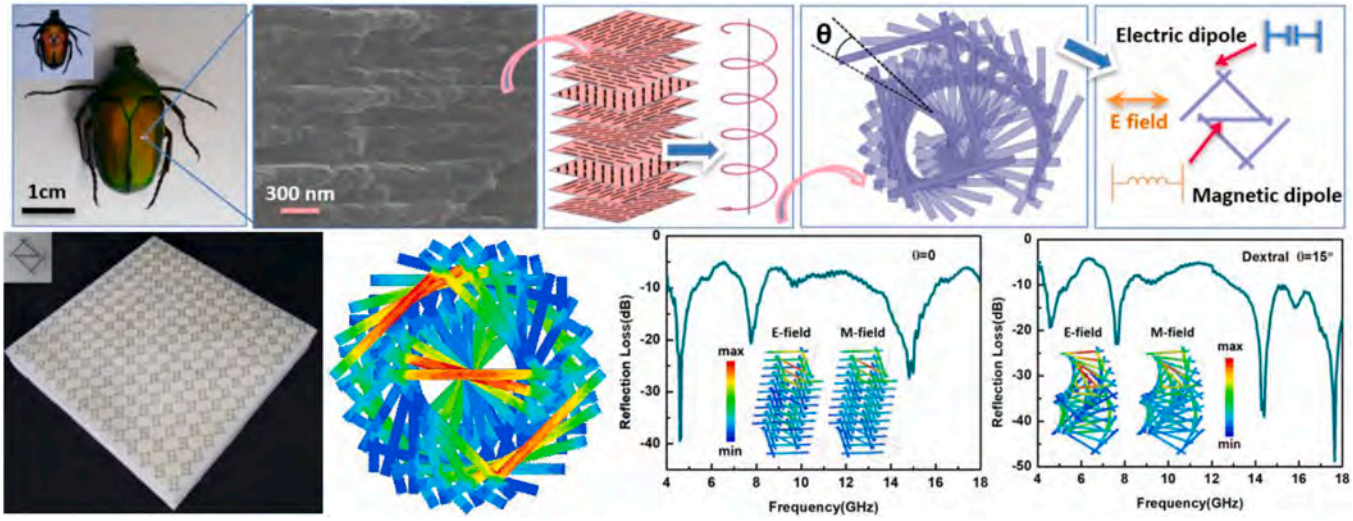

Fig. 28. Chiral micro structure of beetles and corresponding bionic structrues [264].

absorption EM wave by rotate the polarization, by construct the dextral intrinsic chiral structure (twisted 15°), there are six absorption peaks within 4–18 GHz frequency range, while the extrinsic structure (none twisted) are only four. And this bionic metamaterials used the porous matrix, which could be found in any natural models [265,266], realized ultrasonic wave absorption, water wave absorption, as well as impact resistance.

Some natural concept also could be used in microwave absorption materials, such as Qian et al. prepared an intelligent stealth metamaterial based on deep learning model [267], which derived from the self-adaptive concept of chameleon. That metamaterial with reconfigurable metasurface that tuned by deep learning artificial neural network, and could dynamically adapt to the changing background environment, and achieve adaptive stealth.

11.2. Metamaterial perfect absorbers

Metamaterial Perfect Absorbers (MPAs) based on a metamaterial high impedance surface is postulated. They consist of arrays of split resonant rings above a ground plane with a dielectric between them [268]. All the incident waves will be reflected and generate large electric fields on the surface of the metamaterial. A resistive sheet places on the outward surface of the metamaterials could absorb the energy of EM waves before reflecting it back, such as the thin thickness for Salisbury Screen. However, the original theoretical prediction still requires a much thinner dielectric layer than the operational wavelength.

Although the previous design does utilize metamaterials to create MAMs, the absorption mechanism is not the same as many traditional MAMs. The first experimental demonstration is designed by Landy in 2008 [269]. The combined design allows for individual tuning of the

electric and magnetic responses. The electric response derives from the top split resonant ring structure, and the magnetic response results from anti-parallel currents between the top and bottom metal layers. The high absorptivity is also experimentally realized or numerically predicted in the THz regime in 2008, Mid-infrared frequency frequencies in 2010, Near infrared frequencies in 2008, and in the visible light frequency in 2011 [270,271]. the versatility of the MPA utilization of a number of configurations which include: polarization dependent or independent absorptivity, variable angular dependent light absorptivity (both wide and narrow), broad or narrow frequency band absorptivity. A few particular examples are demonstrated in detail as follows.

11.2.1. Polarization independence

Polarization independent magnetic metamaterials are first proposed for near infrared frequencies to eliminate bianisotropy. Electric metamaterials are also proposed for both polarization dependent and polarization independent dielectric response. The design achieves polarization independent absorptivity by introducing structures, as show in Fig. 29 [272]. These metamaterials mentioned above have EM absorption by using unit cells with $\pi/2$ rotation symmetry. However, it is demonstrated that approximate polarization independent absorption is possible by utilizing an asymmetric unit cell. In this case, the unit cell without $\pi/2$ symmetry could also get the polarization independent absorption based on other mechanisms [273].

Chiral metamaterials could also achieve polarization independent absorption. Unlike the standard 3-layer design, this group utilizes a chiral version consisting of two stacked rings which can create inductive effect to increase the EM wave absorption [274]. A folded eta-shaped metamaterial shows that it is capable of generating gigantic optical chirality and spectrally breaking the spin degeneracy of optical transmission at multiband. A remarkable circular dichroism approaching unity is experimentally achieved, with the maximum transmittance exceeding 93% [275]. These MAMs shows absorption properties using rotationally symmetric structures or other symmetry structures for the EM spectrum in various bands, such as infrared frequencies and THz frequencies.

11.2.2. Broad angle and broad bandwidth adaptivity

It is possible to create resonance in multiple bands by adjusting resonance frequencies. By simulation, it is possible to improve the effective impedance for the whole system by structure design, such as the multilayer structures and nested elements used in the microwave and THz ranges. Some researches utilize higher order modes to get a broad resonance or a multi-resonant response. The device consisting of planar single unit-cell layer of metamaterial yields over 95% absorption and reaches an absorptivity of 77% at 1.145 THz [276]. Water-based [277] materials is also used recently to broaden the microwave absorbing bandwidth, which have been proposed and investigated by employing water as primary element. The paper designed two structure: the one is water-droplet structure, the other is water-tube structure. The dielectric permittivity of water unit rapidly decreases with the increasing frequency while the loss tangent significantly increases in the microwave region. Simulation and experimental investigation show that the induced currents loop in the droplets will couple to EM wave to increase the energy attenuation.

11.3. Digitally coded control metamaterials

In 2014, the concept of encoding metamaterials is firstly proposed by Cui [278]in Southeast University. So far, many attempts have been made to exploit dynamic metasurfaces. To realize the metamaterials coding, 0 and Π phase responses are introduced to mimic the '0' and '1' elements of 1-bit digital so that they can be controlled by a biased diode. This concept can be extended to 2 bits or more bits to realize different functionalities, thereby realizing coding metamaterials. Then, He [279] utilizes split-ring resonators to realize 3-bit digital coding states, and demonstrates the capabilities of manipulating both EM and acoustic waves simultaneously. He also designs programmable metasurfaces [280] which allow dynamic and real-time control of EM waves in sub-wavelength resolution. By combining metamaterials with computer, the discrete elements are controlled to realize multiple functions including steering, bending, focusing, and random scattering of EM waves.

11.3.1. Frequency coding metamaterials

Frequency coding metamaterials [281] can control EM energy radiation with fixed spatial coding pattern when frequency changes. Due to different frequency sensitivities of unit cells, two units with the same phase responding to the initial frequency may have different phase response to higher-frequency microwave. The authors design four different structures as show in the Fig. 30. The anisotropic encoding metamaterials [281] are fabricated. The coding behaviors are dependent on the polarization status of the EM waves propagating in different directions. The author experimentally demonstrates an ultrathin and flexible polarization-controlled anisotropic coding metasurface that works in the terahertz regime using specially designed coding elements. It reveals that the anisotropic coding metasurfaces can generate a beam splitter and realize simultaneous anomalous reflections and polarization conversions, thus provide powerful control on different polarized EM waves.

11.3.2. Structure coding metamaterials

By adjusting structures and periodic arrangements, polarization conversion can be achieved with metamaterials. It has been demonstrated [282] theoretically and experimentally that a specific

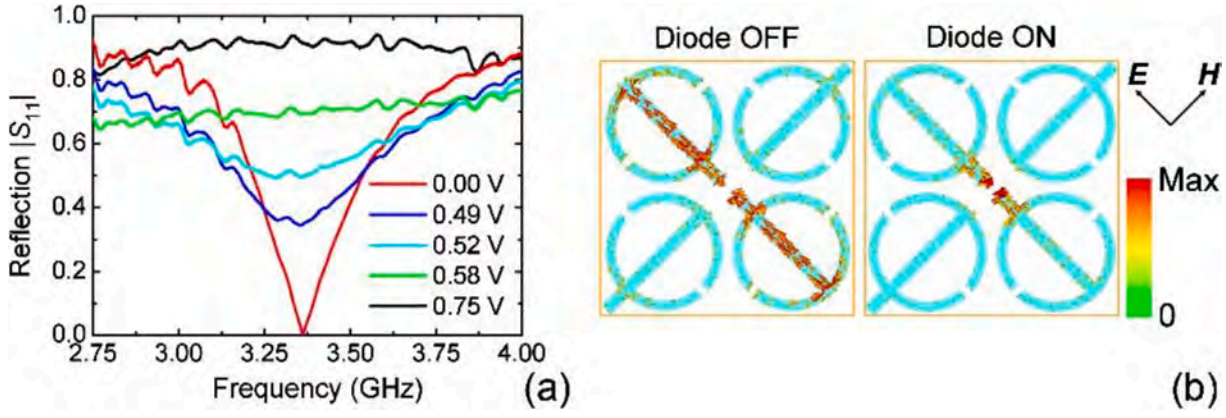

Fig. 29. (a) Measured reflection under normal incidence at different forward bias voltages (indicated in the inset). (b) Surface current density distribution on ELCs at peak absorption frequency for one particular polarization [272].

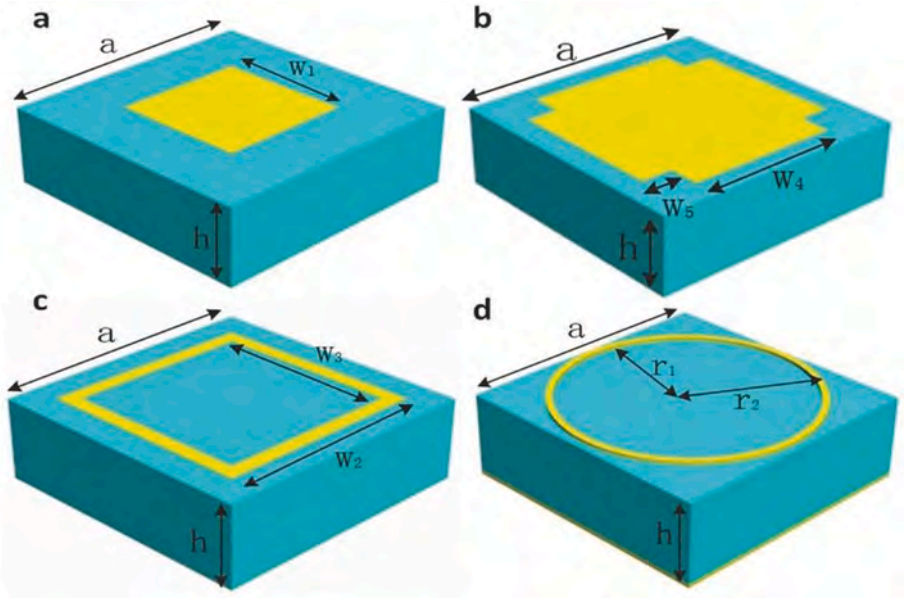

Fig. 30. The four digital units of frequency coding metamaterials and their reflection response curves. a) Square block. b) Crisscross. c) Square loop. d) Circular loop [281].

gradient-index metasurface can convert a propagating waves to a surface waves with nearly 100%. The structure consisting of a metallic 'H' and a metal sheet which are separated by a dielectric spacer is designed. Simulation research shows that the surface waves generated on the meta-surface can indeed be guided out to flow on the mushroom as a surface plasmon polaritons. It is demonstrated that gradient-index metasurface is a bridge to link propagating waves and surface waves in the microwave region. Another sandwiched structure [283] composing of double L arrays and two orthogonal metallic sub-wavelength gratings is proposed. Its polarization conversion rate is over 0.99 in 0.20–1.97 THz which is almost 1.74 times of that in other works. A reflective Pancharatnam-Berry phase metasurface is fabricated by standard print circuit board technique and tested in microwave range. Experiments and simulations validate that a free and independent realization of the cone angle and OAM mode would able to achieve by this metasurface, which greatly simplifies the design process of conical beam generation. Xu [284] also adjusts the patch size to achieve the full range (2π) reflective phase, thereby paves a way to generate the OAM beams for wireless communication applications.

11.4. Adjustable smart absorbing material

Fabrication of smart stealth material and structure is an innovative way to obtain improved stealth material. By manipulating the intrinsic physical parameters and structure of materials, the EM response and resonance peaks are regulated, which allows the control on their response to EM waves. Smart EM stealth materials and structures have excellent flexibility which helps reduce the thickness and mass of materials, and broaden the response bandwidth of microwave.

There are two types of smart EM wave response structures: active control and passive control type. The active control structure usually works with an active control device. The change of EM response can be realized by controlling the structure parameters actively. In contrast, the passive control smart EM response structure mostly have open architecture which can be adjusted by changing environment or external field. Therefore, for the active control structure, the match between structure and control device should be considered.

11.4.1. Passive control smart absorbing materials

1. Loaded lumped elements control

The most typical passive control material is obtained by adding electric controllable lumped elements into the frequency selection surface (FSS) structure. By controlling the voltage or current of the external power, the resistance, capacitance, and inductance of the components are controlled, resulting in the change of resonance frequency and absorption performance. A passive adjustable absorber loaded with PIN diode is designed [285]. When the absorber is loaded with different current, different absorption depth and frequency will be obtained. The absorptivity over 90% can be obtained in the range of 9–13 GHz. A opened gap is designed on the metal ring, which realized the movement of absorption peak between 6 and 17 GHz [286]. In addition, many studies have been carried out by loading PIN diodes or varactor diodes between dipoles to get a broadband absorption. The absorbing/reflecting and absorbing/transmitting functions can be regulated by controlling the characteristics of PIN diode [287,288].

2. Mechanical performance control

By adjusting the mechanical parameters of structure, the resonance frequency and absorption performance can be controlled. A V-type adjustable structure can achieve adjustable performance by adjusting the folding angle [289]. The periodic units of the structure are arranged on the dielectric sheets in an origami-like manner. During the folding and unfolding process, the interaction between incident field and elements lead to a change of resonance frequency. The resonant frequency moves by 19% when the folding angle changes from 0° to 60°.

3. Other passive control methods

In addition, many new passive control smart absorbers have been studied. Scholars have made in-depth research on optical passive control smart absorber and plasma passive control smart absorber [290]. A tunable absorber made of discrete plasma shell is fabricated by integrating the ceramic gas seal cavity (plasma shell) with a tightly coupled loss resonance layer. By changing the voltage of maintainer, the plasma can be modeled as a frequency dependent inductor, which provides a

dynamic absorption to the microwave with various frequency.

11.4.2. Active control smart absorbing material

Active control smart material is a kind of adaptive material system, which can obtain information from environment, then react to that by changing structure to coordinate with the environment. At present, active control electronic devices are widely used in different field. Sb medium with temperature response characteristic is introduced into the metamaterial structure, and the absorption peak gradually increases from 0.82 to 1.02 THz with the temperature changing from 160 K to 350 K [291]. By phase and frequency modulation, environment open EM metamaterials can introduce or remove polar water molecules and ice crystals in different weather conditions. Thus, the intrinsic properties are regulated, and the smart regulation of EM properties corresponding to environmental humidity and temperature is realized. It should be emphasized that active control on EM stealth not only works in microwave frequency but also in the optical band. By controlling the thickness of nanometer silicon film (within 1/4 optical wavelength), the phase interference cancellation is constructed [292]. On this basis, the electrochemical cell is constructed, and the voltage is used to control the lithium ion deblocking behavior in the nanometer silicon film in the electrochemical cell. The intrinsic properties of the silicon film can be adjusted to make the device interfere with the reflected light.

The smart EM response can be realized by designing the related EM wave induction system and material control system. The coding adjustable metasurface and the artificial neural network model based on the deep learning algorithm are researched for microwave absorption.

11.5. Summary and prospects

The application of biomimetic materials in absorbing materials is still in its infancy, while the natural organisms have evolved for billions of years, their structures have become perfect for regulating EM waves, so the current researchers' attempts have shown that this research paradigm is effective and can be used in MAMs. In the future, with the research on biological models, more biological models suitable for MAMs will be found, which will promote the development of absorbing materials. Furthermore, additional the EM wave absorption model in nature, there are many models could realize multifunctional properties such as flexibility, impact-resistance, etc., which in favor of the integration of MAM. Metamaterial perfect absorbers has become a hotspot which many scholars and institutions are researching in recent years. It can flexibly adjust the absorption performance and facilitate wideband absorption. The integration of coded metamaterials and computers becomes a new way to regulate the electromagnetic radiation behavior and second harmonic. The proposal of this concept not only simplifies the design and optimization processes of metamaterials, but also constructs the axial direction of metamaterials in which physical spaces replace digital spaces which enable people to understand and explore metamaterials from the perspective of information science. More importantly, the digital coding and characterization of metamaterials is very conducive to combining some active devices (such as diodes and MEMS switches, etc.) under the control of field position gate array and other circuit systems to digitally quantify EM waves in real time to achieve a variety of completely different functions. The development of smart EM response system is still in its infancy. The rapid development of many disciplines has created a dynamic interdisciplinary environment for this field. At present, both the smart EM response system and materials have many scientific problems to be solved especially the integration mechanism of design and manufacture.

12. Conclusion

This overview restricts itself primarily to the MAMs working at 2–18 GHz bands. The most commonly researched MAMs currently are introduced including carbon materials, metal oxides, ceramic materials, conductive polymers, and alloys. The MAMs applied for harsh high temperature environment, infrared-compatible purpose, and multiband compatibility metamaterials are also involved. We present MAMs from their electromagnetic properties, loss mechanisms, structure, fabrication method, regulation approaches, designing principles, current applications, and future prospects which concern with many fields of science and technology including nanotechnology, material chemistry, polymer science, solid state physics, optics, and electromagnetism, etc. In this fashion, a comprehensively overview over the MAMs for their theoretical and experimental advances in recent year can be summarized as follows:

1. Integrating two or more kinds of materials is a useful strategy to achieve outstanding absorption performance, which has been devoted to tuning the electromagnetic parameters and adjusting the impedance matching characteristics. Significant synergetic effects and enhanced interfacial can be produced by combining magnetic (alloys, ferrites, metal oxides), dielectric (ceramics, MnO_2, ZnO), and conductive materials (conductive polymers, carbon materials) through heterogeneous electromagnetic couplings.
2. Microstructure effect the microwave absorbing performance significantly. Surface modification, heat treatment, atom doping, ball milling, chemical control, etc, are used to regulate the microstructure. Alloys with flaky particles showing larger shape anisotropy can get larger permeability and better EM absorption performance than others. Some materials with the structure of nanowires, nanotubes, nanorods, and core-shell can achieve unique electrical transport or exciting emissions. The network structure composed of different nanoparticles could increase the specific surface area of the material and improve the conductive loss, which attributes to the migration of activated electrons in the network.
3. Currently, ceramic materials and carbon materials are most used to explore and optimize high temperature dielectric properties. Ceramic materials are resistant for high temperature, corrosion, oxidation, etc., and show high strength, modulus, hardness due to the covalent and ionic bonding. In addition, high temperature absorbing materials in harsh environment must have good structural stability, oxidation resistance and dielectric constant temperature stability. HEA is one the new candidate if MAMs used in high temperature condition. While the main reason limiting the application of alloys at high temperatures is their low Curie temperature. The composition controlling, material modification and structure optimization can be used to improve the magnetic properties of the alloys.
4. First-principles calculation are one of the most widely used method to analyze the energy, electronic properties, magnetic properties, structure information, microparticle interactions, etc. They are mainly focusing on the explanation the variations of dielectric performance between the defective model and the origin model, and also on the magnetic materials for analyzing the phase transition assisted twinning by estimating the stacking fault energies, and temperature-dependent phase stabilities of different structures.
5. Besides the composition of absorbent, its microstructure, coating thickness, and the structure of coating can also influence the microwave absorption performance of coating. Metamaterial are presented to obtain excellent microwave absorbing properties which are far beyond that of the materials can achieve, even some lossless materials can show huge microwave absorption. By structure designing, digital coding, and active controlling, the metamaterials can show multiband compatibility on microwave absorption.

Declaration of competing interest

The authors declare that they have no known competing financial interests or personal relationships that could have appeared to influence the work reported in this paper.

Acknowledgements

The authors acknowledge the Supported by Program for the National Natural Science Foundation of China (No. 52071053, U1704253), the National Key R&D Program of China (2017YFB0703103), and Fundamental Research Funds for the Central Universities (DUT20GF111) and the China Postdoctoral Science Foundation (2020M670748).

References

[1] Zhang Y, Si H, Liu S, et al. Facile synthesis of BN/Ni nanocomposites for effective regulation of microwave absorption performance. J Alloys Compd 2021;850:156680.
[2] Amano M, Kotsuka Y. A method of effective use of ferrite for microwave absorber. IEEE Trans Microw Theor Tech 2003;51:238–45.
[3] Jiang Z, Si H, Chen X, et al. Simultaneous enhancement of impedance matching and the absorption behavior of BN/RGO nanocomposites for efficiency microwave absorption. Composites Communications 2020;22:100503.
[4] Wang H, Xiu X, Wang Y, et al. Based composites as a dual-functional material for ultralight broadband radar absorbing honeycombs. Compos B Eng 2020;202:108378.
[5] Zhang J, Li Z, Qi X, et al. Constructing flower-like core@ shell $MoSe_2$-based nanocomposites as a novel and high-efficient microwave absorber. Compos B Eng 2021;222:109067.
[6] Wang C, Wang B, Cao X, et al. 3D flower-like Co-based oxide composites with excellent wideband electromagnetic microwave absorption. Compos B Eng 2021;205:108529.
[7] Li J, Miao P, Chen K, et al. Highly effective electromagnetic wave absorbing prismatic Co/C nanocomposites derived from cubic metal-organic framework. Compos B Eng 2020;182:107613.
[8] Su J, Zhou W, Liu Y, et al. Effect of carbon black on dielectric and microwave absorption properties of carbon black/cordierite plasma-sprayed coatings. J Therm Spray Technol 2015;24:826–35.
[9] Wei R, Zhang H, Wang H, et al. Phase transitions and magnetic properties of $Fe_{30}Co_{29}Ni_{29}Zr_7B_4Cu_1$ high-entropy alloys. J Alloys Compd 2019;789:762–7.
[10] Min D, Zhou W, Qing Y, et al. Single-layer and double-layer microwave absorbers based on graphene nanosheets/epoxy resin composite. Nano 2017;12:1750089.
[11] Kuang J, Jiang P, Liu W, et al. Synergistic effect of Fe-doping and stacking faults on the dielectric permittivity and microwave absorption properties of SiC whiskers. Appl Phys Lett 2015;106:212903.
[12] Raveendran , M A, Sebastian T, Raman S. Applications of microwave materials: a review. 2019 J Electron Mater 2018;48:2601–34.
[13] Kwak BS, Choi WH, Noh YH, et al. Nickel-coated glass/epoxy honeycomb sandwich composite for broadband RCS reduction. Compos B Eng 2020;191:107952.
[14] Zhang Y, Meng H, Shi Y, et al. TiN/Ni/C ternary composites with expanded heterogeneous interfaces for efficient microwave absorption. Compos B Eng 2020;193:108028.
[15] Wang H, Meng F, Huang F, et al. Interface Modulating CNTs@PANi hybrids by controlled unzipping of the walls of CNTs to achieve tunable high-performance microwave absorption. ACS Appl Mater Interfaces 2019;11:12142–53.
[16] Jiang Y, Chen Y, Liu Y, et al. Lightweight spongy bone-like graphene@SiC aerogel composites for high-performance microwave absorption. Chem Eng J 2018;337:522–31.
[17] Green M, Chen X. Recent progress of nanomaterials for microwave absorption. Journal of Materiomics 2019;5:503–41.
[18] Liang C, Qiu H, Han Y, et al. Superior electromagnetic interference shielding 3D graphene nanoplatelets/reduced graphene oxide foam/epoxy nanocomposites with high thermal conductivity. J Mater Chem C 2019;7:2725–33.
[19] Huangfu Y, Ruan K, Qiu H, et al. Fabrication and investigation on the PANI/MWCNT/thermally annealed graphene aerogel/epoxy electromagnetic interference shielding nanocomposites. Compos Appl Sci Manuf 2019;121:265–72.
[20] Li J, Huang H, Zhou Y, et al. Research progress of graphene-based microwave absorbing materials in the last decade. J Mater Res 2017;32:1213.
[21] Jia H, Zhou W, Nan H, et al. Enhanced high temperature dielectric polarization of barium titanate/magnesium aluminum spinel composites and their potential in microwave absorption. J Eur Ceram Soc 2020;40:728–34.
[22] Song W, Cao M, Hou Z, et al. High-temperature microwave absorption and evolutionary behavior of multiwalled carbon nanotube nanocomposite. Scripta Mater 2009;61:201–4.
[23] Yuan X, Cheng L, Guo S, et al. High-temperature microwave absorbing properties of ordered mesoporous inter-filled SiC/SiO2 composites. Ceram Int 2017;43:282–8.
[24] Yin M, Bai X, Lv J, et al. Significant magnetism enhancement and weak spin-orbit coupling effect in $Mn_{(13-n)}Co_n$ (n = 0-13) bimetal alloy clusters. J Magn Magn Mater 2019;481:203–11.
[25] Silveira OJ, de Carvalho LC, Alves HWL, et al. Interplay between magnetic, metal/insulator and topological phases in $Hg_{1-x}Mn_xTe$ alloys: prediction of a ferromagnetic Weyl semimetal at x = 0.25. J Phys Condens Matter 2019;31:435502.
[26] Tariq A, Qurat Ul A, Nazir S. Cu-doping impact on the electronic and magnetic properties of Co_2ZrSn. Phys B Condens Matter 2020;580:411836.
[27] Dawson JA, Chen H, Tanaka I. First-principles calculations of oxygen vacancy formation and metallic behavior at a beta-MnO_2 grain boundary. ACS Appl Mater Interfaces 2015;7:1726–34.
[28] Song L, Duan Y, Zhang Y, et al. Promoting defect formation and microwave loss properties in δ-MnO_2 via Co doping: a first-principles study. Comput Mater Sci 2017;138:288–94.
[29] Gao S, Yang S, Wang H, et al. CoNi alloy with tunable magnetism encapsulated by N-doped carbon nanosheets toward high-performance microwave attenuation. Compos B Eng 2021;215:108781.
[30] Wu Y, Han M, Tang Z, et al. Eddy current effect on the microwave permeability of Fe-based nanocrystalline flakes with different sizes. J Appl Phys 2014;115:163902.
[31] Gao H, Wang J, Xu B, et al. Broadband metamaterial absorber based on magnetic substrate and resistance rings. Mater Res Express 2019;6:045803.
[32] Han M, Guo W, Wu Y, et al. Electromagnetic wave absorbing properties and hyperfine interactions of Fe-Cu-Nb-Si-B nanocomposites. Chin Phys B 2014;23:083301.
[33] Yang W, Zhang Y, Qiao G, et al. Tunable magnetic and microwave absorption properties of $Sm_{1.5}Y_{0.5}Fe_{17-x}Si_x$ and their composites. Acta Mater 2018;145:331–6.
[34] Murugaiyan P, Mitra A, Panda AK, et al. Electromagnetic interference shielding effectiveness of amorphous and nanocomposite soft magnetic ribbons. Phys B Condens Matter 2019;568:13–7.
[35] Liu T, Zhou P, Xie J, et al. Electromagnetic and absorption properties of urchinlike Ni composites at microwave frequencies. J Appl Phys 2012;111:093905.
[36] Liu J, Cao M, Luo Q, et al. Electromagnetic property and tunable microwave absorption of 3D nets from nickel chains at elevated temperature. ACS Appl Mater Interfaces 2016;8:22615–22.
[37] Cheng Y, Ji G, Li Z, et al. Facile synthesis of FeCo alloys with excellent microwave absorption in the whole Ku-band: effect of Fe/Co atomic ratio. J Alloys Compd 2017;704:289–95.
[38] Yan J, Huang Y, Liu P, et al. Large-scale controlled synthesis of magnetic FeCo alloy with different morphologies and their high performance of electromagnetic wave absorption. J Mater Sci Mater Electron 2017;28:3159–67.
[39] Liu Q, Cao Q, Zhao X, et al. Insights into size-dominant magnetic microwave absorption properties of CoNi microflowers via off-axis electron holography. ACS applied materials 2015;7:4233–40.
[40] Quan B, Liang X, Ji G, et al. Cross-linking-derived synthesis of porous Co_xNi_y/C nanocomposites for excellent electromagnetic behaviors. ACS Appl Mater Interfaces 2017;9:38814–23.
[41] Zhao B, Guo X, Zhao W, et al. Facile synthesis of yolk-shell Ni@ void@ SnO_2 (Ni_3Sn_2) ternary composites via galvanic replacement/Kirkendall effect and their enhanced microwave absorption properties. Nano Research 2017;10:331–43.
[42] Zhao B, Shao G, Fan B, et al. Facile preparation and enhanced microwave absorption properties of core–shell composite spheres composited of Ni cores and TiO_2 shells. Phys Chem Chem Phys 2015;17:8802–10.
[43] Hu H, Gao T, Zhao X, et al. Ultralight and high-elastic carbon foam with hollow framework for dynamically tunable electromagnetic interference shielding at gigahertz frequency. Carbon 2019;153:330–6.
[44] Wang X, Li J, Zhang N, et al. Evolution of hyperfine structure and magnetic characteristic in Fe-Si-Cr alloy with increasing heat treatment temperature. Mater Des 2016;96:314–22.
[45] Wei J, Wang T, Li F. Effect of shape of Fe_3Al particles on their microwave permeability and absorption properties. J Magn Magn Mater 2011;323:2608–12.
[46] Sun X, He J, Song Z, et al. Sodiumphosphinate-assisted synthesis of P-doped FeCo microcubes and their electromagnetic scattering characteristics. J Alloys Compd 2020;820:153280.
[47] Wang X, Shi G, Shi F, et al. Synthesis of hierarchical cobalt dendrites based on nanoflake self-assembly and their microwave absorption properties. RSC Adv 2016;6:40844–53.
[48] Wu N, Xu D, Wang Z, et al. Achieving superior electromagnetic wave absorbers through the novel metal-organic frameworks derived magnetic porous carbon nanorods. Carbon 2019;145:433–44.
[49] Cai X, Jiang X, Xie W, et al. Effect of particle size on the preparation and microwave absorption properties of FeSiAl magnetically soft alloy hollow microspheres. Defence Technology 2018;14:477–83.
[50] Li Y, Shi G, Tong M, et al. Effects of Al content in Fe-Al raw material alloy on shape and microwave absorption of Fe-based nanocapsules prepared by arc discharged method. J Mater Sci Mater Electron 2019;30:20058–68.
[51] Yeh JW, Chen SK, Lin SJ, et al. Nanostructured high-entropy alloys with multiple principal elements: novel alloy design concepts and outcomes. Adv Eng Mater 2004;6:299–303.
[52] Yang P, Liu Y, Zhao X, et al. Electromagnetic wave absorption properties of mechanically alloyed FeCoNiCrAl high entropy alloy powders. Adv Powder Technol 2016;27:1128–33.
[53] Yang P, Liu Y, Zhao X, et al. Electromagnetic wave absorption properties of $FeCoNiCrAl_{0.8}$ high entropy alloy powders and its amorphous structure prepared by high-energy ball milling. J Mater Res 2016;31:2398–406.
[54] Duan Y, Wen X, Zhang B, et al. Optimizing the electromagnetic properties of the $FeCoNiAlCr_x$ high entropy alloy powders by composition adjustment and annealing treatment. J Magn Magn Mater 2020;497:165947.
[55] Zhang B, Duan Y, Cui Y, et al. Improving electromagnetic properties of $FeCoNiSi_{0.4}Al_{0.4}$ high entropy alloy powders via their tunable aspect ratio and elemental uniformity. Mater Des 2018;149:173–83.

[56] Li Y, Shang S, Zhang W. Synthesis and electromagnetic wave absorption properties of FeCoNi($Si_{0.6}Al_{0.2}B_{0.2}$) high-entropy nanocrystalline alloy powders. AIP Adv 2019;9:125045.

[57] Zhang B, Duan Y, Wen X, et al. FeCoNiSi$_x$Al$_{0.4}$ high entropy alloy powders with dual-phase microstructure: improving microwave absorbing properties via controlling phase transition. J Alloys Compd 2019;790:179–88.

[58] Zhang B, Duan Y, Yang X, et al. Tuning magnetic properties based on FeCoNiSi$_{0.4}$Al$_{0.4}$ with dual-phase nano-crystal and nano-amorphous microstructure. Intermetallics 2020;117:106678.

[59] Zhang B, Duan Y, Cui Y, et al. A new mechanism for improving electromagnetic properties based on tunable crystallographic structures of FeCoNiSi$_x$Al$_{0.4}$ high entropy alloy powders. RSC Adv 2018;8:14936–46.

[60] Kim H, Park S, Kim S, et al. Microwave Absorption and shielding property of Fe-Si-Al alloy/MWCNT/polymer nanocomposites. Langmuir 2019;35:6950–5.

[61] Huang L, Liu X, Chuai D, et al. Flaky FeSiAl alloy-carbon nanotube composite with tunable electromagnetic properties for microwave absorption. Sci Rep 2016;6:35377.

[62] Liu D, Zhang Y, Zhou C, et al. A facile strategy for the core-shell FeSiAl composites with high-efficiency electromagnetic wave absorption. J Alloys Compd 2020;818:152861.

[63] Feng Y, Tang C, Qiu T. Effect of ball milling and moderate surface oxidization on the microwave absorption properties of FeSiAl composites. Mater Sci Eng, B 2013;178:1005–11.

[64] Zheng H, Yao W, Sun H, et al. Highly enhanced microwave absorption properties of CoFeBSiNb metallic glasses through corrosion. J Magn Magn Mater 2018;468:109–14.

[65] Wang Y, Wang W, Sun J, et al. Microwave-based preparation and characterization of Fe-cored carbon nanocapsules with novel stability and super electromagnetic wave absorption performance. Carbon 2018;135:1–11.

[66] Liu Z, Che R, Wei Y, et al. Broadening microwave absorption via a multi-domain structure. Apl Mater 2017;5:046104.

[67] Song L, Duan Y, Liu J, et al. Assembled Ag-doped α-MnO_2@ δ-MnO_2 nanocomposites with minimum lattice mismatch for broadband microwave absorption. Compos B Eng 2020;199:108318.

[68] Duan Y, Pang H, Zhang Y, et al. Morphology-controlled synthesis and microwave absorption properties of β-MnO_2 microncube with rectangular pyramid. Mater Char 2016;112:206–12.

[69] Guan H, Xie J, Chen G, et al. Facile synthesis of α-MnO_2 nanorods at low temperature and their microwave absorption properties. Mater Chem Phys 2014;143:1061–8.

[70] Niu Y, Li XP. Flexible polymer composites with enhanced wave absorption properties based on beta-manganese dioxide nanorods and PVDF. Inorg Chem Commun 2015;55:25–9.

[71] Hazarika A, Deka BK, Kong K, et al. Microwave absorption and mechanical performance of α-MnO_2 nanostructures grown on woven Kevlar fiber/reduced graphene oxide-polyaniline nanofiber array-reinforced polyester resin composites. Compos B Eng 2018;140:123–32.

[72] Wang H, Zhang Z, Dong C, et al. Carbon spheres@MnO_2 core-shell nanocomposites with enhanced dielectric properties for electromagnetic shielding. For Rep 2017;7:15841.

[73] She W, Bi H, Wen Z, et al. Tunable microwave absorption frequency by aspect ratio of hollow polydopamine@α-MnO_2 microspindles studied by electron holography. ACS Appl Mater Interfaces 2016;8:9782.

[74] Xiang H, Guo Y, Zhang Z, et al. Fabrication of MnO_2@Fe rod-like composite with controllable weight ratios of Fe/MnO_2 and excellent wideband electromagnetic absorption performance. J Alloys Compd 2019;773:150–7.

[75] Qiao M, Lei X, Ma Y, et al. Dependency of tunable microwave absorption performance on morphology-controlled hierarchical shells for core-shell Fe_3O_4@MnO_2 composite microspheres. Chem Eng J 2016;304:552–62.

[76] Wang L, Huang Y, Li C, et al. Hierarchical graphene@Fe_3O_4 nanocluster@carbon@MnO_2 nanosheet array composites: synthesis and microwave absorption performance. Phys Chem Chem Phys 2015;17:5878–86.

[77] Chen X, Jia Z, Feng A, et al. Hierarchical Fe_3O_4@carbon@MnO_2 hybrid for electromagnetic wave absorber. J Colloid Interface Sci 2019;553:465–74.

[78] Luo H, Zhang X, Huang S, et al. Infrared emissivity and microwave transmission behavior of flaky aluminum functionalized pyramidal-frustum shaped periodic structure. Infrared Phys Technol 2019;99:123–8.

[79] Wang R, He M, Zhou Y, et al. Metal organic frameworks self-templated cubic hollow Co/N/C@MnO_2 composites for electromagnetic wave absorption. Carbon 2019;156:388.

[80] Wang Y, Gao X, Lin C, et al. Metal organic frameworks-derived Fe-Co nanoporous carbon/graphene composite as a high-performance electromagnetic wave absorber. J Alloys Compd 2019;785:765–73.

[81] Huang Y, Zhang N, Wang M, et al. Facile synthesis of hollow ZnxFe$_{3-x}$O$_4$@porous MnO_2/rGO conductive network composites for tunable electromagnetic wave absorption. Ind Eng Chem Res 2018;57:14878–88.

[82] Qin Y, Zhang M, Guan Y, et al. Laser absorption and infrared stealth properties of Al/ATO composites. Ceram Int 2019;45:14312–5.

[83] Hu J, Shen Y, Xu LH, et al. Facile preparation of flower-like MnO_2/reduced graphene oxide (RGO) nanocomposite and investigation of its microwave absorption performance. Chem Phys Lett 2019;739:136953.

[84] Yang Z, Li M, Zhang Y, et al. Constructing uniform Fe_3O_4@C@MnO_2 microspheres with yolk-shell interior toward enhancement in microwave absorption. J Alloys Compd 2019;817:152795.

[85] Sunny V, Kurian P, Mohanan P, et al. A flexible microwave absorber based on nickel ferrite nanocomposite. J Alloys Compd 2010;489:297–303.

[86] Mulyawan A, Adi WA, Yunasfi Y. Raman spectroscopy study, magnetic and microwave absorbing properties of modified barium strontium monoferrite Ba$_{1-x}$Sr$_x$Fe$_2$O$_4$. Malaysian Journal of Fundamental and Applied Sciences 2018;14:73–7.

[87] Gordani GR, Mohseni M, Ghasemi A, et al. Microstructure, magnetic and microwave absorptive behavior of doped W-type hexaferrite nanoparticles prepared by co-precipitation method. Mater Res Bull 2016;76:187–94.

[88] Yasmin N, Abdulsatar S, Hashim M, et al. Structural and magnetic studies of Ce-Mn doped M-type $SrFe_{12}O_{19}$ hexagonal ferrites by sol-gel auto-combustion method. J Magn Magn Mater 2019;473:464–9.

[89] Alam RS, Moradi M, Rostami M, et al. Structural, magnetic and microwave absorption properties of doped Ba-hexaferrite nanoparticles synthesized by co-precipitation method. J Magn Magn Mater 2015;381:1–9.

[90] Hou T, Wang B, Ma M, et al. Preparation of two-dimensional titanium carbide ($Ti_3C_2T_x$) and $NiCo_2O_4$ composites to achieve excellent microwave absorption properties. Compos B Eng 2020;180:107577.

[91] Zhang M, Zhang J, Lin H, et al. Designable synthesis of reduced graphene oxide modified using $CoFe_2O_4$ nanospheres with tunable enhanced microwave absorption performances between the whole X and Ku bands. Compos B Eng 2020;190:107902.

[92] Chang Y, Zhang Y, Li L, et al. Microwave absorption in 0.1-18 GHz, magnetic and structural properties of $SrFe_{12-x}Ru_xO_{19}$ and $BaFe_{12-x}Ru_xO_{19}$. J Alloys Compd 2020;818:152930.

[93] Zhang H, Jia Z, Feng A, et al. In situ deposition of pitaya-like Fe_3O_4@C magnetic microspheres on reduced graphene oxide nanosheets for electromagnetic wave absorber. Compos B Eng 2020;199:108261.

[94] Shu R, Zhang J, Guo C, et al. Facile synthesis of nitrogen-doped reduced graphene oxide/nickel-zinc ferrite composites as high-performance microwave absorbers in the X-band. Chem Eng J 2020;384:123266.

[95] Liu P, Yao Z, Zhou J. Fabrication and microwave absorption of reduced graphene oxide/$Ni_{0.4}Zn_{0.4}Co_{0.2}Fe_2O_4$ nanocomposites. Ceram Int 2016;42:9241–9.

[96] Peng J, Peng Z, Zhu Z, et al. Achieving ultra-high electromagnetic wave absorption by anchoring $Co_{0.33}Ni_{0.33}Mn_{0.33}Fe_2O_4$ nanoparticles on graphene sheets using microwave-assisted polyol method. Ceram Int 2018;44:21015–26.

[97] Lin Y, Dai J, Yang H, et al. Graphene multilayered sheets assembled by porous $Bi_2Fe_4O_9$ microspheres and the excellent electromagnetic wave absorption properties. Chem Eng J 2018;334:1740–8.

[98] Wang S, Zhao Y, Xue H, et al. Preparation of flower-like $CoFe_2O_4$@graphene composites and their microwave absorbing properties. Mater Lett 2018;223:186–9.

[99] Xu F, Ma L, Gan M, et al. Preparation and characterization of chiral polyaniline/barium hexaferrite composite with enhanced microwave absorbing properties. J Alloys Compd 2014;593:24–9.

[100] Xu F, Ma L, Huo Q, et al. Microwave absorbing properties and structural design of microwave absorbers based on polyaniline and polyaniline/magnetite nanocomposite. J Magn Magn Mater 2015;374:311–6.

[101] Qian K, Yao Z, Lin H, et al. The influence of Nd substitution in Ni-Zn ferrites for the improved microwave absorption properties. Ceram Int 2020;46:227–35.

[102] Xiang J, Hou Z, Zhang X, et al. Facile synthesis and enhanced microwave absorption properties of multiferroic $Ni_{0.4}Co_{0.2}Zn_{0.4}Fe_2O_4$/$BaTiO_3$ composite fibers. J Alloys Compd 2018;737:412–20.

[103] Shen J, Feng J, Li L, et al. Synthesis and excellent electromagnetic absorbing properties of copolymer (N-methylpyrrole-co-pyrrole) and Ba-Nd-Cr ferrite. J Alloys Compd 2015;632:490–9.

[104] Du Y, Liu W, Qiang R, et al. Shell thickness-dependent microwave absorption of core-shell Fe_3O_4@C composites. ACS Appl Mater Interfaces 2014;6:12997–3006.

[105] Khan MA, Riaz S, Ali I, et al. Structural and magnetic behavior evaluation of Mg-Tb ferrite/polypyrrole nanocomposites. Ceram Int 2015;41:651–6.

[106] Macdiarmid AG. Polyaniline and polypyrrole: where are we headed? Synth Met 1997;84:27–34.

[107] Liu J, Duan Y, Song L, et al. Constructing sandwich-like polyaniline/graphene oxide composites with tunable conjugation length toward enhanced microwave absorption. Org Electron 2018;63:175–83.

[108] Lei Y, Zhou J, Yao Z, et al. Self-assembly of porous polyaniline microspheres via template-free interfacial method for high-performance electromagnetic absorption property. Mater Lett 2020;265:127389.

[109] Shi Y, Chen J, Dai J, et al. Frequency selective absorbing property of nanoring-shaped polyaniline with broadband absorption. J Mater Sci Mater Electron 2020;31:3622–30.

[110] Hao B, Li L, Wang Y, et al. Electrical and microwave absorbing properties of polypyrrole synthesized by optimum strategy. J Appl Polym Sci 2013;127:4273–9.

[111] Xie A, Wu F, Jiang W, et al. Chiral induced synthesis of helical polypyrrole (PPy) nano-structures: a lightweight and high-performance material against electromagnetic pollution. J Mater Chem C 2017;5:2175–81.

[112] Motojima S, Noda Y, Hoshiya S, et al. Electromagnetic wave absorption property of carbon microcoils in 12-110 GHz region. J Appl Phys 2003;94:2325–30.

[113] Zhang Y, Huang Y, Zhang T, et al. Broadband and tunable high-performance microwave absorption of an ultralight and highly compressible graphene foam. Adv Mater 2015;27:2049–53.

[114] Wang Y, Du Y, Qiang R, et al. Interfacially engineered sandwich-like rgo/carbon microspheres/rGO composite as an efficient and durable microwave absorber. Advanced Materials Interfaces 2016;3:1500684.

[115] Qiao M, Lei X, Ma Y, et al. Well-defined core-shell Fe_3O_4@Polypyrrole composite microspheres with tunable shell thickness: synthesis and their superior

microwave absorption performance in the Ku band. Ind Eng Chem Res 2016;55:6263–75.
[116] Varshney S, Singh K, Ohlan A, et al. Synthesis, characterization and surface properties of Fe_2O_3 decorated ferromagnetic polypyrrole nanocomposites. J Alloys Compd 2012;538:107–14.
[117] Li L, Liu S, Lu L. Synthesis and significantly enhanced microwave absorption properties of cobalt ferrite hollow microspheres with protrusions/polythiophene composites. J Alloys Compd 2017;722:158–65.
[118] Acharya S, Alegaonkar P, Datar S. Effect of formation of heterostructure of $SrAl_4Fe_8O_{19}$/RGO/PVDF on the microwave absorption properties of the composite. Chem Eng J 2019;374:144–54.
[119] Zhang Y, Lyu X, Yang Z, et al. Facile chemical synthesis of amorphous FeB alloy nanoparticles and their superior electromagnetic wave absorption performance. J Phys Chem Solid 2019;126:143–9.
[120] Wang Y, Dai X, Jiang W, et al. The hybrid of SnO_2 nanoparticle and polypyrrole aerogel: an excellent electromagnetic wave absorbing materials. Mater Res Express 2016;3:075023.
[121] Tian C, Du Y, Xu P, et al. Constructing Uniform Core-Shell PPy@PANI Composites with tunable shell thickness toward enhancement in microwave absorption. ACS Appl Mater Interfaces 2015;7:20090–9.
[122] Wang J, Or SW, Tan J. Enhanced microwave electromagnetic properties of core/shell/shell-structured Ni/SiO_2/polyaniline hexagonal nanoflake composites with preferred magnetization and polarization orientations. Mater Des 2018;153:190–202.
[123] Tian X, Meng F, Meng F, et al. Synergistic enhancement of microwave absorption using hybridized Polyaniline@helical CNTs with dual chirality. ACS Appl Mater Interfaces 2017;9:15711–8.
[124] Li J, Tan Y, Chen Y, et al. Constructing multiple interfaces in polydimethylsiloxane/multi-walled carbon nanotubes nanocomposites by the incorporation of cotton fibers for high-performance electromagnetic interference shielding and mechanical enhancement. Appl Surf Sci 2019;466:657–65.
[125] Chen X, Meng F, Zhou Z, et al. One-step synthesis of graphene/polyaniline hybrids by in situ intercalation polymerization and their electromagnetic properties. Nanoscale 2014;6:8140–8.
[126] Yu H, Wang T, Wen B, et al. Graphene/polyaniline nanorod arrays: synthesis and excellent electromagnetic absorption properties. J Mater Chem 2012;22:21679.
[127] Makeiff DA, Huber T. Microwave absorption by polyaniline–carbon nanotube composites. Synth Met 2006;156:497–505.
[128] Wu F, Sun M, Jiang W, et al. A self-assembly method for the fabrication of a three-dimensional (3D) polypyrrole (PPy)/poly(3,4-ethylenedioxythiophene) (PEDOT) hybrid composite with excellent absorption performance against electromagnetic pollution. J Mater Chem C 2016;4:82–8.
[129] Wang H, Meng F, Huang F, et al. Interface Modulating CNTs@PANi hybrids by controlled unzipping of the walls of CNTs to achieve tunable high-performance microwave absorption. ACS Appl Mater Interfaces 2019;11:12142–53.
[130] Xu F, Wu D, Fu R, et al. Design and preparation of porous carbons from conjugated polymer precursors. Mater Today 2017;20:629–56.
[131] Qi Y, Qi L, Liu L, et al. Facile synthesis of lightweight carbonized hydrochars decorated with dispersed ZnO nanocrystals and enhanced microwave absorption properties. Carbon 2019;150:259–67.
[132] Liu J, Zhang J, Li Y, et al. Microwave absorbing properties of barium hexa-ferrite/polyaniline core-shell nano-composites with controlled shell thickness. Mater Chem Phys 2015;163:470–7.
[133] Wang F, Wang N, Han X, et al. Core-shell FeCo@carbon nanoparticles encapsulated in polydopamine-derived carbon nanocages for efficient microwave absorption. Carbon 2019;145:701–11.
[134] Kim J, Kim G, Kim SY, et al. Fabrication of highly flexible electromagnetic interference shielding polyimide carbon black composite using hot-pressing method. Compos B Eng 2021;221:109010.
[135] Dong J, Zhou W, Qing Y, et al. Dielectric and microwave absorption properties of CB doped SiO_{2f}/PI double-layer composites. Ceram Int 2018;44:14007–12.
[136] Qin H, Liao Q, Zhang G, et al. Microwave absorption properties of carbon black and tetrapod-like ZnO whiskers composites. Appl Surf Sci 2013;286:7–11.
[137] Tang J, Bi S, Wang X, et al. Excellent microwave absorption of carbon black/reduced graphene oxide composite with low loading. J Mater Sci 2019;54:13990–4001.
[138] Wu F, Liu Z, Xiu T, et al. Fabrication of ultralight helical porous carbon fibers with CNTs-confined Ni nanoparticles for enhanced microwave absorption. Compos B Eng 2021;215:108814.
[139] Chu Z, Cheng H, Xie W, et al. Effects of diameter and hollow structure on the microwave absorption properties of short carbon fibers. Ceram Int 2012;38:4867–73.
[140] Sun Z, Yan Z, Yue K, et al. Novel high-performance electromagnetic absorber based on Nitrogen/Boron co-doped reduced graphene oxide. Compos B Eng 2020;196:108132.
[141] Zuo Y, Yao Z, Lin H, et al. Digital light processing 3D printing of graphene/carbonyl iron/polymethyl methacrylate nanocomposites for efficient microwave absorption. Compos B Eng 2019;179:107533.
[142] Feng W, Wang Y, Chen J, et al. Microwave absorbing property optimization of starlike ZnO/reduced graphene oxide doped by ZnO nanocrystal composites. Phys Chem Chem Phys 2017;19:14596–605.
[143] Zhang Y, Gao S, Xing H. Reduced graphene oxide wrapped cube-like $ZnSnO_3$: as a high-performance microwave absorber. J Alloys Compd 2019;777:544–53.
[144] a Zhang K, Chen J, Yue S, et al. Facile synthesis of core-shell CI/SiO_2 decorated RGO sheets composite for excellent electromagnetic wave absorption performance covering the whole X-band. Compos Appl Sci Manuf 2020;130.
b Li G, Cui Y, Zhang N, et al. The precipitation in annealing and its effect on permittivity of Fe-Si-Al powders. Phys B Condens Matter 2016;481:1–7.
[145] Liu P, Huang Y, Yan J, et al. Construction of CuS nanoflakes vertically aligned on magnetically decorated graphene and their enhanced microwave absorption properties. ACS Appl Mater Interfaces 2016;8:5536–46.
[146] Vietmeyer F, Seger B, Kamat PV. Anchoring ZnO particles on functionalized single wall carbon nanotubes. Excited State Interactions and Charge Collection. Adv Mater 2007;19:2935–40.
[147] Pang H, Abdalla AM, Sahu RP, et al. Low-temperature synthesis of manganese oxide–carbon nanotube-enhanced microwave-absorbing nanocomposites. J Mater Sci 2018;53:16288–302.
[148] Yang Q, Liu L, Hui D, et al. Microstructure, electrical conductivity and microwave absorption properties of γ-FeNi decorated carbon nanotube composites. Compos B Eng 2016;87:256–62.
[149] Qi X, Hu Q, Cai H, et al. Heteronanostructured Co@carbon nanotubes-graphene ternary hybrids: synthesis, electromagnetic and excellent microwave absorption properties. Sci Rep 2016;6:1–15.
[150] Wang T, Yu W, Zhou C, et al. Self-healing and flexible carbon nanotube/polyurethane composite for efficient electromagnetic interference shielding. Compos B Eng 2020;193:108015.
[151] Wu G, Jia Z, Zhou X, et al. Interlayer controllable of hierarchical MWCNTs@C@Fe_xO_y cross-linked composite with wideband electromagnetic absorption performance. Compos Appl Sci Manuf 2020;128:105687.
[152] Chen X, Jia Z, Feng A, et al. Hierarchical Fe_3O_4@carbon@MnO_2 hybrid for electromagnetic wave absorber. J Colloid Interface Sci 2019;553:465–74.
[153] Wang Y, Wang H, Ye J, et al. Magnetic CoFe alloy@C nanocomposites derived from ZnCo-MOF for electromagnetic wave absorption. Chem Eng J 2020;383:123096.
[154] Wang L, Yu X, Li X, et al. MOF-derived yolk-shell Ni@C@ZnO Schottky contact structure for enhanced microwave absorption. Chem Eng J 2020;383:123099.
[155] Zhu W, Ye F, Li M, et al. In-situ growth of wafer-like Ti_3C_2/Carbon nanoparticle hybrids with excellent tunable electromagnetic absorption performance. Compos B Eng 2020;202:108408.
[156] Guan H, Wang Q, Wu X, et al. Biomass derived porous carbon (BPC) and their composites as lightweight and efficient microwave absorption materials. Compos B Eng 2020;207:108562.
[157] Zhou Y, Wang S, Li D, et al. Lightweight and recoverable ANF/rGO/PI composite aerogels for broad and high-performance microwave absorption. Compos B Eng 2021;213:108701.
[158] Sotiropoulos A, Koulouridis S, Masouras A, et al. Carbon nanotubes films in glass fiber polymer matrix forming structures with high absorption and shielding performance in X-Band. Compos B Eng 2021;217:108896.
[159] Li Y, Qing Y, Zhou Y, et al. Unique nanoporous structure derived from Co_3O_4–C and Co/CoO–C composites towards the ultra-strong electromagnetic absorption. Compos B Eng 2021;213:108731.
[160] Xiang Z, Xiong J, Deng B, et al. Rational design of 2D hierarchically laminated Fe_3O_4@nanoporous carbon@rGO nanocomposites with strong magnetic coupling for excellent electromagnetic absorption applications. J Mater Chem C 2020;8:2123–34.
[161] Wang L, Wen B, Bai X, et al. Facile and green approach to the synthesis of zeolitic imidazolate framework nanosheet-derived 2D Co/C composites for a lightweight and highly efficient microwave absorber. J Colloid Interface Sci 2019;540:30–8.
[162] Zhang Y, Chen Y, Qin Q, et al. Synthesis of FeCoNiCuZn single-phase high-entropy alloy by high-frequency electromagnetic-field assisted ball milling. J Magn Magn Mater 2020;498:166151.
[163] Lan X, Liang C, Wu M, et al. Facile synthesis of highly defected silicon carbide sheets for efficient absorption of electromagnetic waves. J Phys Chem C 2018;122:18537–44.
[164] Zhou J, Wei B, Yao Z, et al. Preparation of hollow SiC spheres with biological template and research on its wave absorption properties. J Alloys Compd 2020;819:153021.
[165] Zhang M, Lin H, Ding S, et al. Net-like SiC@ C coaxial nanocable towards superior lightweight and broadband microwave absorber. Compos B Eng 2019;179:107525.
[166] Xiao S, Mei H, Han D, et al. Sandwich-like SiCnw/C/Si_3N_4 porous layered composite for full X-band electromagnetic wave absorption at elevated temperature. Compos B Eng 2020;183:107629.
[167] Du B, Qian J, Hu P, et al. Fabrication of C-doped SiC nanocomposites with tailoring dielectric properties for the enhanced electromagnetic wave absorption. Carbon 2020;157:788–95.
[168] Ye X, Chen Z, Li M, et al. Microstructure and microwave absorption performance variation of SiC/C foam at different elevated-temperature heat treatment. ACS Sustainable Chem Eng 2019;7:18395–404.
[169] Cheng Y, Tan M, Hu P, et al. Strong and thermostable SiC nanowires/graphene aerogel with enhanced hydrophobicity and electromagnetic wave absorption property. Appl Surf Sci 2018;448:138–44.
[170] Dong S, Lyu Y, Li X, et al. Construction of MnO nanoparticles anchored on SiC whiskers for superior electromagnetic wave absorption. J Colloid Interface Sci 2020;559:186–96.
[171] Liang C, Liu C, Wang H, et al. SiC-Fe_3O_4 dielectric-magnetic hybrid nanowires: controllable fabrication, characterization and electromagnetic wave absorption. J Mater Chem 2014;2:16397–402.
[172] Wei X, Xu G, Ren Z, et al. Size-controlled synthesis of $BaTiO_3$ nanocrystals via a hydrothermal route. Mater Lett 2008;62:3666–9.

[173] Zhang M, Zheng J, Liang L, et al. Preparation and microwave absorption properties of Ag-doped $BaTiO_3$ nanocomposites. J Magn Magn Mater 2014;368:198–201.

[174] Liu Y, Feng Y, Wu X, et al. Microwave absorption properties of La doped barium titanate in X-band. J Alloys Compd 2009;472:441–5.

[175] Cui L, Tian C, Tang L, et al. Space-confined synthesis of core-shell $BaTiO_3$@carbon microspheres as a high-performance binary dielectric system for microwave absorption. ACS Appl Mater Interfaces 2019;11:31182–90.

[176] Ran J, Guo M, Zhong L, et al. In situ growth of $BaTiO_3$ nanotube on the surface of reduced graphene oxide: a lightweight electromagnetic absorber. J Alloys Compd 2019;773:423–31.

[177] Shi G, Li Y, Ai L, et al. Two step synthesis and enhanced microwave absorption properties of polycrystalline $BaTiO_3$ coated Ni nanocomposites. J Alloys Compd 2016;680:735–43.

[178] Wang X, Li Q, Su Z, et al. Enhanced microwave absorption of multiferroic Co_2Z hexaferrite-$BaTiO_3$ composites with tunable impedance matching. J Alloys Compd 2015;643:111–5.

[179] Wang Z, Cheng Z, Fang C, et al. Recent advances in MXenes composites for electromagnetic interference shielding and microwave absorption. Compos Appl Sci Manuf 2020;136:105956.

[180] Wang L, Chen L, Song P. Fabrication on the Annealed $Ti_3C_2T_x$ MXene/epoxy nanocomposites for electromagnetic interference shielding application. Compos B Eng 2019;171:111–8.

[181] Gong K, Zhou K, Qian X, et al. MXene as emerging nanofillers for high-performance polymer composites: a review. Compos B Eng 2021;217:108867.

[182] Dai Y, Wu X, Liu Z, et al. Highly sensitive, robust and anisotropic MXene aerogels for efficient broadband microwave absorption. Compos B Eng 2020;200:108263.

[183] Liang L, Li Q, Yan X, et al. Multifunctional Magnetic $Ti_3C_2T_x$ MXene/graphene aerogel with superior electromagnetic wave absorption performance. ACS Nano 2021;15:6622–32.

[184] Li X, Yin X, Song C, et al. Self-assembly core–shell graphene-bridged hollow mxenes spheres 3D foam with ultrahigh specific em absorption performance. Adv Funct Mater 2018;28:1803938.

[185] Li X, Yin X, Xu H, et al. Ultralight MXene-coated, interconnected SiCnws three-dimensional lamellar foams for efficient microwave absorption in the X-band. ACS Appl Mater Interfaces 2018;10:34524–33.

[186] Ning M, Lu M, Li J, et al. Two-dimensional nanosheets of MoS_2: a promising material with high dielectric properties and microwave absorption performance. Nanoscale 2015;7:15734–40.

[187] Ning M, Man Q, Tan G, et al. Ultrathin MoS_2 nanosheets encapsulated in hollow carbon spheres: a case of a dielectric absorber with optimized impedance for efficient microwave absorption. ACS Appl Mater Interfaces 2020;12:20785–96.

[188] Ning M, Jiang P, Ding W, et al. Phase manipulating toward molybdenum disulfide for optimizing electromagnetic wave absorbing in gigahertz. Adv Funct Mater 2021;31:2011229.

[189] Cao M, Song W, Hou Z, et al. The effects of temperature and frequency on the dielectric properties, electromagnetic interference shielding and microwave-absorption of short carbon fiber/silica composites. Carbon 2010;48:788–96.

[190] Wen B, Cao M, Hou Z, et al. Temperature dependent microwave attenuation behavior for carbon-nanotube/silica composites. Carbon 2013;65:124–39.

[191] Liu Y, Luo F, Su J, et al. Dielectric and microwave absorption properties of Ti_3SiC_2/cordierite composite ceramics oxidized at high temperature. J Alloys Compd 2015;632:623–8.

[192] Jia H, Zhou W, Nan H, et al. High temperature microwave absorbing properties of plasma sprayed $La_{0.6}Sr_{0.4}FeO_{3-\delta}/MgAl_2O_4$ composite ceramic coatings. Ceram Int 2020;46:6168–73.

[193] Wan F, Luo F, Zhou Y, et al. A glass coating for SiC fiber reinforced aluminum phosphate matrix ($SiC_f/AlPO_4$) composites for high-temperature absorbing wave applications. Surf Coating Technol 2015;264:9–16.

[194] Li E, Wen Q, Yang H, et al. Novel temperature stable $NiSnTa_2O_8$ microwave dielectric ceramics with trirutile structure. Ceram Int 2020;46:6079–84.

[195] Li K, Chen G, Li X, et al. High-temperature dielectric properties and pyrolysis reduction characteristics of different biomass-pyrolusite mixtures in microwave field. Bioresour Technol 2019;294:122217.

[196] Wang J, Wang Z, Jia Y, et al. High temperature soft magnetic properties of $(Fe_xCo_{1-x})_{73.5}Cu_1Mo_3Si_{13.5}B_9$ (x=0.5,1) alloys. J Magn Magn Mater 2013;328:62–5.

[197] Xie Z, Wang Z, Han Y, et al. Influence of Ge on crystallization kinetics, microstructure and high-temperature magnetic properties of Si-rich nanocrystalline FeAlSiBCuNbGe alloy. J Non-Cryst Solids 2017;463:1–5.

[198] Zhang L, Wang Z, Xu Y. Superior high-temperature magnetic softness for Al-doped FeCo-based nanocrystalline alloys. J Non-Cryst Solids 2018;481:148–51.

[199] Jayaraman T, Thotakura G, Rathi A. Phase evolution, structure, and magnetic characterization of mechanosynthesized $Ni_{40}Fe_{30}Co_{30}$ medium-entropy alloy. J Magn Magn Mater 2019;489:165466.

[200] Guo L, Liang F, Wen X, et al. Uniform magnetic chains of hollow cobalt mesospheres from one-pot synthesis and their assembly in solution. Adv Funct Mater 2007;17:425–30.

[201] Duan Y, Liu Z, Jing H, et al. Novel microwave dielectric response of Ni/Co-doped manganese dioxides and their microwave absorbing properties. J Mater Chem 2012;22:18291–9.

[202] Duan Y, Liu Z, Zhang Y, et al. A theoretical study of the dielectric and magnetic responses of Fe-doped α-MnO_2 based on quantum mechanical calculations. J Mater Chem C 2013;1:1990–4.

[203] Duan Y, Chen J, Zhang Y, et al. The theoretical study on electronic structure and electromagnetic properties of α-MnO_2 based on crystal defects. Eur Phys J Appl Phys 2014;68:30901.

[204] Yang Z, Wang X, Huang Y. First-principles study on the doping effects of Al in α-MnO_2. Curr Appl Phys 2015;15:1556–61.

[205] Alfaruqi MH, Islam S, Lee J, et al. First principles calculations study of α-MnO_2 as a potential cathode for Al-ion battery application. J Mater Chem 2019;7:26966–74.

[206] Duan Y, Zhang Y, Chen J, et al. Frequency response of microwave dielectric based on tunable crystallographic defects of β-MnO_2. Mater Chem Phys 2015;157:1–7.

[207] Tompsett DA, Middlemiss DS, Islam MS. Importance of anisotropic Coulomb interactions and exchange to the band gap and antiferromagnetism of β-MnO_2 from DFT+U. Phys Rev B 2012;86:205126.

[208] Song L, Duan Y, Liu J, et al. Transformation between nanosheets and nanowires structure in MnO_2 upon providing Co^{2+} ions and applications for microwave absorption. Nano Research 2019;13:95–104.

[209] Wei H, Yin X, Li X, et al. Controllable synthesis of defective carbon nanotubes/$Sc_2Si_2O_7$ ceramic with adjustable dielectric properties for broadband high-performance microwave absorption. Carbon 2019;147:276–83.

[210] Ye F, Song Q, Zhang Z, et al. Direct growth of edge-rich graphene with tunable dielectric properties in porous Si_3N_4 ceramic for broadband high-performance microwave absorption. Adv Funct Mater 2018;28:1707205.

[211] Yang H, Yuan J, Li Y, et al. Silicon carbide powders: temperature-dependent dielectric properties and enhanced microwave absorption at gigahertz range. Solid State Commun 2013;163:1–6.

[212] Kuang B, Dou Y, Wang Z, et al. Enhanced microwave absorption properties of Co-doped SiC at elevated temperature. Appl Surf Sci 2018;455:383–90.

[213] Mahapatra AS, Mitra A, Mallick A, et al. XRD, HRTEM, magnetic, dielectric and enhanced microwave reflection loss of $GaFeO_3$ nanoparticles encapsulated in multi-walled carbon nanotubes. Ceram Int 2016;42:3826–35.

[214] Ray A, Basu T, Behera B, et al. Role of Gd-doping in conduction mechanism of BFO-PZO nanocrystalline composites: experimental and first-principles studies. J Alloys Compd 2018;768:198–213.

[215] Deng J, Zhang X, Zhao B, et al. Fluffy microrods to heighten the microwave absorption properties through tuning the electronic state of Co/CoO. J Mater Chem C 2018;6:7128–40.

[216] Moitra D, Dhole S, Ghosh BK, et al. Synthesis and microwave absorption properties of $BiFeO_3$ nanowire-RGO nanocomposite and first-principles calculations for insight of electromagnetic properties and electronic structures. J Phys Chem C 2017;121:21290–304.

[217] Ullah I, Mehmood S, Ali Z, et al. Theoretical studies of the electronic structure and magnetic properties of aluminum-rich intermetallic alloy $Al_{13}Fe_4$. Int J Mod Phys B 2018:1850201.

[218] Alsaad AM, Ahmad AA, Qattous HA. Structural, electronic and magnetic properties of M_xPt_{1-X}, (M= Co, Ni and V) binary alloys. Heliyon 2019;5:e02433.

[219] Luo H, Chen F, Wang X, et al. A novel two-layer honeycomb sandwich structure absorber with high-performance microwave absorption. Compos Appl Sci Manuf 2019;119:1–7.

[220] Mushtaq M, Dar SA, Sattar MA, et al. First-principles study of structural, electronic, magnetic, thermodynamic and mechanical properties of ferromagnetic Mn_2MoAl Heuslar alloy. J Mol Graph 2019;95:107507.

[221] Li J, Zhang Z, Sun Y, et al. The thermodynamic, electronic and magnetic properties of Ni_2MnX (X=Ge, Sn, Sb) Heusler alloys: a quasi-hormonic Debye model and first principles study. Phys B Condens Matter 2013;409:35–41.

[222] Zipporah M, Robinson M, Julius M, et al. Perpendicular magnetic anisotropy in nearly fully compensated ferrimagnetic Heusler alloy $Mn_{0.75}Co_{1.25}VIn$: an ab initio study. J Magn Magn Mater 2017;442:343–9.

[223] Mushtaq M, Sattar MA, Dar SA, et al. Search for half-metallicity in new ferrimagnetic quaternary Mn_XMoAl (X= Co and Ti) Heusler alloys: a DFT based investigation. Mater Chem Phys 2020;245:122779.

[224] Zuo T, Gao M, Ouyang L, et al. Tailoring magnetic behavior of $CoFeMnNi_X$ (X= Al, Cr, Ga, and Sn) high entropy alloys by metal doping. Acta Mater 2017;130:10–8.

[225] Fathalian A, Jalilian J, Shahidi S. First principle study of the electronic and magnetic properties of a single iron atomic chain encapsulated in boron nitrite nanotubes. Solid State Commun 2011;151:1635–9.

[226] Dashora A, Suthar M, Kumar K, et al. Study of magnetism in Fe doped $CoCr_2O_4$ using magnetic Compton scattering and first-principles computations. J Alloys Compd 2020;824:153883.

[227] Mardani R, Kazerani MR, Shahmirzaee H. Investigating magnetic properties of $Co_{68}Fe_4B_{15}Si_{13}$ amorphous alloy by molecular dynamics and DFT calculations. Mod Phys Lett B 2017;31:1750094.

[228] Wei P, Zhu D, Huang S, et al. Effects of the annealing temperature and atmosphere on the microstructures and dielectric properties of ZnO/Al_2O_3 composite coatings. Appl Surf Sci 2013;285:577–82.

[229] Liang Z, Zhou W, Liu T, et al. Influence of ZnO content and annealing temperature on the dielectric properties of ZnO/Al_2O_3 composite coatings. J Alloys Compd 2011;509:5903–7.

[230] You W, She W, Liu Z, et al. High-temperature annealing of an iron microplate with excellent microwave absorption performance and its direct micromagnetic analysis by electron holography and Lorentz microscopy. J Mater Chem C 2017;5:6047–53.

[231] Pan Y, Ma G, Liu X, et al. Electromagnetic and microwave absorption properties of coatings based on spherical and flaky carbonyl iron. J Mater Sci Mater Electron 2019;30:18123–34.

[232] Liu L, Duan Y, Ma L, et al. Microwave absorption properties of a wave-absorbing coating employing carbonyl-iron powder and carbon black. Appl Surf Sci 2010; 257:842–6.
[233] Song C, Yin X, Han M, et al. Three-dimensional reduced graphene oxide foam modified with ZnO nanowires for enhanced microwave absorption properties. Carbon 2017;116:50–8.
[234] Qing Y, Zhou W, Luo F, et al. Epoxy-silicone filled with multi-walled carbon nanotubes and carbonyl iron particles as a microwave absorber. Carbon 2010;48: 4074–80.
[235] Gill N, Singh J, Puthucheri S, et al. Thin and broadband two-layer microwave absorber in 4-12 GHz with developed flaky cobalt material. Electronic Materials Letters 2018;14:288–97.
[236] Shi G, Zhang B, Wang X, et al. Enhanced microwave absorption properties of core double-shell type Fe@C@$BaTiO_3$ nanocapsules. J Alloys Compd 2016;655:130–7.
[237] Li S, Huang Y, Ding L, et al. Synthesis and enhancement of microwave absorption property by coating silicon dioxide and polyaniline for Fe-Co alloy. J Magn Magn Mater 2019;486:165259.
[238] Yang Z, Luo F, Hu Y, et al. Dielectric and microwave absorption properties of TiO_2/Al_2O_3 coatings and improved microwave absorption by FSS incorporation. J Alloys Compd 2016;678:527–32.
[239] Shah A, Wang Y, Huang H, et al. Microwave absorption and flexural properties of Fe nanoparticle/carbon fiber/epoxy resin composite plates. Compos Struct 2015; 131:1132–41.
[240] Song W, Zhou Z, Wang L, et al. Constructing repairable meta-structures of ultra-broad-band electromagnetic absorption from three-dimensional printed patterned shells. ACS Appl Mater Interfaces 2017;9:43179–87.
[241] Yuan L, Weng X, Xie J, et al. Effects of shape, size and solid content of Al pigments on the low-infrared emissivity coating. Mater Res Innovat 2015;19:325–30.
[242] Yan X, Xu G. Corrosion and mechanical properties of epoxy-polyurethane/bronze composite coatings with low infrared emissivity. Surf Coating Technol 2010;205: 2307–12.
[243] Song L, Shen X, Cheng G, et al. Infrared Emissivity of $La_{0.8}Sr_{0.2}MnO_3$ with three different structures. J Wuhan Univ Technol -Materials Sci Ed 2018;33:338–42.
[244] Wu G, Yu D. Preparation of a novel infrared low-emissive coating from the Cu powder modified by the polyethylene wax. Infrared Phys Technol 2012;55:26–31.
[245] Wu G, Yu D. Preparation and characterization of a new low infrared-emissivity coating based on modified aluminum. Prog Org Coating 2013;76:107–12.
[246] Chu H, Zhang Z, Liu Y, et al. Silver particles modified carbon nanotube paper/glassfiber reinforced polymer composite material for high temperature infrared stealth camouflage. Carbon 2016;98:557–66.
[247] Ye X, Zheng C, Xiao X, et al. Synthesis, characterization and infrared emissivity study of SiO_2/Ag/TiO_2 "sandwich" core-shell composites. Mater Lett 2015;141: 191–3.
[248] Loka C, Park KR, Lee KS. Multi-functional TiO_2/Si/Ag(Cr)/TiN_x coatings for low-emissivity and hydrophilic applications. Appl Surf Sci 2016;363:439–44.
[249] Zhang W, Lv D. Preparation and characterization of Ge/TiO_2//Si/SiO_2 one-dimensional heterostructure photonic crystal with infrared spectrally selective low emissivity. Opt Mater 2019;96:109333.
[250] Fuquan B, Wang JL, Tang N, et al. A study of magnetic properties of $SmFe_{12-x}Nb_x$ compounds. J Magn Soc Jpn 1999;23:456–8.
[251] Liu Q, Xing H, Wang H, et al. Microwave absorbing and infrared radiation properties of Al@multi-walled carbon nanotubes composites. J Mater Sci Mater Electron 2019;30:19760–9.
[252] Zhou P, Zhang J, Li W, et al. AOPC 2019: Advanced laser materials and laser technology 2019;11333:1.
[253] Solovyev AA, Rabotkin SV, Kovsharov NF. Polymer films with multilayer low-E coatings. Mater Sci Semicond Process 2015;38:373–80.
[254] Chen X, Tian C, Chen T. Composite grating structure for laser and infrared compatible stealth with high visible transmittance. Optik 2019;183:863–8.
[255] Hu C, Xu G, Shen X, et al. The epoxy-siloxane/Al composite coatings with low infrared emissivity for high temperature applications. Appl Surf Sci 2010;256: 3459–63.
[256] Zhang B, Xu G, Liu C, et al. Low infrared emissivity of the $Cr_{39}Ni_7C$/inorganic silicate coatings with excellent heat-resistant. Infrared Phys Technol 2018;92: 234–9.
[257] Guo T, Xu G, Tan S, et al. Controllable synthesis of ZnO with different morphologies and their morphology-dependent infrared emissivity in high temperature conditions. J Alloys Compd 2019;804:503–10.
[258] Kuo W, Hsu J, Nien C, et al. Moth-eye-inspired biophotonic surfaces with antireflective and hydrophobic characteristics. ACS Appl Mater Interfaces 2016;8: 32021–30.
[259] Siddique RH, Gomard G, Hölscher H. The role of random nanostructures for the omnidirectional anti-reflection properties of the glasswing butterfly. Nat Commun 2015;6:6909.
[260] Zhang W, Zhang D, Fan T, et al. Novel photoanode structure templated from butterfly wing scales. Chem Mater 2009;21:33–40.
[261] Lv J, Ding D, Yang X, et al. Biomimetic chiral photonic crystals. Angew Chem Int Ed 2019;58:7783–7.
[262] Nguyen TD, MacLachlan MJ. Double twisted photonic honeycomb frameworks with mesoporous structures. Advanced Optical Materials 2019;7:1801275.
[263] Huang L, Duan Y, Dai X, et al. Bioinspired metamaterials: multibands electromagnetic wave adaptability and hydrophobic characteristics. Small 2019; 0:1902730.
[264] Huang L, Duan Y, Liu J, et al. Bioinspired gyrotropic metamaterials with multifarious wave adaptability and multifunctionality. Advanced Optical Materials 2020;8:2000012.
[265] Wang Y, Zhang C, Ren L, et al. Sound absorption of a new bionic multi-layer absorber. Compos Struct 2014;108:400–8.
[266] Cui Y, Gong H, Wang Y, et al. A thermally insulating textile inspired by polar bear hair. Adv Mater 2018;30:1706807.
[267] Qian C, Zheng B, Shen Y, et al. Deep-learning-enabled self-adaptive microwave cloak without human intervention. Nat Photonics 2020;14:383–90.
[268] Fante RL, McCormack MT. Reflection properties of the salisbury screen. IEEE Trans Antenn Propag 1988;36:1443–54.
[269] Landy NI, Sajuyigbe S, Mock JJ, et al. Perfect metamaterial absorber. Phys Rev Lett 2008;100:4.
[270] Tao H, Landy NI, Bingham CM, et al. A metamaterial absorber for the terahertz regime: design, fabrication and characterization. Opt Express 2008;16:7181–8.
[271] Aydin K, Ferry VE, Briggs RM, et al. Broadband polarization-independent resonant light absorption using ultrathin plasmonic super absorbers. Nat Commun 2011;2:045131.
[272] Zhu B, Feng Y, Zhao J, et al. Switchable metamaterial reflector/absorber for different polarized electromagnetic waves. Appl Phys Lett 2010;97:051906.
[273] Cheng Y, Cheng Z, Mao X, et al. Ultra-thin multi-band polarization-insensitive microwave metamaterial absorber based on multiple-order responses using a single resonator structure. Materials 2017;10:1241.
[274] Wang B, Koschny T, Soukoulis CM. Wide-angle and polarization-independent chiral metamaterial absorber. Phys Rev B 2009;80:033108.
[275] Yang S, Liu Z, Yang H, et al. Intrinsic chirality and multispectral spin-selective transmission in folded eta-shaped metamaterials. Advanced Optical Materials 2020;8:1901448.
[276] Landy NI, Bingham CM, Tyler T, et al. Design, theory, and measurement of a polarization-insensitive absorber for terahertz imaging. Phys Rev B 2009;79: 125104.
[277] Zhao J, Wei S, Wang C, et al. Broadband microwave absorption utilizing water-based metamaterial structures. Opt Express 2018;26:8522–31.
[278] Cui T, Qi M, Wan X, et al. Coding metamaterials, digital metamaterials and programmable metamaterials, Light. Science & Applications 2014;3:218.
[279] Bai G, Ma Q, Cao W, et al. Manipulation of electromagnetic and acoustic wave behaviors via shared digital coding metallic metasurfaces. Advanced Intelligent Systems 2019;1:1900038.
[280] Zhang X, Yu Q, Jiang W, et al. Polarization-controlled dual-programmable metasurfaces. Advanced Science 2020;7:1903382.
[281] Wu H, Liu S, Wan X, et al. Controlling energy radiations of electromagnetic waves via frequency coding metamaterials. Adv Sci 2017;4:1700098.
[282] Sun S, He Q, Xiao S, et al. Gradient-index meta-surfaces as a bridge linking propagating waves and surface waves. Nat Mater 2012;11:426–31.
[283] Cao W, Wu L, Zhang C, et al. Asymmetric transmission of acoustic waves in a waveguide via gradient index metamaterials. Sci Bull 2019;64:808–13.
[284] Xu B, Wu C, Wei Z, et al. Generating an orbital-angular-momentum beam with a metasurface of gradient reflective phase. Opt Mater Express 2016;6:3940.
[285] Tennant A, Chambers B. Adaptive radar absorbing structure with PIN diode controlled active frequency selective surface. Smart Mater Struct 2003;13:122.
[286] Martynyuk AE, Martinez Lopez JI, Martynyuk NA. Active frequency-selective surfaces based on loaded ring slot resonators. Electron Lett 2005;41:2.
[287] Ghosh S, Srivastava KV. Polarisation-independent switchable absorber/reflector. Electron Lett 2016;52:1141–3.
[288] Ghosh S, Srivastava KV. Polarization-insensitive single-and broadband switchable absorber/reflector and its realization using a novel biasing technique. IEEE Trans Antenn Propag 2016;64:3665–70.
[289] Fuchi K, Tang J, Crowgey B, et al. Origami tunable frequency selective surfaces. IEEE Antenn Wireless Propag Lett 2012;11:473–5.
[290] Payne K, Xu K, Choi JH, et al. Electrically tunable microwave absorber based on discrete plasma-shells. IEEE Trans Antenn Propag 2019;67:6523–31.
[291] Zheng W, Li W, Chang S. A thermally tunable terahertz metamaterial absorber. Optoelectron Lett 2015;11:18–21.
[292] Bao Y, Han Y, Yang L, et al. Bioinspired controllable electro-chemomechanical coloration films. Adv Funct Mater 2018;29:1806383.